

This electronic thesis or dissertation has been downloaded from the King's Research Portal at <https://kclpure.kcl.ac.uk/portal/>



Haemodynamic and physiological principles of paradoxical low gradient aortic stenosis

McConkey, Hannah

Awarding institution:
King's College London

The copyright of this thesis rests with the author and no quotation from it or information derived from it may be published without proper acknowledgement.

END USER LICENCE AGREEMENT



Unless another licence is stated on the immediately following page this work is licensed

under a Creative Commons Attribution-NonCommercial-NoDerivatives 4.0 International

licence. <https://creativecommons.org/licenses/by-nc-nd/4.0/>

You are free to copy, distribute and transmit the work

Under the following conditions:

- Attribution: You must attribute the work in the manner specified by the author (but not in any way that suggests that they endorse you or your use of the work).
- Non Commercial: You may not use this work for commercial purposes.
- No Derivative Works - You may not alter, transform, or build upon this work.

Any of these conditions can be waived if you receive permission from the author. Your fair dealings and other rights are in no way affected by the above.

Take down policy

If you believe that this document breaches copyright please contact librarypure@kcl.ac.uk providing details, and we will remove access to the work immediately and investigate your claim.

King's College London
University of London, Faculty of Life Sciences and Medicine
Cardiovascular Division, Rayne Institute, BHF Centre of Research Excellence
St Thomas' Hospital, London

Thesis Submitted for the Degree of Doctor of Philosophy 2019

Haemodynamic and physiological principles of paradoxical low gradient aortic stenosis

Hannah Zélie Ruth McConkey
ATCL MBBS MRCP MA (Cantab)

Supervisors:

Professor Bernard Prendergast
Professor Simon Redwood

Financial support from the British Heart Foundation is gratefully acknowledged. This research was supported by a Clinical Research Training Fellowship (FS/16/51/32365).



TABLE OF CONTENTS

AIM AND OVERVIEW	5
Acknowledgements	9
List of Tables	11
List of Figures	13
List of Abbreviations	15
Related Material	17
1 THE HORNETS' NEST OF CORONARY MICROCIRCULATION IN AORTIC STENOSIS...	18
1.1 Abstract.....	19
1.2 Introduction	19
1.3 Cardiac-Coronary Coupling in Health	20
1.4 Myocardial Blood Supply in Health	23
1.4.1 Coronary Wave Intensity Analysis	24
1.5 Cardiac-Coronary Coupling in AS.....	25
1.6 Disrupted Coronary Flow in AS.....	27
1.7 Aortic Valve Flow and Pressure Gradients	36
1.7.1 Low gradient aortic stenosis	38
1.7.2 Structural Remodeling in Low Gradient AS	39
1.8 Physiological Assessment of Coronary Stenoses in the Setting of AS	41
1.9 Clinical Implications of Impaired Coronary Flow.....	42
1.10 Conclusion.....	43
1.11 Objectives and Hypotheses	44
2 METHODS.....	45
2.1 Introduction	46
2.2 Ethical Approval	46
2.3 Recruitment	46
2.3.1 Patient Selection	47
2.3.2 Patient Journey	47
2.4 Cardiac MRI Protocol	48
2.4.1 CMR Acquisition	49
2.5 Catheter Laboratory Protocol.....	51
2.5.1 Pressure Volume Loop Assessment.....	52
2.5.1.1 Properties of the Conductance Catheter.....	53
2.5.1.2 INCA Console and Conduct NT Software	54
2.5.1.3 Conductance Catheter Insertion and Calibration.....	55
2.5.2 Coronary Assessment	55
2.5.2.1 Properties of the ComboWire.....	56
2.5.2.2 The ComboMap System	58
2.5.2.3 ComboWire Insertion.....	58

2.5.3	Coronary Sinus Access	59
2.5.4	Stress Protocol	59
2.5.5	Serum Sampling and Analysis	60
2.5.6	Histological Sampling and Storage	61
2.6	Analysis of Invasive Parameters	62
2.6.1	Left Ventricular Parameters with SimpleWires	62
2.6.2	Coronary Datasets with CardiacWaves	63
2.7	Analysis of Non-Invasive Datasets	63
2.7.1	MRI Volumetric, Strain and Flow Analysis using CVI42	63
2.7.2	Quantitative MRI Perfusion Analysis using MATLAB	64
2.7.3	MRI ECV Analysis	66
2.7.4	Computed Tomography Calcium Scoring	66
2.7.5	Echocardiographic assessment	67
2.8	Grading aortic stenosis	67
2.9	Physiological Indices	69
2.10	Statistical Analysis	71
3	STUDY PATIENTS	72
4	ISCHAEMIA IN AORTIC STENOSIS	76
4.1	Introduction	77
4.1.1	Invasive Physiology	77
4.1.2	Wave intensity analysis	79
4.1.3	Other Invasive Indices of Ischaemia	80
4.1.4	Non-Invasive Indices of Ischaemia	81
4.2	Results	83
4.2.1	Aortic and Coronary Physiology in AS	83
4.2.2	Subendocardial Viability	86
4.2.3	Coronary Flow Reserve	86
4.2.4	Microvascular Resistance	87
4.2.5	Wave Intensity Analysis during hyperaemia, pacing and following TAVI	88
4.2.6	Wave Intensity Analysis in LGAS vs HGAS	94
4.2.7	Coronary Perfusion Efficiency	94
4.2.8	Myocardial Perfusion Reserve Index	95
4.2.9	Endocardium-Epicardium Gradients	95
4.2.10	Serum Biomarkers	96
4.3	Discussion and summary	97
5	CONTRACTILITY, LUSITROPY AND HYPERTROPHY IN AORTIC STENOSIS	99
5.1	Introduction	100
5.1.1	Invasive Assessment of Myocardial Mechanics	100
5.1.2	Non-Invasive Assessment of Myocardial Mechanics	102
5.2	Results	103
5.2.1	Cardiac Magnetic Resonance Imaging Assessment	104
5.2.2	Left Ventricular Mass	104
5.2.3	Tissue Tracking	107
5.2.4	Remodeling Patterns between Cohorts	108
5.2.5	Echocardiography for Left Ventricular Assessment	109
5.2.6	Valvulo-Arterial Impedance	110
5.2.7	Pressure-Volume Loop Assessment of the Left Ventricle	111
5.2.8	Reflection Coefficient and Augmentation Index	116
5.2.9	Tissue and Serum Results	118

5.3	Discussion and summary	118
6	MYOCARDIAL FIBROSIS IN AORTIC STENOSIS	120
6.1	Introduction	121
6.1.1	Pathogenesis of Fibrosis	121
6.1.2	Fibrosis in AS	124
6.1.3	Interstitial and Replacement Fibrosis in Aortic Stenosis	125
6.2	Results	126
6.2.1	LGE results	126
6.2.2	T ₁ Mapping for Interstitial Fibrosis	127
6.2.3	Aortic Valve Calcification and Correlations	128
6.3	Summary	129
7	CARDIAC-CORONARY COUPLING PRE- AND POST-TAVI	131
7.1	Introduction	132
7.1.1	The Cardiomyocyte	132
7.1.2	Cardiac Excitation-Contraction Coupling	133
7.1.3	Preload and Afterload	134
7.1.4	Ventricular-Arterial Coupling	135
7.2	Results	136
7.2.1	Haemodynamic Changes with Intervention	140
7.2.2	VA results	141
7.3	Summary	143
8	SYNTHESIS	144
8.1	Introduction	145
8.2	Ventricular Disparity between LGAS and HGAS	145
8.3	Coronary Disparity between LGAS and HGAS	146
8.4	Structural and Functional Effects of TAVI	147
	Limitations	149
	Future Directions	150
	References	151

AIM AND OVERVIEW

This thesis details work from one single multifaceted study. It examines the divergent clinical and pathophysiological features of high gradient and paradoxical low gradient aortic stenosis and their respective responses to transcatheter aortic valve implantation. The background to the research described evolved from my interest in valvular heart disease, and the clinical enigma of paradoxical low gradient aortic stenosis. Together with my supervisors, Professors Bernard Prendergast and Simon Redwood, and collaborators, Professors Mike Marber and Philippe Pibarot, the concept and methodology was conceived, and a BHF Clinical Research Training Fellowship grant allowed the entirety of this work to take place. I was wholly responsible for the successful HRA, REC and R&D applications, and created all the study documents from scratch. I have single-handedly recruited and consented all patients and collected and analysed all data.

Chapter 1 and 2 describe the background and methodology used for the work completed with baseline characteristics being displayed in **chapter 3**. In **chapter 4**, the associated parameters of ischaemia are researched, and in **chapter 5**, the differences in left ventricular remodelling and dynamic function are outlined. **Chapter 6** investigates the relationship of both replacement and interstitial fibrosis in the cohorts studied, and **chapter 7** explores the relationship between coronary and left ventricular physiology. **Chapter 8** summarises salient findings and suggests future work.

ABSTRACT

Background

Low gradient severe aortic stenosis (LGAS) accounts for up to 35% of severe aortic stenosis cases and is associated with unfavourable outcomes when compared to high gradient aortic stenosis (HGAS). Controversy and conflicting evidence exist regarding this disease entity, yet the contributing pathophysiology is poorly understood. There is a paucity of invasive data to help characterise this phenomenon of distinct remodelling - how do they respond to valve intervention and what makes them “high-risk”?

Methods

Patients with severe symptomatic AS and normal LVEF were dichotomised according to their mean aortic valve pressure gradient of less than or greater to 40mmHg. Patients listed for trans-catheter aortic valve implantation (TAVI) underwent 3T stress perfusion cardiac magnetic resonance imaging (CMR) pre-(within 24 hours) and post-(4-8 months) TAVI. Left ventricular (LV) mechanics and coronary flow and pressure parameters were measured during hyperaemia and rapid pacing, immediately before and after TAVI, using a conductance LV catheter and dual-pressure and Doppler sensor–tipped guidewire in the mid-left anterior descending coronary artery.

Results

24 patients were recruited resulting in 19 suitable datasets (LGAS N=9, HGAS N=10, equally matched for comorbidities and symptoms. LGAS was characterised by smaller indexed LV end diastolic volumes ($p=0.010$) and indexed LV mass ($p=0.037$). Stress global endocardium-epicardium gradient did not change following TAVI (0.94 [0.81,0.98] to 0.95 [0.80,1.0], $p=0.694$) whereas global myocardial perfusion reserve index improved following TAVI (2.1 [1.8,2.3] to 2.4 [2.3,2.8], $p=0.029$). There was a less significant gradient in LGAS patients (0.959 ± 0.089 to 0.846 ± 0.100 , $p=0.018$) but a trend toward reduced MPRI in this group (1.88 ± 0.32 vs 2.30 ± 0.64 , $p=0.091$).

Baseline Characteristics	LGAS (n=9)	HGAS (n=10)	P value
Age (years)	84 \pm 6	85 \pm 5	0.768
Male (%)	33	10	0.303
Mean aortic valve pressure gradient (mmHg)	32 \pm 5	67 \pm 22	<0.001
Diabetes mellitus (%)	67	20	0.070
Hypertension (%)	78	60	0.628
Prior stroke (%)	33	10	0.303
Obstructive airways disease (%)	33	10	0.303
Indexed aortic valve area (cm ² /m ²)	0.490	0.336	0.008
TAVI anaesthesia: conscious sedation	89	90	0.942
Haemoglobin (g/l)	125 (112,130)	124 (113,136)	0.604
eGFR (ml/min)	57 \pm 21	63 \pm 18	0.751
Pre-TAVI BNP (ng/l)	720 (369,983)	1355 (935,6957)	0.058

Post-TAVI BNP (ng/l)	530 (290,915)	500 (144,1457)	0.950
Body Surface Area (m ²)	1.83±0.17	1.71±0.13	0.097
Non-invasive systolic blood pressure (mmHg)	150±19	136±27	0.198
LV end diastolic volume index (ml/m ²)	76 (60,80)	83 (75,87)	0.010
LV mass index (g/m ²)	56.3±8.5	71.1±18.1	0.037
LV ejection fraction (%)	64.5±4.2	60.9±5.9	0.143
CT calcium score (Ag units)	2328 (1474,3655)	2982 (2686,6085)	0.028
Indexed CT calcium score (Ag/m ²)	1152 (825,1924)	1799 (1581,3383)	0.017

Pre-TAVI, baseline coronary data demonstrated lower coronary augmentation pressure ($p=0.035$) and augmentation index (AIx, $p=0.028$) in the LGAS group along with reduced time-averaged peak Doppler flow velocity (APV, $p=0.022$) and coronary velocity time integral (VTI, $p=0.006$). These patients also exhibited a shorter ejection time ($p=0.022$), proportionately larger forward compression wave areas and smaller backward expansion waves (BEW) during rest, hyperaemia and rapid pacing when compared to HGAS patients. They also demonstrated increased inhibitory forward expansion waves ($p=0.021$). Lower baseline end LV systolic pressure ($p=0.004$), inotropy (dP/dt^+ , $p=0.031$), lusitropy (dP/dt^- , $p=0.050$), pressure volume area ($p=0.020$), and stroke work ($p=0.019$) were observed in the LGAS group along with reduced LV volumes during hyperaemia ($p=0.040$) and pacing ($p=0.003$). Pacing at 90bpm induced minimal response in the LGAS ventricles, but a more profound impact in HGAS ventricles on the delta change in end systolic volume ($-12\pm45\%$ vs $+31\pm31\%$, $p=0.048$) and ejection fraction ($-1\pm15\%$ vs $-19\pm12\%$, $p=0.016$).

Post-TAVI, the hyperaemic BEW fell sharply ($p<0.001$) in both groups, along with coronary VTI ($p=0.018$) and APV ($p=0.024$), whilst coronary AP and AIx remained lower in LGAS patients ($p=0.035$ and $p=0.028$, respectively). The LGAS group displayed a less profound drop in dP/dt^+ ($-19\pm15\%$ vs $-37\pm9\%$, $p=0.013$) and dP/dt^- ($-17\pm19\%$ vs $-39\pm15\%$, $p=0.015$) at rest following intervention. Diastolic microvascular resistance was increased in LGAS patients during hyperaemia following TAVI ($p=0.025$). Repeat CMR demonstrated statistically significant reduction in indexed LV volume and mass ($p=0.003$ and $p<0.001$, respectively) with significant increase in 3D global peak radial, circumferential and longitudinal strain ($p=0.006$, $p=0.010$ and $p=0.013$, respectively). There was no difference in remodelling patterns or follow up perfusion assessment between cohorts.

Conclusion

This is the first study detailing the combined invasive and CMR pathophysiological changes associated with LGAS. Despite invasive parameters indicating a disease of less severe AS, blunted microvascular-originating waves, and disproportionate myopathic and ischaemic changes in the LGAS group may underlie the adverse prognosis associated with this poorly understood condition.

Acknowledgements

Firstly, I would like to thank the participants who selflessly and willingly consented to be subjects in this study. Without their generous cooperation, this research would not have materialised. Each and every one enriched my experience of research, as I got to know them and their families.

I have had immense opportunity whilst being a research fellow at St Thomas' and this is entirely down to my supervisors – I have been privileged and thank them for taking me on. They had an open-door policy, and any query was answered immediately no matter where in the world they were. I am grateful for their encouragement, constructive criticism and expert guidance. Not least among their roles was the deliverance of a complex and demanding invasive research protocol. Professor Bernard Prendergast models attentive clinical acumen and careful consideration of patient management, and is a master curator of words both written and spoken. Professor Simon Redwood is a skilled interventionalist, wizard of cardiac physiology, dynamic cardiologist and an inspiration in his understanding and enthusiasm for research. If any of their traits have rubbed off in any small part, then I am fortunate.

I would also like to thank the following people:

- Professor Mike Marber, for his significant input into the design of this study and his godfather approach to cardiovascular research – wise, calm and always able to provide a solution.
- Professor Amedeo Chiribiri, for his clinical and research tutoring in cardiac MRI, our endless hours analyzing perfusion datasets and for treating me like his own student. He was continually excited by this project and impassioned me to invest in MRI.
- Professor Philippe Pibarot, for his enthusiasm, guidance and support for the project.
- Dr Jack Lee, who has a phenomenal grasp of physiology and inspired development in my approach in interpreting results, with the use of SimpleWires.

- Dr James Clark and Dr Richard Heads, for teaching me bench work techniques and helping with histopathology analysis.

Many other nursing, physiologist and administrative colleagues made this research possible – Howie Ellis, Bina Patel, Gemma Beilby, Paula Ghandour, Karen Wilson, and Lucy Hewett to name a few. The catheter laboratory staff, with warmth and kindness, never failed to offer assistance during research study days – this was greatly appreciated.

Thanks to my fellow Tommy's researchers, a fun and energetic bunch whom I am honoured to call my friends – we have shared many happy times together. This support has enhanced the academic experience, whilst mutually benefitting our respective projects.

Lastly, my family - my wonderful husband Richard, brother Kris, and parents. Their love, support, encouragement and wisdom has made this possible.



List of Tables

TABLE 1-1: INVASIVE PHYSIOLOGICAL MEASURES IN AS FROM PREVIOUS STUDIES (PRESENTED IN CHRONOLOGICAL ORDER) .	29
TABLE 1-2: NON-INVASIVE PHYSIOLOGICAL MEASURES IN AS FROM PREVIOUS STUDIES (PRESENTED IN CHRONOLOGICAL ORDER)	31
TABLE 1-3: CLASSIFICATION OF CORONARY MICROVASCULAR DYSFUNCTION ⁶⁵	34
TABLE 2-1: INCLUSION AND EXCLUSION CRITERIA	47
TABLE 2-2: STEP BY STEP GUIDE TO THE INVASIVE PROTOCOL	51
TABLE 2-3: HOW SERUM RESULTS WERE COLLATED	61
TABLE 2-4: TABLE OF INVASIVE INDICES USED IN THIS STUDY	69
TABLE 3-1: BASELINE CHARACTERISTICS OF 19 ANALYSED PATIENT RESULTS	74
TABLE 3-2: BASELINE CHARACTERISTICS: LFLG VS HGAS	75
TABLE 4-1: THE HAEMODYNAMIC IMPACT OF HYPERAEMIA PRE- AND POST-TAVI FROM ALL PAIRED DATASETS	84
TABLE 4-2: THE HAEMODYNAMIC IMPACT OF PACING PRE- AND POST-TAVI FROM ALL PAIRED DATASETS	84
TABLE 4-3: THE HAEMODYNAMIC IMPACT OF TAVI DURING THREE PHYSIOLOGICAL STATES FROM ALL PAIRED DATASETS.....	85
TABLE 4-4: CORONARY AND AORTIC HAEMODYNAMIC INDICES IN LGAS AND HGAS COHORTS. RESULTS DISPLAYED WHEN P<0.010 FOR LGAS THEN HGAS WITH SD OR IQR IN BRACKETS.	85
TABLE 4-5: HYPERAEMIC WAVE INTENSITY ANALYSIS RESULTS PRE- AND POST-TAVI FROM ALL PAIRED DATASETS	90
TABLE 4-6: RAPID PACING WAVE INTENSITY ANALYSIS RESULTS PRE- AND POST-TAVI FROM ALL PAIRED DATASETS	91
TABLE 4-7: THE IMPACT OF TAVI (PRE- VS POST) ON CORONARY WAVE INTENSITY ANALYSIS RESULTS FROM ALL PAIRED DATASETS	92
TABLE 4-8: PRE-TAVI CORONARY WAVE INTENSITY ANALYSIS RESULTS IN LGAS AND HGAS COHORTS. RESULTS DISPLAYED WHEN P<0.010 FOR LGAS THEN HGAS WITH SD OR IQR IN BRACKETS.	93
TABLE 4-9: RESULTS FROM AORTIC AND CORONARY SINUS SERUM SAMPLING	96
TABLE 5-1: CARDIAC REMODELLING PHENOTYPES IN AORTIC STENOSIS	100
TABLE 5-2: PRE-TAVI BASELINE CHARACTERISTICS AND CARDIAC MAGNETIC RESONANCE FINDINGS	104
TABLE 5-3: PAIRED (PRE- AND POST-TAVI) MRI RESULTS IN ALL PATIENTS (18 PAIRS), VALUES ARE PRESENTED AS THE MEAN ± SD OR MEDIAN WITH INTERQUARTILE RANGE AS APPROPRIATE	106
TABLE 5-4: STRAIN MRI RESULTS IN ALL PATIENTS (18 PAIRS), VALUES ARE PRESENTED AS THE MEAN ± SD OR MEDIAN WITH INTERQUARTILE RANGE AS APPROPRIATE	107
TABLE 5-5: LGAS VS HGAS PRE-TAVI CMR STRAIN RESULTS	108
TABLE 5-6: LGAS VS HGAS FOLLOW-UP CARDIAC MAGNETIC RESONANCE SCAN RESULTS.....	109
TABLE 5-7: LGAS VS HGAS CHANGE IN MRI PARAMETERS FOLLOWING INTERVENTION	109
TABLE 5-8: INVASIVE RESULTS FROM INDUCED HYPERAEMIA IN ALL PAIRED DATASETS	113
TABLE 5-9: INVASIVE RESULTS FROM PACING IN ALL PAIRED DATASETS	114
TABLE 5-10: THE IMPACT OF TAVI (PRE- VS POST) ON CARDIAC MECHANICS DURING THREE PHYSIOLOGICAL SETTINGS IN ALL PAIRED DATASETS	115

TABLE 5-11: INVASIVE RESULTS IN LGAS AND HGAS COHORTS FOR RESTING AND HYPERAEMIC STATES. RESULTS DISPLAYED WHEN $P < 0.010$ FOR LGAS THEN HGAS WITH SD OR IQR IN BRACKETS.	117
TABLE 6-1: LGAS AND HGAS RESULTS FOR MYOCARDIAL COMPONENTS	127
TABLE 7-1: INFLUENCES OF VARIABLES ON PARAMETERS OF VENTRICULAR FUNCTION ²⁷²	134
TABLE 7-2: THE EFFECT OF HYPERAEMIA ON FULL PRESSURE-VOLUME LOOP RESULTS IN ALL PAIRED DATASETS	137
TABLE 7-3: THE EFFECT OF PACING ON FULL PRESSURE-VOLUME LOOP RESULTS IN ALL PAIRED DATASETS	138
TABLE 7-4: THE IMPACT OF TAVI (PRE- VS POST) ON FULL PRESSURE VOLUME LOOP RESULTS DURING EACH PHYSIOLOGICAL SETTING IN ALL PAIRED DATASETS	139
TABLE 7-5: FULL PRESSURE-VOLUME LOOP RESULTS IN LGAS AND HGAS COHORTS PRE-TAVI. RESULTS DISPLAYED WHEN $P < 0.010$ FOR LGAS THEN HGAS WITH SD OR IQR IN BRACKETS. NO DIFFERENCES WERE FOUND POST-TAVI BETWEEN COHORTS.	142

List of Figures

FIGURE 1-1: MYOCARDIAL CONTRACTION RESULTS IN MUSCLE SHORTENING AND THICKENING TO CAUSE EXTRAVASCULAR CORONARY COMPRESSION. THE MECHANISM OF MYOCARDIUM-VESSEL INTERACTION IS A COLLECTIVE EFFECT OF CONTRACTION-INDUCED INTRA-MYOCYTE PRESSURE AND LV PRESSURE-DERIVED INTERSTITIAL PRESSURE ¹¹ . ADAPTED FROM WESTERHOF <i>ET AL</i> (2006) ¹²	21
FIGURE 1-2: DIAGRAMMATIC REPRESENTATION OF THE EXTRAVASCULAR FORCES AND INTRALUMINAL PRESSURES AFFECTING MYOCARDIAL LAYERS, DEMONSTRATING GREATER SUBENDOCARDIAL CONTRACTION DURING SYSTOLE. P_{LUMEN} , PRESSURE IN THE LEFT VENTRICULAR LUMEN; $P_{INTRAMURAL}$, INTRAMURAL PRESSURE; $P_{PERICARDIUM}$, PRESSURE IN THE PERICARDIAL SPACE. ADAPTED FROM DUNCKER & BACHE AND BELL & FOX ^{25,26}	22
FIGURE 1-3: THE FOUR DOMINANT CORONARY WAVES DURING THE CARDIAC CYCLE IN RELATION TO HEMODYNAMIC INDICES (NOT TO SCALE). BCW: BACKWARD COMPRESSION WAVE, FCW: FORWARD COMPRESSION WAVE, FEW: FORWARD EXPANSION WAVE, BEW: BACKWARD EXPANSION WAVE.....	24
FIGURE 1-4: IMPAIRMENT OF CFR IN PROGRESSIVE AS: SIMULATED RESTING AND HYPEREMIC MEAN CORONARY BLOOD FLOW AS A FUNCTION OF THE SEVERITY OF AS AND ESTIMATED ORIFICE AREA. INDUCED HYPEREMIA IS FUNDAMENTALLY IMPORTANT DURING CIRCULATORY ASSESSMENT IN AS SINCE ADAPTIVE HYPEREMIA IS ALREADY ESTABLISHED AT BASELINE — SEVERAL WELL-CITED STUDIES ARE FLAWED IN THIS RESPECT. ADAPTED FROM GARCIA <i>ET AL</i> ⁶¹	27
FIGURE 1-5: FACTORS IMPLICATED IN DISRUPTED CORONARY FLOW AND REDUCED CFR IN AS. COMPENSATORY MECHANISMS FAIL DUE TO STRUCTURAL AND MECHANICAL EFFECTS UPON THE VENTRICLE AND CORONARY CIRCULATION. THERE IS REDUCED PHYSIOLOGICAL RESERVE AS A RESULT OF INADEQUATE MYOCARDIAL OXYGEN SUPPLY AND INCREASED OXYGEN DEMAND.	35
FIGURE 1-6: CLASSIFICATION OF AS ACCORDING TO FLOW (LOW-FLOW [LF] <35ML/M ² , NORMAL-FLOW [NF] >35ML/M ²) AND GRADIENT (LOW-GRADIENT [LG] MPG <40MMHG, HIGH-GRADIENT [HG] MPG >40MMHG). LOW-FLOW LOW-GRADIENT CAN BE FURTHER SUBDIVIDED INTO “CLASSICAL” AND “PARADOXICAL” ACCORDING TO THE PRESENCE OR ABSENCE OF IMPAIRED LV FUNCTION.	36
FIGURE 1-7: PATTERNS OF CARDIAC REMODELING BASED ON NORMAL OR INCREASED MASS TO VOLUME RATIO (CONCENTRIC REMODELLING AND CONCENTRIC HYPERTROPHY) AND NORMAL LV WALL THICKNESS (CONCENTRIC REMODELING) OR HYPERTROPHY (CONCENTRIC AND ECCENTRIC). ADAPTED FROM GJESDAL <i>ET AL</i> ⁸⁷	37
FIGURE 2-1: STUDY PATIENT FLOW DIAGRAM.....	48
FIGURE 2-2: THUMBNAIL SEQUENCE OF MRI PROTOCOL FROM OSIRIX	49
FIGURE 2-3: A CONDUCTANCE CATHETER (LEFT), THE CD LEYCOM PANEL (MIDDLE), AND THE INCA CONSOLE (RIGHT)	54
FIGURE 2-4: SCHEMATIC OF THE CONNECTIONS BETWEEN THE CONDUCTANCE CATHETER AND COMBOWire	55
FIGURE 2-5: COMBOWire IN THE LEFT ANTERIOR DESCENDING CORONARY ARTERY	56
FIGURE 2-6: FLUOROSCOPIC IMAGE SHOWING THE ELEMENTS OF THE INVASIVE PROTOCOL	59
FIGURE 2-7: AN EXAMPLE OF A CASE BEING ANALYSED WITHIN SIMPLEWires	62
FIGURE 2-8: LEFT: SIGNAL INTENSITY CURVE GENERATED FROM DUAL BOLUS GADOLINIUM SEQUENCE, RIGHT: MANUAL SEGMENTATION OF LATE GADOLINIUM SCAR IMAGING IN MATLAB	64

FIGURE 2-9: KINGS COLLEGE LONDON CUSTOM DESIGNED PERFUSION ANALYSIS PLATFORM.....	65
FIGURE 3-1: STUDY FLOW CHART OF PATIENT RECRUITMENT	73
FIGURE 4-1: THE AORTIC WAVEFORM AND ASSOCIATED DERIVATIONS.....	78
FIGURE 4-2: DIFFERENCES IN AORTIC WAVEFORM IN NORMAL AND AORTIC STENOSIS.....	79
FIGURE 4-3: A TYPICAL FLOW VELOCITY WAVEFORM AT REST IN A PATIENT WITH SEVERE AS. THERE IS ALMOST ENTIRELY DIMINISHED FLOW DURING SYSTOLE.	80
FIGURE 4-4: CONSIDERATIONS RELATING TO MICROVASCULAR RESISTANCE AND TONE	81
FIGURE 4-5: CFR RESULTS	87
FIGURE 4-6: PAN-CARDIAC MICROVASCULAR RESISTANCE PRE- AND POST-TAVI	88
FIGURE 4-7: CORONARY PERFUSION EFFICIENCY	94
FIGURE 4-8: PRE-TAVI MPR AND ENDOCARDIUM-EPICARDIUM GRADIENT RESULTS FOR LGAS AND HGAS PATIENTS.....	95
FIGURE 5-1: THE END-DIASTOLIC AND END-SYSTOLIC PRESSURE VOLUME RELATIONSHIP IN A PATIENT WITH AS.....	101
FIGURE 5-2: LVMI IN LGAS VS HGAS.....	105
FIGURE 5-3: CORRELATION BETWEEN MPG AND LVMI.....	106
FIGURE 5-4: MAXIMUM AND MINIMUM DP/DT IN LGAS AND HGAS PATIENTS	111
FIGURE 6-1: SCHEMATIC DIAGRAM OF THE PATHOGENESIS OF FIBROSIS.....	122
FIGURE 6-2: MOLECULAR SIGNALING INVOLVED BETWEEN CARDIAC FIBROBLASTS AND CARDIOMYOCYTES	124
FIGURE 6-3: LATE GADOLINIUM DEMONSTRATING REPLACEMENT FIBROSIS. TOP PANEL: THREE PATIENTS WITH LGAS FEATURING SUBENDOCARDIAL FIBROSIS; BOTTOM PANEL: MIDWALL FIBROSIS IN TWO PATIENTS WITH HGAS (THERE WAS NO CROSSOVER IN THIS PATTERN OF LGE)	127
FIGURE 7-1: FIGURE DEMONSTRATING THE CARDIAC EXCITATION-CONTRACTION ON A CELLULAR LEVEL	133
FIGURE 7-2: HAEMODYNAMIC INDICES USED IN PRESSURE-VOLUME LOOP DATASETS	135

List of Abbreviations

A

ABG: arterial blood gas
 AHA: American Heart Association
 Alx: augmentation index
 AL: immunoglobulin-derived light chains
 AS: aortic stenosis
 AP: augmentation pressure
 APV: time-averaged peak Doppler flow velocity
 APV_h: APV during hyperaemia
 APV_r: APV during resting conditions
 AUC: area under the curve
 AVA: aortic valve area
 AVC: aortic valve calcification
 AVG: aortic valve gradient

B

BEW: backward expansion wave
 BCW: backward compression wave
 BI: Buckberg index
 bMR: baseline microvascular resistance
 BNP: b-type natriuretic peptide
 bPPD: baseline coronary pulse pressure in diastole
 Br: baseline resistance
 BSA: body surface area
 bSSFP: balanced steady state free precession sequence

C

CBF: coronary blood flow
 CBFV: coronary blood flow velocity
 CBFVI: coronary blood flow velocity indexed for LV mass
 CFLM: cardiac function laboratory modular
 CFR: coronary flow reserve
 CI: cardiac index
 CMR: cardiac magnetic resonance
 CO: cardiac output
 CS: coronary sinus
 CTGF: connective tissue growth factor

D

DICOM: digital imaging and communications in medicine
 DICOMDIR: DICOM directory
 dP: change in pressure
 dP/dt_{max}: isovolumetric contraction
 dP/dt_{min}: isovolumetric relaxation
 DPT: diastolic perfusion time
 DT: diastolic time

DTF: diastolic time fraction
 DTI: diastolic time index
 dU: change in flow velocity

E

E_a: effective arterial elastance
 ECHO: echocardiography
 ECV: extracellular volume fraction
 ECM: extracellular matrix
 EDP: end diastolic pressure
 EDPVR: end diastolic pressure volume relationship
 EDV: end diastolic volume
 Ees: end systolic elastance
 ESP: end systolic pressure
 ESPVR: end systolic pressure volume relationship
 ESV: end systolic volume
 ET: ejection time

F

FCW: forward compression wave
 FEW: forward expansion wave
 FFR: fractional flow reserve

G

GLS: global longitudinal strain

H

hAPV: hyperaemic average peak Doppler flow velocity
 hDPT: hyperaemic diastolic perfusion time
 HFpEF: heart failure with preserved ejection fraction
 HGAS: high-gradient aortic stenosis
 hMR: hyperaemic microvascular resistance
 hPPd: hyperaemic pulse pressure in diastole
 HR: heart rate
 hTransmural MBF: hyperaemic transmural myocardial blood flow

I

ICAM: intercellular adhesion molecule 1
 iFR: instantaneous wave-free ratio
 IMR: index of microvascular resistance
 IPV: instantaneous peak velocity
 IRAS: integrated research application system
 IVSd: interventricular septum in diastole

L

LAD: left anterior descending artery
LFLG: low-flow low-gradient
LFHG: low-flow high-gradient
LGAS: low-gradient aortic stenosis
LGE: late-gadolinium enhancement
LV: left ventricle
LVEF: left ventricular ejection fraction
LVH: left ventricular hypertrophy
LVIDd: left ventricular internal diameter in diastole
LVMI: indexed left ventricular mass
LVMM: left ventricular muscle mass
LVOT: left ventricular outflow tract

M

M/V: mass to volume ratio
MATLAB: matrix laboratory
MBF: myocardial blood flow
MDT: multidisciplinary team
MOLL: modified Look-Locker inversion recovery
MMP: matrix metalloproteinases
MPG: mean pressure gradient
MRI: magnetic resonance imaging
MPR: myocardial perfusion reserve
MPRI: indexed myocardial perfusion reserve
MTA: material transfer agreement
MR: microvascular resistance
MR_{dias}: wave-free microvascular resistance
MyC: cardiac myosin-binding protein C

N

NFHG: normal-flow high-gradient
NFLG: Normal-flow low-gradient

O

OCT: optimal cutting temperature

P

PCr/ATP: phosphocreatine/adenosine triphosphate
Pa: mean aortic pressure
Pd: mean distal coronary pressure
PE: potential energy
PET: positron emission tomography
pLFLG: paradoxical low-flow low-gradient
PRSW: preload recruitable stroke work
PVA: pressure-volume area
PVL: pressure-volume loop
PW: pulse wave spectral Doppler
PWd: posterior wall in diastole

R

Γ : reflection coefficient
RPP: rate-pressure product
RWT: relative wall thickness

S

SAP: systolic arterial pressure
SAVR: surgical aortic valve replacement
sBP_{AO}: aortic systolic blood pressure
Sci: Frank-Starling contractile state index
SI* β : peak signal intensity x rate of signal rise
SMA: α -smooth muscle actin
SR: systolic resistance
STS: society of thoracic surgeons
SV: stroke volume
SVi: indexed stroke volume
SW: stroke work

T

T₁: longitudinal recovery time
T1_{BloodPC}: post-contrast blood pool recovery time
T1_{BloodNative}: native blood pool recovery time
T1_{MyoPC}: post-contrast myocardial recovery time
T1_{MyoNative}: native myocardial recovery time
T1TFE: kt-turbo-gradient echo sequence
Tau (τ): relaxation time constant
TAVI: transcatheter aortic valve implantation
TE: echo time
TEE: transoesophageal echocardiography
TFE: turbo field echo
TIMP: tissue inhibitors of metalloproteinases
Tmn_{hyp}: transit mean times during hyperaemia
Tmn_{rest}: transit mean times at rest
TR: repetition time
TTI: tension time index
TTR: transthyretin

V

Va: ventricular-arterial coupling
VCAM: vascular cell adhesion molecule
VENC: velocity encoding
V_{max}: peak velocity
VTI: velocity time integral

W

WI⁺: proximal originating waves
WI⁻: distal originating waves
WIA: wave intensity analysis
WI^{net}: net wave intensity

Z

Zva: valvulo-arterial impedance

Related Material

PUBLICATION

McConkey HZR, Marber M, Chiribiri A, Pibarot P, Redwood SR, Prendergast BD. Coronary Microcirculation in Aortic Stenosis: a physiological hornet's nest. Circ Cardiovasc Interv. 2019 Aug;12(8):e007547.

ABSTRACT

HZR. McConkey, M. Marber, J. Lee, H. Ellis, J. Joseph, C. Allen, H. Rahman, T. Patterson, C. Scannell, P. Pibarot, A. Chiribiri, S. Redwood, BD. Prendergast. Invasive and non-invasive characterisation of low gradient aortic stenosis. ESC 2019. European Heart Journal 40 Supplement 1, P6484

AWARDS

Finalist, Young Investigator Award 2019/20, British Cardiovascular Intervention Society

British Heart Foundation Clinical Research Training Fellowship 2016-2019 (£297,432)

British Heart Foundation Travel Award, 2019

1 THE HORNETS' NEST OF CORONARY MICROCIRCULATION IN AORTIC STENOSIS

1.1 Abstract

Aortic stenosis (AS) is a heterogeneous disorder. Variations in the pathological and physiological responses to pressure overload are incompletely understood and generate a range of flow and pressure gradient patterns which ultimately cause varying microvascular effects. The impact of cardiac-coronary coupling depends upon these pressure and flow effects. In this article, we explore important concepts concerning cardiac physiology and the coronary microcirculation in AS, and their impact on myocardial remodelling, aortic valve flow patterns and clinical progression.

1.2 Introduction

*“There is a form of cardiac lesion, not infrequent in occurrence,
which has a clinical picture so characteristic
that it deserves more frequent recognition than it commonly receives.”*

Henry A Christian, 18th July 1931¹

Severe symptomatic AS has a bleak prognosis^{2,3} and no medical treatment exists. As the population ages, the clinical importance and burden of AS are increasing, yet its diagnosis and management are multifaceted, especially in the era of percutaneous interventions. AS is characterised by progressive valve narrowing which clinically manifests as dyspnoea, syncope and angina despite normal coronary arteries, and patients have a truncated lifespan of around two years without intervention. However, symptomatology is subjective and confounded by co-morbidities (particularly in the aging population), and assessment of transvalvular pressures is heavily flow-dependent. The clinician is therefore faced with the challenge of evaluating discordant parameters and balancing the potential risks and benefits of valve intervention.

In 1616, William Harvey was the first to propose that blood circulates because of pulsatile cardiac force⁴. Interactions between the cardiac cycle and coronary circulatory flow were described in 1696 by Scaramucci who suggested that the coronary vasculature is filled in

THE HORNETS' NEST OF CORONARY MICROCIRCULATION IN AORTIC STENOSIS

diastole and squeezed empty during systole⁵. Cardiac-coronary coupling is pertinent in AS, since alterations to the coronary microcirculation are synonymous with the pathophysiology of progressive disease. Disruption to the coronary circulation by ventricular hypertrophy, high left ventricular pressure, low coronary perfusion pressure and extravascular forces (amongst many other factors) reduce physiological reserve. The ominous symptom of angina correlates with impaired myocardial perfusion reserve (MPR) and is strongly associated with increased ventricular mass index⁶. The fact that clinical symptoms occur at the end of the ischemic cascade (whereas perfusion abnormalities can be detected earlier) places great expectation on the physiological evaluation of AS⁷.

Patients with AS and an aortic valve area (AVA) less than 1cm² exhibit distinct pathophysiological responses to pressure overload. The ventricle remodels in response to pressure overload in different ways, generating a range of flow and pressure gradient patterns which ultimately cause varying microvascular effects. Detailed understanding of the pressure-flow relationship in this setting is important in fully understanding a patient's symptoms, and the complex relationship between disrupted coronary flow, left ventricular mechanics and surrogate markers of ischemia.

1.3 Cardiac-Coronary Coupling in Health

Normal resting coronary blood flow comprises around 4% of total cardiac output⁸ and both oxygen extraction and the myocardial metabolic rate are high when compared to skeletal muscle. During the cardiac cycle, cardiac contraction cyclically increases intramural tissue and microvascular pressures to impede systolic flow. This contraction induces greater subendocardial resistance and blood displacement in comparison with the subepicardium^{9,10}. Once the aortic valve closes and left ventricular (LV) relaxation ensues, the coronary vessels embedded in the myocardium recoil and blood flow accelerates.

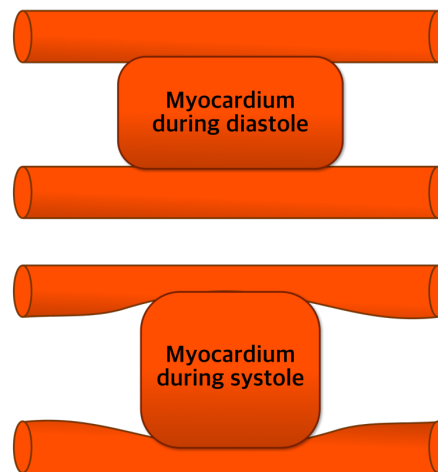


Figure 1-1: Myocardial contraction results in muscle shortening and thickening to cause extravascular coronary compression. The mechanism of myocardium-vessel interaction is a collective effect of contraction-induced intra-myocyte pressure and LV pressure-derived interstitial pressure¹¹. Adapted from Westerhof *et al* (2006)¹².

Coronary flow is dictated by this effect of cardiac contraction – the intramyocardial pump – which pushes blood backwards and draws it in during systole and diastole, respectively¹³ (Figure 1-1), but is also modulated by aortic and LV pressure, and inotropic state. The waterfall model¹⁴ proposes that external hydrostatic vascular pressure causes temporary partial collapse of the lumen. Distal luminal pressure therefore becomes similar to external (or intramyocardial) tissue pressure. This external pressure is presumed to result from intra-ventricular cavity pressure, creating a force against the myocardial walls that reduces from subendocardium to subepicardium. The intramyocardial pump model¹⁵ expands on this further to allow phase-lag between arterial and venous flows, and the role of vascular compliance.

Subendocardial vulnerability to ischemia in normal hearts therefore reflects changes in two main factors¹⁶:

1. Increased tension due to systolic compression and increased subendocardial wall stress, accompanied by increased myocardial oxygen requirements¹⁷. Both invasive and non-invasive studies have demonstrated increasing intramyocardial pressure from the epicardial to the endocardial surface of the ventricular wall¹⁸⁻

THE HORNETS' NEST OF CORONARY MICROCIRCULATION IN AORTIC STENOSIS

2. Decreased subendocardial perfusion, secondary to:

- a. Systolic backflow from endocardial to epicardial vessels causing preferential epicardial blood flow²¹
- b. Thinned subendocardial vessel walls relative to their respective subepicardial counterparts^{22,23} making them more prone to external pressure and stress
- c. Greater subendocardial vascular volume density²⁴ – although, with fewer (but larger) perfusion territories, the subendocardium is perfused by a small subset of penetrating arteries (Figure 1-2)

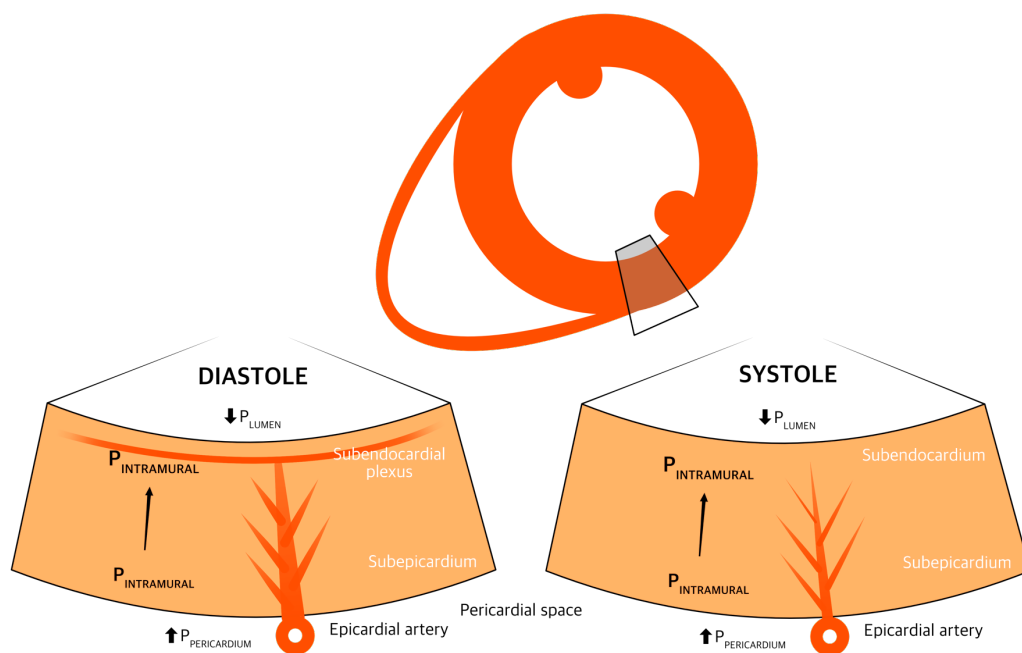


Figure 1-2: Diagrammatic representation of the extrinsic forces and intraluminal pressures affecting myocardial layers, demonstrating greater subendocardial contraction during systole. P_{LUMEN} , pressure in the left ventricular lumen; $P_{INTRAMURAL}$, intramural pressure; $P_{PERICARDIUM}$, pressure in the pericardial space. Adapted from Duncker & Bache and Bell & Fox^{25,26}.

According to Laplace's law, circumferential wall tension is equal to the product of the vessel pressure and radius, divided by wall thickness ($T=P.r/Th$) meaning that the diameter-to-thickness ratio of the vessel or chamber plays an important role. Wall tension and extravascular compressive forces are therefore greatest in the innermost layers of the LV wall. Supporting intramyocardial pressure as a strong determinant of subendocardial blood flow, an early study on anaesthetised dogs demonstrated a flow

gradient favouring the subendocardium during hyperaemia in cardiac arrest (thereby minimising intramyocardial pressures). However, when tissue pressures were maximised by rapid pacing and coronary perfusion maintained through autoperfusion, the gradient of flow favoured the subepicardium²⁷. At low preload, intramyocardial pressure shuts off systolic coronary blood flow across the entire LV wall²⁸. Conversely, there is preferential subepicardial blood flow at high preload²⁹. Coronary blood flow is therefore a balance between intravascular arterial and extravascular tissue pressure³⁰.

1.4 Myocardial Blood Supply in Health

The coronary vascular bed acts as the primary gatekeeper to myocardial blood supply. Resting myocardial blood flow (MBF) is greatest in the subendocardium (endocardial/epicardial flow ratio 1.29-1.35^{13,31}) but subepicardial MBF is augmented during adenosine-induced hyperaemia to a greater extent. During systole, there is significant subendocardial underperfusion due to the aforementioned physical determinants (transmural perfusion endocardial to epicardial ratio 0.38¹³). After a period of ischemia, reactive hyperaemia is earliest in the subepicardium⁹ and this delayed subendocardial response is thought to be due to sluggish reopening of the coronary vasculature embedded in ischemic, poorly compliant myocardium.

Among many other mechanisms, the gradient in coronary perfusion pressure (difference between aortic and LV end diastolic pressure [EDP]) facilitates coronary perfusion, and flow is determined by the product of the net velocity-time integral (VTI) and cross-sectional arterial area ($Q=VA$). The largest cross-sectional area exists in the microvasculature where reduced velocity allows adequate time for capillary bed gas transfer. In normal hearts, aortic and LV pressures are coupled during systolic ejection and higher perfusion pressure gradients enable coronary perfusion during diastole. There is a non-linear connection between cross-sectional area and transmural pressure since vascular tone is influenced by metabolic/neurohormonal mediators and physical forces. According to Ohm's law, flow through a vascular bed is equal to the perfusion pressure gradient divided by vessel resistance, $8\eta/\pi^4$ (Hagen-Poiseuille's equation, where η is

THE HORNETS' NEST OF CORONARY MICROCIRCULATION IN AORTIC STENOSIS

blood viscosity, l is vessel length, and r is vessel radius). Microvascular resistance (MR) is therefore primarily determined by lumen diameter and vasodilatation is the principle means of microcirculatory autoregulation.

During maximal coronary vasodilatation, coronary flow depends on the relative duration of diastole³². This diastolic time fraction (DTF, the length of diastole/length of cardiac cycle) has an inverse relationship with heart rate and is also determined by other modulators of systolic duration (such as altered myocyte contraction). Decreased coronary perfusion pressure induces an increase in DTF, which in turn reduces the duration of intra-myocardial vessel compression.

1.4.1 Coronary Wave Intensity Analysis

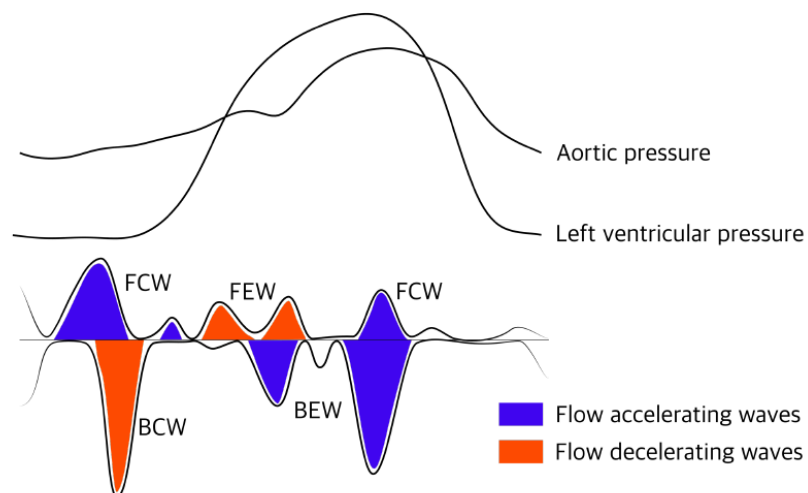


Figure 1-3: The four dominant coronary waves during the cardiac cycle in relation to hemodynamic indices (not to scale). BCW: backward compression wave, FCW: forward compression wave, FEW: forward expansion wave, BEW: backward expansion wave.

Studies of wave intensity analysis (WIA) have identified four main coronary waves within the cardiac cycle in health and disease³³ (Figure 1-3). Quantification of net wave intensity through the product of changes in pressure and flow velocity makes it possible to segregate components of coronary flow into forward or backward travelling waves from

THE HORNETS' NEST OF CORONARY MICROCIRCULATION IN AORTIC STENOSIS

the aorta or microcirculation, and those caused by suction (expansion) or compression – blood can be pushed into or pulled out of the coronary circulation.

Flow from the coronary circulation to the myocardium is largely determined by the prominent backward expansion wave (BEW), originating at the onset of LV relaxation. The decelerating backward compression wave (BCW) and forward expansion wave (FEW) impede coronary flow, while the BEW and forward compression wave (FCW) are accelerating waves. Information concerning the size, direction and duration of coronary waves throughout the cardiac cycle has helped us understand coronary flow in normal hearts, in AS¹⁹ and transcatheter aortic valve implantation (TAVI)^{34,35}, hypertrophic cardiomyopathy³⁶ and several other settings^{33,37-42}.

1.5 Cardiac-Coronary Coupling in AS

The pathophysiology of calcific degenerative AS has two distinct phases: initiation and propagation⁴³. The former overlaps with the development of atherosclerosis, centred around endothelial disruption and activation of inflammatory responses. Progressive AS induces left ventricular hypertrophy (LVH) to increase contractile force and reduce wall stress⁴⁴, in response to progressive and eventually insurmountable afterload. Compressive forces resulting from rising intracavitary pressure determine coronary perfusion pressure and limit coronary circulatory response to increased myocardial demand – an association related to the extent of LVH⁴⁵. Oxygen requirements increase whilst perfusion through the small perforating coronary network is compromised by fixed elevated systolic wall stress^{46,47} and reduced relative capillary density⁴⁸, creating supply-demand mismatch. These structural changes of vascular rarefaction, compressive forces and perivascular fibrosis, and functional changes, such as reduced diastolic perfusion time (DPT, defined as [RR interval]-[S₁-S₂ interval] x heart rate) and endothelial and smooth muscle dysfunction, all exert adverse effects.

Preferential coronary flow shifts from the endocardium to epicardium resulting in a significant decrease in subendocardial (but not subepicardial) MBF⁴⁹. This reversal of

THE HORNETS' NEST OF CORONARY MICROCIRCULATION IN AORTIC STENOSIS

normal endocardial-epicardial blood flow ratio⁵⁰ at rest is fundamental to the pathophysiology of AS, resulting in subendocardial ischemia⁵¹, apoptosis⁴⁷ and fibrosis – clinically manifest as angina despite normal epicardial coronary arteries. Non-invasive detection of this shift in resting endocardial-epicardial ratio could be utilised to guide timing of valve intervention.

Severe AS exhibits an array of flow parameters but there is significant LV outflow tract obstruction in all forms, typically accompanied by LVH⁵² which may cause dynamic obstruction in late systole with systolic anterior motion of the mitral valve. Unlike hypertrophic cardiomyopathy, where there is a strong linear relationship between peak-to-peak gradient and peak instantaneous gradients, significant scatter exists in AS patients⁵³.

One study demonstrated that severity of AS and parameters of LV workload (but not LVH or diastolic indices) have important roles in determining coronary flow reserve (CFR)⁵⁴. Another study, however, correlated impaired perfusion reserve with valve stenosis, myocardial fibrosis and strongly with LVH⁴⁵. Cardiac amyloid is common in this population and may confound results.

There are strong similarities in the pathogenic manifestations of AS and hypertension, i.e. interstitial and perivascular fibrosis, cardiomyocyte hypertrophy, reduced DPT, increased diastolic filling pressure (compressing the endocardium) and diastolic dysfunction, capillary rarefaction⁵⁰ and arteriolar remodelling⁵⁵. However, key differences exist. The BEW is the most important contributor to coronary blood flow and a measure of microcirculatory function – it is increased at rest in AS^{34,35} but reduced in isolated LVH³³, probably as a result of lower wall stress and slower isovolumetric LV relaxation (dp/dt_{min}). Furthermore, there is a direct relationship between systolic coronary velocity and systolic perfusion pressure in hypertensive patients with no AS – extravascular compressive forces which normally impede systolic coronary flow may be overcome in the setting of higher perfusion pressure⁵⁶.

THE HORNETS' NEST OF CORONARY MICROCIRCULATION IN AORTIC STENOSIS

Following TAVI or surgical aortic valve replacement (SAVR), there is restoration of myocardial perfusion, oxygenation, energetics and contractility, accompanied by improved microcirculatory function as a result of the relief of mechanical obstruction and wall stress, and eventual LVH regression^{57,58}. Indexed stroke volume drops sharply (41 ± 8 to $33 \pm 10 \text{ ml/m}^2$, $p < 0.001$) as a result of increased systemic vascular resistance ($p < 0.001$), despite no clear difference in global afterload measured by valvulo-arterial impedance (Z_{va})⁵⁹. Hyperaemic microvascular resistance (hMR) decreases after TAVI, independent of resting haemodynamics⁶⁰. Remaining hypertrophy continues to influence coronary physiology with improved (but not normalised) CFR.

1.6 Disrupted Coronary Flow in AS

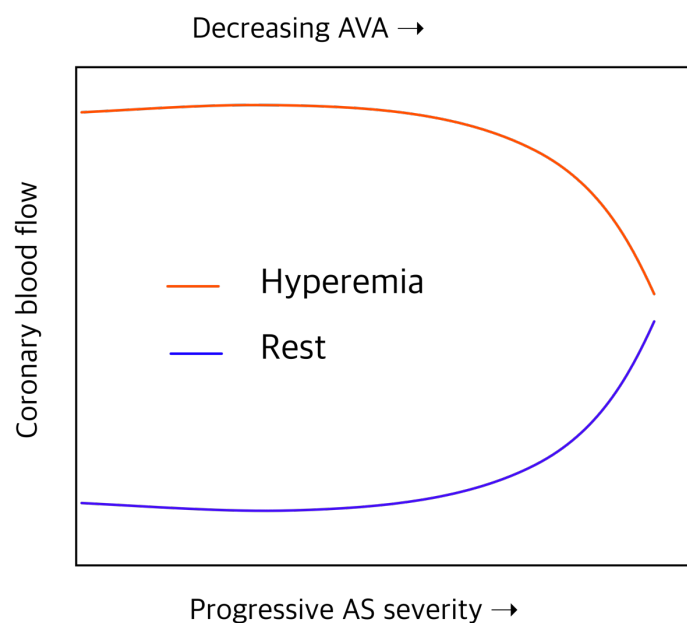


Figure 1-4: Impairment of CFR in progressive AS: simulated resting and hyperemic mean coronary blood flow as a function of the severity of AS and estimated orifice area. Induced hyperemia is fundamentally important during circulatory assessment in AS since adaptive hyperemia is already established at baseline – several well-cited studies are flawed in this respect. Adapted from Garcia *et al*⁶¹.

Microcirculatory autoregulation induces vasodilation to minimise MR and increase total resting MBF, resulting in reduced CFR^{35,62,63} and MPR⁶⁴ due to paired inability to further vasodilate (**Error! Reference source not found.**). Low coronary perfusion pressure⁶⁵,

THE HORNETS' NEST OF CORONARY MICROCIRCULATION IN AORTIC STENOSIS

extravascular compressive forces⁶⁶ and reduced DPT^{46,55,60} all appear to play a role. Reduced DPT due to prolonged systole in AS supports the maldistribution theory⁶⁷.

In contrast to normal physiology, the relative contribution of accelerating waves to total wave intensity decreases with exercise and hyperaemia in AS¹⁹. The contrary is true for decelerating waves: the BCW increases with exercise and hyperaemia, thereby hampering flow and driving ischemia. Davies *et al* analyzed wave intensity in the left main stem at programmed heart rates before and after TAVI (albeit without inducing hyperaemia) and demonstrated progressive reduction (rather than the expected increase) in the BEW with increasing heart rate³⁴. This paradoxically blunted microvascular response normalised following TAVI where induced tachycardia caused the BEW to increase rather than decrease, probably due to a sharp reduction in afterload. A chronological summary of relevant invasive and non-invasive coronary physiology and AS studies are displayed in Table 1-1 and Table 1-2, respectively.

Before valve intervention, forward flow is delayed, and peak systolic flow and VTI reduced⁶⁸. In comparison to normal hearts, the aortic-ventricular diastolic relationship impairs coronary perfusion^{34,69}. Following TAVI however, all coronary waves augment (apart from the BCW³⁵), inducing an immediate increase in coronary flow⁷⁰. In particular, the FCW improves and its onset is shortened³⁵. Increased aortic diastolic pressure (with consequent forward pressure at the coronary ostia) accompanied by decreased LVEDP and increased DPT causes an elevated driving pressure across the coronary bed. In part, improved forward flow may be due to the resolution of abnormal helical and eccentric vertical flow patterns seen in AS⁷¹ which reduce high fluid pressure and the associated Venturi effect in the proximal aorta and coronary ostia.

THE HORNETS' NEST OF CORONARY MICROCIRCULATION IN AORTIC STENOSIS

Table 1-1: Invasive physiological measures in AS from previous studies (presented in chronological order)

COHORTS	N	CORONARY INDICES		SYSTEMIC/ VALVE INDICES	MYOCARDIAL INDICES	ISCHEMIC/OTHER INDICES		
Fallen EL <i>et al</i> 1967 ⁷² Left heart and coronary sinus catheterisation with baseline and hyperaemic measurements using Isoproterenol in patients with severe AS								
		Hyperaemic CBF			Hyperaemic myocardial oxygen extraction	Hyperaemic lactate production		
No angina	7	↑			↓	○		
Angina without CAD	5	○			○	↑		
Angina with CAD	6	↑			↓	↑		
Marcus ML et al 1982 ⁶³ Coronary reactive hyperaemia response following 20 second LAD occlusion in symptomatic severe AS patients during SAVR								
		Coronary reserve	Repayment-debt area ratio					
Controls	8	○	○					
Severe AS	14	↓	↓					
Julius BK <i>et al</i> 1997 ⁷³ Invasive rest and dipyridamole stress data in patients without coronary disease								
		CFR	Resting and minimal CR per 100g LVMM	LV peak systolic pressure	LV wall stress	Resting CSBF	Peak CSBF	ST depression on stress ECG
Controls	7	○	○	○	○	○	○	
Severe AS – angina	11	↓	○	↑	○	↑	○	
Severe AS + angina	18	↓↓	○	↑↑	↑	↑	↓	↑
Davies <i>et al</i> 2006 ³³ Invasive coronary physiology at the time of angiography in patients without coronary disease or aortic stenosis								
		Mean CFV	BEW	FCW:BEW ratio				
Controls	10	○	○	○				
LVH	10	○	↓	↓				
Davies <i>et al</i> 2011 ³⁴ Invasive coronary physiology at baseline and during rapid pacing before and after TAVI in patients with severe symptomatic AS								

THE HORNETS' NEST OF CORONARY MICROCIRCULATION IN AORTIC STENOSIS

		BEW	Flow velocity				Pressure time integral		
Pre-TAVI rest	11	o		o			o		
Pre-TAVI 120bpm	11	↓		o			↓		
Post-TAVI rest	11	↓		o			o		
Post-TAVI 120bpm	11	o		o			↓		
Wiegerinck <i>et al</i> 2015⁶⁰									
Invasive coronary physiology immediately pre- and post-TAVI									
		bCFV	hCFV	CFR	bMR	hMR	hAPV		
Controls	28	o	o	o	o	o	o		
Pre-TAVI	27	↑	↓	↓	↓	o	↓		
Post-TAVI	27	↑	o	o	↓	↓	o		
Rolandi <i>et al</i> 2016³⁵									
Invasive coronary physiology immediately pre- and post-TAVI									
		CFR	bBEW	hBEW	Coronary bPPd and hPPd	Systolic VTI rest and hyperaemia			
Controls	12	o	o	o	o	o			
Pre-TAVI	15	↓	↑	↓	o	↑			
Post-TAVI	15	↓	↑↑	o	↑	↑↑			
Lumley <i>et al</i> 2016¹⁹									
Rest and exercise coronary physiology with stress echocardiography in a subset (n=13) of severe AS patients									
		Hyperaemic CBF	Fall in MR with hyperaemia	Exercise CFR	Hyperaemic CFR		Resting myocardial workload	Exercise myocardial workload	
Controls	38	o	↓	o	o		o	o	
Severe AS	22	↓	↓↓	o	↓		↑	↑	
Gutiérrez-Barrios <i>et al</i> 2017⁷⁴									
Rest and hyperaemic invasive coronary physiology									
		CFR	Tmn _{rest}	Tmn _{hyp}	IMR	Br		Correlation of LVMI with CFR	
Controls	10	o	o	o	o	o			
Severe AS	36	↓	Faster	Slower	↑	↓		-0.32, p<0.050	

THE HORNETS' NEST OF CORONARY MICROCIRCULATION IN AORTIC STENOSIS

Abbreviations: ↑ indicates a higher measure, ↓ a lower measure where “o” is the baseline comparison. AS: aortic stenosis, bBEW: baseline BEW, bCFV: baseline CFV, BEW: backward expansion wave, bMR: baseline microvascular resistance, bPPD: baseline coronary pulse pressure in diastole, Br: baseline resistance, CAD: coronary artery disease, CBF: coronary blood flow, CFV: coronary flow velocity, CFR: coronary flow reserve, CR: coronary resistance, CSBF: coronary sinus blood flow, FCW: forward compression wave, hAPV: hyperaemic average peak flow velocity, hBEW: hyperaemic BEW, hCFV: hyperaemic CFV, hMR: hyperaemic microvascular resistance, hPPd: hyperaemic pulse pressure in diastole, IMR: index of microvascular resistance, LAD: left anterior descending artery, LVH: left ventricular hypertrophy, LVMI: indexed left ventricular mass, MR: microvascular resistance, SAVR: surgical aortic valve replacement, TAVI: transcatheter aortic valve implantation, Tmn_{hyp}: transit mean times during hyperaemia, Tmn_{rest}: transit mean times at rest, VTI: velocity time integral

Table 1-2: Non-invasive physiological measures in AS from previous studies (presented in chronological order)

COHORTS	N	CORONARY INDICES				SYSTEMIC/VALVE HEMODYNAMIC INDICES		MYOCARDIAL INDICES		ISCHEMIC/OTHER INDICES
Omran H <i>et al</i> 1996 ⁷⁵ TEE Doppler of the LAD in patients with at least moderate AS and normal coronary arteries										
		Peak systolic velocity	Peak diastolic velocity	Systolic VTI	Diastolic acceleration time	AVA	Pressure gradient	LVMI	LV wall stress	
Controls	15	o	o	o	o			o		
All AS	58	↓	↓	↓	↑			↑		
Symptomatic vs asymptomatic AS	34 vs 12	Lower	Higher	Smaller	Longer	Smaller	Higher	Higher	Higher	
Hildick-Smith <i>et al</i> 2000 ⁷⁶ Echocardiographic rest and hyperaemic LAD Doppler data in patients with severe AS pre- and 6-months post-SAVR										
		CFR	Hyperaemic peak systolic velocity	Hyperaemic peak diastolic velocity				LVMI		
Pre-SAVR	24	↓	↓	↓				↑		
Post-SAVR	24	o	o	o				o		
Rajappan <i>et al</i> 2002 ⁴⁶ CMR, ECHO and PET data from 20 patients with moderate-severe AS (asymptomatic and symptomatic)										
		CFR				AVA	hDPT	hTransmural MBF		
Controls	20	o						o		
Mod-severe AS	20	↓				Increase linearly	Significant correlation	↓		

THE HORNETS' NEST OF CORONARY MICROCIRCULATION IN AORTIC STENOSIS

					related to hMBF	with hMBF and CFR		
Galiuto <i>et al</i> 2006⁴⁷								
Contrast and Doppler echocardiographic data from patients with severe symptomatic AS awaiting SAVR, LV biopsy during SAVR								
		Baseline CFV	CFVI	CFR		LVMi	SI*β	Apoptosis
Controls	5	○	○	○		○	○	○
Severe AS + LVH	11	↑	↓	↓		↑	↓	↑
Steadman <i>et al</i> 2012⁶⁴								
Cardiopulmonary exercise testing, CMR and echocardiography in patients with severe AS awaiting SAVR								
					Peak AV Velocity	MPR	LVMi	Septal E/e'
Association with MPR	46				β=-0.34, p=0.020		β=0.51, p<0.001	β=-0.33, p=0.030
Association with peak VO ₂	46					β=0.45, p=0.004		β=-0.34, p=0.020
Mahmod M <i>et al</i> 2014⁴⁵								
CMR in 28 patients with severe AS (3 asymptomatic, 25 symptomatic) – 14 of the 25 symptomatic patients were rescanned 8 months after SAVR								
						MPRI	Circumferential strain	BOLD SI change
Controls	15					○	○	○
Severe AS	28					↓	↓	↓
Post-SAVR	14					○	○	○
Ben-Dor I <i>et al</i> 2014⁷⁰								
Doppler LAD flow using TEE during TAVI								
		Peak systolic coronary velocity	Peak diastolic coronary velocity	Systolic VTI	Diastolic VTI			
Pre-TAVI	90	○	○	○	○			
Post-TAVI	90	↑	↑	↑	↑			
Ahn JH <i>et al</i> 2016⁶								
CMR in patients with severe AS								

THE HORNETS' NEST OF CORONARY MICROCIRCULATION IN AORTIC STENOSIS

Controls	20				MPRI	LVMI	CI	LGE
AS – angina	41				o	o	o	o
AS + angina	43				↓	↑	↑	↑
					↓↓	↑↑	↑↑	↑↑
Singh <i>et al</i> 2017⁷⁷								
Exercise test, echocardiography and CMR in asymptomatic patients with moderate-severe AS								
			AVA	AVG	Global MPR	Stroke volume	Fibrosis	NT-proBNP
No event	127		o	o	o	o	o	o
Event	47		↓	↑	↓	↓	o	↑

Abbreviations: ↑ indicates a higher measure, ↓ a lower measure where “o” is the baseline comparison. AS: aortic stenosis, AVA: aortic valve area, AVG: aortic valve gradient, BNP: b-type natriuretic peptide, BOLD: Blood oxygen level dependent, CBF: coronary blood flow, CFV: coronary flow velocity, CFVI: coronary flow velocity indexed for LV mass, CFR: coronary flow reserve, CI: cardiac index, CMR: cardiac magnetic resonance, ECHO: echocardiography, hDPT: hyperaemic diastolic perfusion time, hTransmural MBF: hyperaemic transmural myocardial blood flow, LAD: left anterior descending artery, LGE: late-gadolinium enhancement, LVH: left ventricular hypertrophy, LVMI: indexed left ventricular mass, MPR: myocardial perfusion reserve, MPRI: indexed myocardial perfusion reserve, PCr/ATP: phosphocreatine/adenosine triphosphate, PET: positron emission tomography, SAVR: surgical aortic valve replacement, SI*β: peak signal intensity (SI) multiplied by the rate of signal rise, TEE: transoesophageal echocardiography, VTI: velocity time integral

THE HORNETS' NEST OF CORONARY MICROCIRCULATION IN AORTIC STENOSIS

LV systolic wall stress index and peak systolic flow velocity⁷⁵ are tightly knit, suggesting that extravascular compressive forces change systolic flow, although these changes are independent of LV mass. This may explain why CFR may not respond immediately to relief of valve obstruction but improves after one year⁷⁸. Other studies have also demonstrated improved subendocardial blood flow at two weeks⁴⁹, CFR at six months⁷⁶ and indexed MPR (MPRI) at eight months⁴⁵ following valve replacement. The evidence is strong for structural and hemodynamic effects as the cause of myocardial ischemia in AS.

Table 1-3: Classification of coronary microvascular dysfunction⁶⁵

	Clinical Setting	Main pathogenetic mechanism
Type 1 Absence of myocardial or obstructive coronary artery disease	Risk factors Microvascular angina	Endothelial dysfunction Smooth muscle cell dysfunction Vascular remodelling
Type 2 Myocardial disease	Hypertrophic cardiomyopathy Dilated cardiomyopathy Anderson-Fabry's disease Amyloidosis Myocarditis Aortic stenosis	Vascular remodelling Smooth muscle cell dysfunction Extramural compression Luminal obstruction
Type 3 Obstructive coronary artery disease	Stable angina Acute coronary syndrome	Endothelial dysfunction Smooth muscle cell dysfunction Luminal obstruction
Type 4 Iatrogenic	Percutaneous coronary angioplasty Coronary artery grafting	Luminal obstruction Autonomic dysfunction

The pathophysiological and clinical manifestations of coronary microvascular dysfunction, described as heightened sensitivity to vasoconstrictor stimuli associated with limited vasodilator capacity, have been previously classified⁵⁵ (Table 1-3). Coronary physiological response to hyperaemia can also be grouped into four categories, depending on the presence of normal or abnormal CFR (>2.0 and <2.0 , respectively) and normal or abnormal hMR (<1.7 and >1.7 mmHg/cm/s, respectively)⁷⁹. The reference standard of microvascular dysfunction is invasive measurement of coronary vascular resistance using pressure and flow during hyperaemia⁸⁰, where hMR is calculated by dividing the mean distal coronary pressure (Pd) by the hyperaemic average peak Doppler flow velocity (hAPV). However, hMR does not determine global microvascular dysfunction but minimal static resistance which is strongly dictated by microcirculatory

THE HORNETS' NEST OF CORONARY MICROCIRCULATION IN AORTIC STENOSIS

remodelling – either intrinsic (arteriolar remodelling or capillary rarefaction) or extrinsic to the vascular tree.

Two reasons for reduced CFR in AS have been proposed. The first hypothesis is that inherent microvascular dysfunction elaborates ischemia, as initially proposed by Ahn *et al*⁶ who demonstrated reduced MPRI in patients with AS and angina using perfusion cardiac magnetic resonance (CMR) imaging (without reporting hemodynamic or microvascular mechanisms)⁸⁰. The second is that ischemic signs and symptoms result from high wall stress and mechanical effects in response to AS, supported by improvement of coronary physiological indices immediately following TAVI.

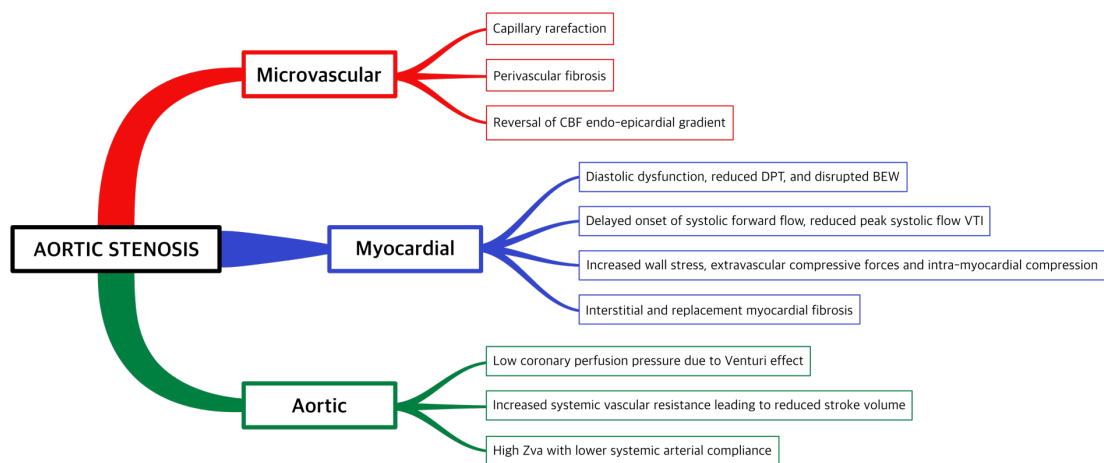


Figure 1-5: Factors implicated in disrupted coronary flow and reduced CFR in AS. Compensatory mechanisms fail due to structural and mechanical effects upon the ventricle and coronary circulation. There is reduced physiological reserve as a result of inadequate myocardial oxygen supply and increased oxygen demand.

Transmural CFR and subendocardial-to-subepicardial perfusion ratio fall directly with decreased hyperaemic DPT in AS (measured using positron emission tomography) and improve with increased hyperaemic DPT and increased AVA after SAVR^{46,78}, supporting a prominent role for hemodynamic conditions in determining CFR - microvascular disease would be expected to yield uniformly reduced transmural perfusion without a gradient⁸⁰. Equally, MPRI may be low in AS patients⁶ due to the resting increase in perfusion (rather than reduced stress perfusion), since MPRI is a relative ratio of stress-to-rest of the

magnetic resonance signal⁸⁰, and independently associated with exercise capacity⁶⁴. Intrinsic endothelial dysfunction does not correlate convincingly with hemodynamic factors that are promptly corrected following TAVI⁶⁰ - proposed mechanisms impacting disrupted microvascular function are illustrated in Figure 1-5.

Lumley *et al*¹⁹ found that perfusion efficiency during exercise in patients with AS was reduced as a result of augmented early systolic deceleration waves (BCW) and attenuated rise in systolic acceleration waves (FCW). Importantly, further assessment found that AS patients and those with normal hearts are able to reduce MR to the same extent. Decreased hMR after TAVI independent of resting haemodynamics has also been demonstrated in patients with severe AS (not differentiated into flow or pressure gradient status)⁶⁰. Clearly, both intra- and extra-myocardial pressures dictate coronary supply, and a combination of factors is likely to be responsible for the distortion of coronary flow and impaired CFR in AS.

1.7 Aortic Valve Flow and Pressure Gradients

The adaptive compensatory response to AS ultimately become maladaptive and results in cardiac decompensation, yet there are several guises with distinct anatomical and physiological characteristics (Figure 1-6 and Figure 1-7). Normal-flow high-gradient (NFHG) AS usually provokes concentric hypertrophy, whereas paradoxical low-flow low-gradient (pLFLG) AS patients demonstrate concentric remodelling⁸¹.

	Gradient	
Flow	NFLG	NFHG
	LFLG	LFHG

Figure 1-6: Classification of AS according to flow (low-flow [LF] <35ml/m², normal-flow [NF] >35ml/m²) and gradient (low-gradient [LG] MPG <40mmHg, high-gradient [HG] MPG >40mmHg). Low-flow low-gradient can be further subdivided into “classical” and “paradoxical” according to the presence or absence of impaired LV function.

The ventricular adaptive response to high afterload in combination with valve obstruction is poorly understood and may be more varied than is currently appreciated. Flow and stroke volume can both be reduced or normal in patients with preserved and reduced LV ejection fraction (LVEF)⁸². Whilst there is clear consensus that symptomatic AS with AVA $<1\text{cm}^2$, peak velocity (V_{max}) $>4\text{m/s}$ and mean pressure gradient (MPG) $>40\text{mmHg}$ warrants intervention, diagnostic ambiguity exists in patients with a small AVA and lower pressure gradients (despite preserved LVEF) where lower stroke volumes contribute significantly to discrepancies⁸³. Ageing, hypertension, diabetes mellitus and dyslipidaemia are associated with microvascular dysfunction and impaired CFR, and there is a higher proportion of diabetes mellitus and hypertension in pLFLG cohorts. These, in turn, are associated with an intrinsic likelihood of impaired CFR⁸⁴⁻⁸⁶, arising as a consequence of non-endothelium-dependent disorders of nitric oxide metabolism, dysregulation of inflammatory cytokines, oestrogen, or adrenergic receptors, and alterations in expression or production of local vasoactive substances such as angiotensin II and endothelin⁶⁵.

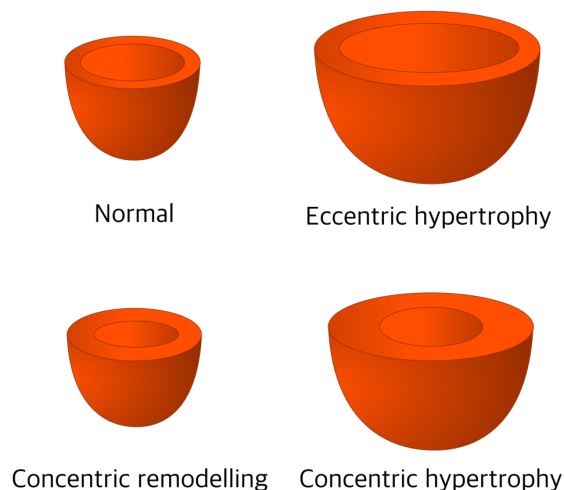


Figure 1-7: Patterns of cardiac remodeling based on normal or increased mass to volume ratio (concentric remodelling and concentric hypertrophy) and normal LV wall thickness (concentric remodeling) or hypertrophy (concentric and eccentric). Adapted from Gjesdal *et al*⁸⁷.

Low-gradient groups may be more susceptible to microvascular disturbance, as evidenced by a higher burden of subendocardial fibrosis on CMR⁸⁸. Since the first

description of pLFLG AS by Hachicha *et al*⁸⁹, there have been conflicting reports and evidence concerning the underlying pathophysiology. Accounting for up to 35% of severe AS cases (with a female preponderance), many are undiagnosed and surgical referral is frequently delayed or overlooked. The syndrome entails the perfect storm of valve, ventricular and vascular abnormalities, with valve stenosis, concentric LV remodelling (culminating in restrictive physiology), and high Zva with markedly lower systemic arterial compliance and higher arterial resistance⁸⁸⁻⁹³.

A low indexed stroke volume (SVi) predicts mortality and risk increases sharply when it is $<35 \text{ ml/m}^{2.94-96}$. Although still controversial, the bulk of evidence suggests that patients with AS and SVi $<35 \text{ ml/m}^2$ have markedly worse outcomes^{84,89,91,93,94,97-109}. Some discrepant studies (which include a high proportion of asymptomatic patients or fail to account for stroke volume)¹¹⁰⁻¹¹³ have been criticised for imprecise data analysis and misclassification¹¹⁴. The phenomenon of distinct remodelling is poorly understood and there is a paucity of invasive data to characterise the cohort and understand factors that predict poor outcome and the response to valve intervention.

European¹¹⁵ and American¹¹⁶ guidelines provide a Class IIA indication for aortic valve intervention in symptomatic pLFLG AS but only after careful confirmation of clinical, hemodynamic and anatomical data (in the normotensive setting), and exclusion of pseudo-stenosis, where the myopathic ventricle fails to generate adequate force. Although survival is improved when it is treated^{82,98,100,109,117,118}, these patients have adverse outcomes during and after valve intervention when compared to other AS cohorts^{84,100,105}, perhaps related to the burden of myocardial fibrosis^{100,113}. This fibrosis also impacts on MPR owing to reduced arteriolar and capillary density.

1.7.1 Low gradient aortic stenosis

AS patients with AVA $<1 \text{ cm}^2$ and MPG $<40 \text{ mmHg}$ can be subdivided into three categories:

1. Classical low-flow low-gradient AS (cLFLG AS) with impaired LVEF and stroke volume $\leq 35 \text{ ml/m}^2$

2. Paradoxical low-flow low-gradient AS (pLFLG AS) with preserved LVEF and stroke volume $\leq 35 \text{ ml/m}^2$
3. Normal-flow low-gradient with preserved LVEF (NFLG AS) and stroke volume $> 35 \text{ ml/m}^2$

Partial characterization of 600 patients with low gradient AS underwent echocardiography, and pre- and post-TAVI right and left heart catheterisation in a German retrospective study¹¹⁹. This demonstrated a greater proportion of female patients, with a significantly higher preponderance of atrial fibrillation and hypertension in the pLFLG AS group. Following TAVI, a significant decrease of systemic vascular resistance index was noted only in pLFLG and not in cLFLG or NFLG patients. Cardiac output and cardiac index was significantly higher in NFLG patients with outcomes in this group significantly more favourable at 5-years. NFLG is no doubt the most difficult to discern - some of these patients may have moderate AS since outcomes are comparable with medical therapy, surgical therapy or incidence of aortic valve intervention¹²⁰. Any error in echocardiographic assessment of the valve haemodynamics may lead to misclassification of the aortic stenosis therefore rigorous assessment is required. In contrast to cLFLG, pLFLG patients are akin to the heart failure with preserved ejection fraction phenotype¹²¹.

1.7.2 Structural Remodeling in Low Gradient AS

The complex collagen weave is responsible for much of the ventricle's passive diastolic stiffness¹²² and remodelling in response to pressure overload causes fibroblast proliferation and collagen I accumulation¹²³. Myocardial collagen deposition is a common end point of many pathologies and accompanies advanced ageing¹²⁴. Myocardial hypertrophy is detrimental to overall survival¹²⁵⁻¹²⁷ and correlates with fibrosis, impaired longitudinal shortening and worsening diastolic function. This fibrosis associated with AS¹²⁸⁻¹³¹ is a crucial determinant of cardiac dysfunction and prognosis^{129,131-134}, and replacement fibrosis may be the result of myocyte apoptosis accounting for progression

to heart failure¹³⁵. Interstitial, subendocardial and mid-wall patterns of fibrosis have been demonstrated in patients with AS and normal coronary arteries^{88,127,133,136-143}.

Whilst endomyocardial biopsy is the gold standard for confirming fibrosis¹⁴⁴, CMR imaging has been widely used in its detection, either using T1 mapping to calculate extracellular volume fraction (ECV) or late gadolinium enhancement (LGE). ECV can detect extracellular volume expansion with diffuse fibrosis, whereas LGE only identifies replacement fibrosis¹⁴⁵.

Patients with pLFLG AS typically have more profound impairment of LV longitudinal function^{106,118,146-148} and more florid myocardial fibrosis, predominantly located in the subendocardium⁸⁸. In comparison to circumferential fibres located in the mid-wall, longitudinal subendocardial fibres (responsible for long-axis function)^{2,149-151} are particularly vulnerable to microvascular ischemia and wall stress^{88,142}. Impaired longitudinal function as a consequence of subendocardial injury, small LV cavity size and increased wall thickness lead to reduced stroke volume and lower flow-dependent valve gradients¹⁵². Reduced stroke volume is primarily due to deficient LV filling (rather than emptying)¹⁰¹ and preserved LVEF should not be construed as “normal” systolic function. Consistent with this theme, a recent study demonstrated that indexed AVA, female gender, an abnormal exercise electrocardiogram and MPR (but not valve gradients or LV function) were independent predictors of event rates in moderate-severe AS⁷⁷.

This distinct remodelling may be explained by decreased cardiac reserve resulting from chronic exposure to high afterload, eventually exceeding the limit of compensatory mechanisms with resulting LV impairment and reduced cardiac output⁸⁹. It is also possible that these patients have a co-existing or secondary heart failure syndrome, akin to heart failure with preserved ejection fraction¹²¹, the aetiology of which is complex and poorly understood. Importantly, these two pathologies (which are both relatively common in older age) are not mutually exclusive and exhibit significant similarities, including impaired LV relaxation and microvascular abnormalities^{46,75,153-156}. Indeed, galactin-3, a novel marker of myocardial fibrosis, has prognostic value in heart failure with reduced or

preserved ejection fraction^{157,158} and is associated with adverse outcomes after TAVI¹⁵⁹ - despite the lack of any association with AS severity¹⁶⁰. Patients with elevated galactin-3 prior to TAVI have lower valve gradients and reduced LVEF (although data were not divided into AS cohorts)¹⁵⁹. Similarly, one study revealed that low flow (but not low LVEF or low gradient) is an independent predictor of early and late mortality following TAVI in high-risk AS patients¹⁰⁵. Comparable to patients with heart failure, LVEF does not correlate with outcomes.

Equally, the peril of low flow does not correlate with aortic valve calcification (AVC). There is less AVC but higher global afterload in pLFLG than other types of AS⁸², suggesting a co-existent ventricular disease entity that may explain why these patients have reduced survival benefit following valve intervention than other subgroups. This would support the theory that pLFLG AS is not "end-stage" normal-flow high-gradient (NFHG) AS¹⁶¹ but a distinct and separate entity¹⁶²⁻¹⁶⁴. Furthermore, the concept of pLFLG AS as a "transition stage" from non-severe to severe⁸² is undermined by a preponderance of myocardial injury and adverse outcomes.

1.8 Physiological Assessment of Coronary Stenoses in the Setting of AS

Symptomatology overlaps in patients with AS and epicardial coronary disease, and distinction may be clinically impossible. Physiological assessment of epicardial coronary stenoses in this setting is challenging due to compounding factors that contribute to myocardial ischemia, such as LVH and excess afterload. Functional evaluation of isolated coronary artery disease is well validated^{165,166} and strongly linked with clinical outcomes but a clear understanding of the pitfalls amidst AS is important for clinicians.

The results of coronary physiological assessment should be interpreted with caution in AS since it is not a true resting state. Distorted values may be caused by several factors:

1. Elevation of coronary sinus outflow and distal coronary pressure¹⁵ which may underestimate the significance of a coronary stenosis

2. Secondary LVH which causes reduced capillary density and abnormal vasoreactivity¹⁶
3. Elevated right atrial pressure¹⁶⁷

LVH causes fixed elevation of coronary resistance which may also be increased by neurohumoral factors that influence the response to adenosine¹⁶⁸ - these include α -adrenoceptor agonists, angiotensin and vasopressin¹⁷, the levels of which may be modulated by medication - adenosine infusion is safe and well-tolerated in patients with AS¹⁸⁻²⁰. LVH is also associated with a lower ischemic threshold as a result of capillary rarefaction²¹ and transmural steal (with disproportionately high subepicardial blood flow). A higher cut-off value level of fractional flow reserve (FFR) to indicate myocardial ischemia is therefore appropriate in patients with AS^{22,23}.

Although data are scarce, two recent publications on the role of FFR and instantaneous wave-free ratio (iFR) in the setting of AS and epicardial coronary disease provide important insights. One study found that diagnostic accuracy of iFR was significantly lower in patients with AS when the standard iFR threshold of 0.89 (to correlate with FFR 0.8) was used²⁰. The authors found that the best iFR threshold to predict an FFR ≤ 0.8 in the setting of AS was 0.83 (although iFR values were widely scattered). Another study found that iFR was not subject to change after TAVI ($p=0.94$) unlike FFR which fell significantly after intervention ($p=0.008$)²⁴. Positive FFR values worsen after TAVI whilst negative FFR values tend to improve¹⁶⁹.

1.9 Clinical Implications of Impaired Coronary Flow

Reduced capacity to augment myocardial oxygenation in response to stress is a physiological hallmark of AS and manifest by angina, dyspnoea and syncope. Up to 40% of patients with AS experience angina despite normal coronary arteries⁷³ and are at increased risk of sudden death¹⁷⁰. These patients have reduced MBF, impaired CFR and increased apoptosis⁴⁷, and are more likely to have impaired reserve^{6,73} and diminished

exercise capacity⁶⁴. One study found that low CFR was the only independent predictor of future cardiovascular events in AS patients¹⁷¹. Exertion accentuates the imbalance between supply and demand, and rising LVEDP blunts the pressure gradient required to achieve adequate coronary perfusion. Any rise in LVEDP or fall in AVA has a deleterious effect on coronary supply^{35,46} and there is a strong association between ventricular load (measured by LV rate-pressure product) and decreased CFR, particularly affecting the subendocardium. Stuttering ischemia yields subclinical LV dysfunction and apoptosis which is linked with myocardial fibrosis¹⁷² - an independent predictor of mortality¹³³.

Biomarkers have an emerging role in the assessment of asymptomatic AS¹⁷³. High-sensitivity troponin I correlates with LVH, fibrosis and clinical event rates¹³⁷, while cardiac myosin binding protein C correlates closely with LV mass, fibrosis and all-cause mortality (but not valve gradient)¹⁷⁴. NT-pro B-natriuretic peptide (BNP) levels are significantly higher in paradoxical and classical low-flow low-gradient AS⁸⁸, and correlate with CFR ≤ 2.5 and parameters of diastolic function¹⁷⁵ - use of BNP in asymptomatic AS is endorsed by recent European guidelines¹¹⁵.

1.10 Conclusion

Patients with AS host a caustic environment where impaired microvascular responses are compounded by high wall stress and hemodynamic load; those with angina (and impaired CFR) are at increased risk of sudden death. Progression of AS is characterised by discrepancies between blood supply and metabolic demand. There is an array of abnormalities in myocardial remodelling, stroke volume, pressure gradients and disordered coronary flow, which contribute to the signatures that determine varying AS phenotypes. These distinctions, which correlate with clinical outcomes, should prompt a directive path of physiological research. All patients with AS are not equal and the optimal timing and modality of treatment might differ according to phenotype. Relying on peak velocity to determine severity is now obsolete. Timing of intervention is crucial in avoiding irreversible myocardial fibrosis and a “burnt out” ventricle. Assessment of microcirculatory function may hold the key.

1.11 Objectives and Hypotheses

The objective of this work is to provide novel mechanistic insight into the aetiology of paradoxical low gradient aortic stenosis, by distinguishing features of a separate entity in comparison to high gradient aortic stenosis, and to better understand the response to aortic valve intervention. Exploration of the relationship between disrupted coronary flow, left ventricular mechanics and biomarker release, along with cardiac magnetic resonance imaging assessment allows meticulous multi-modality assessment.

This disease phenomenon remains poorly understood and detailed invasive characterisation is lacking, therefore this study, to complement available non-invasive research, aims to unravel associated pathophysiological mechanisms and potential interaction with myocardial ischaemia. Enhanced understanding of this high-risk group may direct future research and delineate optimal treatment options such as modality and timing of intervention.

The hypothesis proposes that increased myocardial dysfunction plays a role in the paradoxical low gradient ventricle, and that myocardial remodelling leads to further disruption in coronary flow patterns, especially during stress. Specifically, we hypothesise that the low gradient cohort will exhibit:

1. Depressed forward compression and backward expansion waves at rest and during stress before transcatheter aortic valve implantation
2. A greater proportion and distinct distribution of myocardial fibrosis as measured by cardiac magnetic resonance imaging
3. A higher systemic concentration and transcardiac gradient of lactate and troponin
4. More florid evidence of restriction, based on impaired left ventricular relaxation assessed using the diastolic pressure volume relationship

2 METHODS

2.1 Introduction

This chapter contains the specific methodological techniques used to undertake the research described in this thesis. This multi-faceted study involves several layers of data extraction, and modalities of analysis.

2.2 Ethical Approval

The study was presented at the Cardiovascular Patient Representative Group Meeting 21st March 2016, and the study documents (the Integrated Research Application System [IRAS] form, patient information sheet, protocol, consent form and general practitioner letter) were all created *de novo*.

London Westminster Research Ethics Committee confirmed favourable ethical opinion for this project (reference 16/LO/1619) on 18th October 2016, and the Health Research Authority granted approval (IRAS Project ID 198673) on 31st October 2016.

Guys & St Thomas' NHS Foundation Trust research and development sign-off, incorporating capacity and capability, was granted on 1st December, and the project was listed on the National Institute for Health Research Clinical Research Network Portfolio.

2.3 Recruitment

This thesis was based upon the study of patients with severe, symptomatic aortic stenosis (AS), undergoing trans-femoral trans-catheter aortic valve implantation (TAVI) who were classed as intermediate (Society of Thoracic Surgeons [STS] score 4 – 8) or high (STS score > 8) surgical risk. Recruitment was via the St Thomas' NHS Foundation Trust TAVI waiting list and patients were invited to participate either during an inpatient stay for workup investigations, or after the multidisciplinary team (MDT) meeting by a telephone call.

METHODS

Patients had the patient information sheet for at least a week prior to consent, and written informed consent was obtained for all patients.

2.3.1 Patient Selection

Inclusion and exclusion criteria are presented in Table 2-1. Patients were suffering from severe, symptomatic AS, and referred for TAVI. In order to identify features of AS alone, patients were required to have no other reason to have myocardial scar or ischaemia and needed to be able to have a cardiac MRI scan.

Table 2-1: Inclusion and Exclusion Criteria

Inclusion criteria	Exclusion criteria
<ul style="list-style-type: none">• Severe symptomatic aortic stenosis, referred for trans-femoral TAVI• Preserved left ventricular systolic function (ejection fraction $\geq 50\%$)• Aortic valve area $< 0.6\text{cm}^2/\text{m}^2$• Ability to give informed consent• Life expectancy > 1 year	<ul style="list-style-type: none">• Epicardial coronary artery lesion $\geq 70\%$• More than mild concomitant valve disease• Contraindication to MRI (ferrometallic cerebral aneurysm clips, non-MRI safe pacing device, cochlear implant, ventriculo-peritoneal shunt, metal fragments in the eye, severe claustrophobia or eGFR $< 30\text{ml/min}/1.73\text{m}^2$ contraindicating gadolinium-based contrast agent)• Atrial arrhythmia or bundle branch block• Contraindication to adenosine

2.3.2 Patient Journey

Prior to the decision to undergo TAVI, all patients were formally worked up with coronary and femoral angiography, echocardiography, and a specific clinical ECG-gated computed tomography scan to assess aortic annular dimensions and access route vasculature. Following agreement to participate in the study, patients were contacted within 48-hours of their planned admission for TAVI to explain the schedule of events. Figure 2-1 presents the additional steps undertaken if recruited into the study. Patients were met on arrival to the ward, the day prior to valve intervention, and consented for both TAVI and the research study. A perfusion MRI study was carried out that afternoon, not more than 24-hours prior to TAVI. The following day, the invasive protocol was carried out immediately pre- and post-TAVI. After a minimum of 4 months, patients attended for a clinical review

METHODS

and repeat perfusion MRI study. As part of routine clinical care, all patients also had pre- and post-TAVI blood tests, electrocardiography and echocardiography.

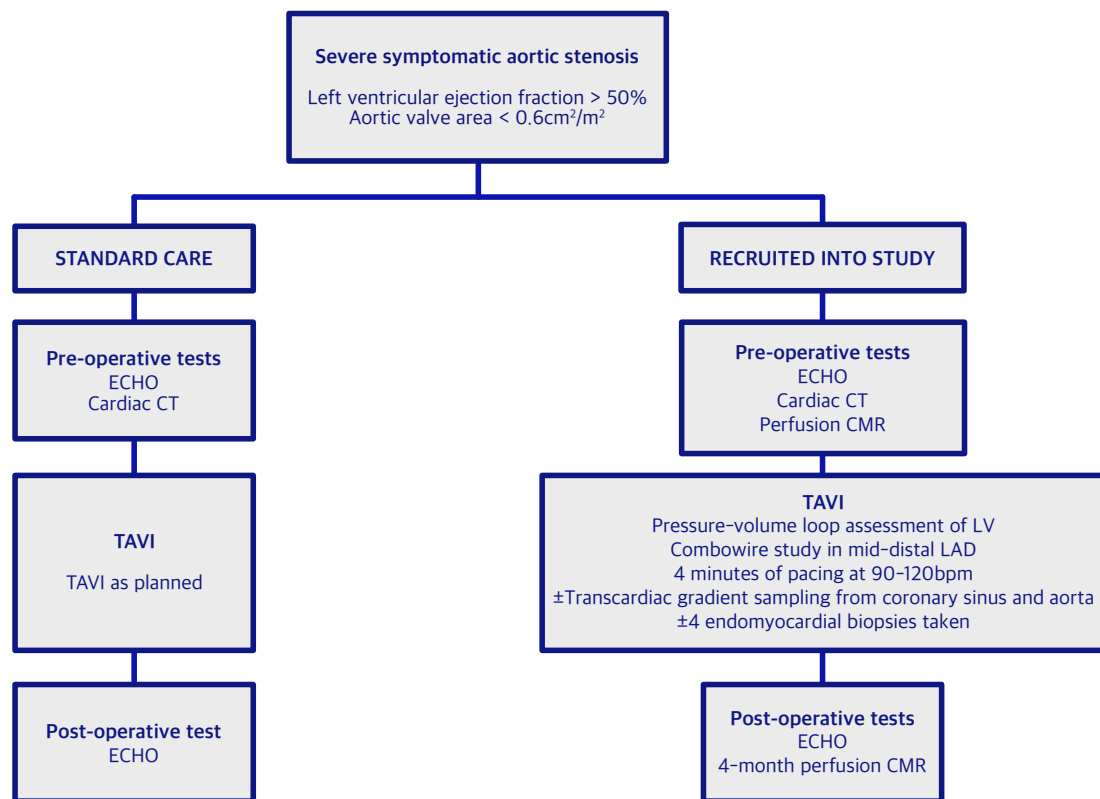


Figure 2-1: Study patient flow diagram

2.4 Cardiac MRI Protocol

Upon arrival, the patients' height, blood pressure and weight (on a consistent set of scales) were recorded, and the body surface area (BSA) calculated using the Mosteller formula¹⁷⁶. Two intravenous cannulae were inserted, one for gadolinium-based contrast, the other for an adenosine infusion as part of the vasodilatation stress protocol. Patients had abstained from caffeinated products for at least 24 hours and also completed a safety questionnaire. After checking that there was no metal or other non-suitable implants on their person, patients were transferred to the scanner. All MRI imaging was performed using a state-of-the-art 3 Tesla scanner (Philips Achieva-TX, Philips Medical Systems, Best, The Netherlands) equipped with 32-channel cardiac phased array receiver coil. Vector-cardiographic trigger was used for cardiac synchronisation. A blood pressure cuff was

METHODS

attached, along with an MR-compatible injector pump and the line through which adenosine infusion would be given. Patients lay supine with their arms by their side, with ear plugs and headphones on, and were handed an emergency buzzer to use if needed.



Figure 2-2: Thumbnail sequence of MRI protocol from Osirix

2.4.1 CMR Acquisition

Figure 2-2 outlines the sequence of scan acquisitions. Localiser scans or “scouts” were first acquired along with pseudo 2- and 4-chamber images using turbo field echo (TFE). To assess left ventricular (LV) myocardial function, volume and mass, 12 consecutive 8mm short-axis images and 2-, 3- and 4-chamber long axis image of the LV were acquired using a cine balanced steady state free precession sequence (bSSFP, 50-phases per cardiac cycle, 1.5-fold SENSE, spatial resolution 2x2mm, temporal resolution at 60bpm of 20ms). Stress and rest perfusion imaging was performed using a high resolution kt-turbo-gradient echo sequence (T1TFE), with three short-axis slices (basal, mid and apical) using a saturation-recovery *k-t* sensitivity encoding accelerated gradient-echo method¹⁷⁷ acquired over every heartbeat covering the standard sixteen American Heart Association (AHA) segments¹⁷⁸ with a typical in-plane spatial resolution of 1.2x1.2mm. Typical

METHODS

imaging parameters: shortest echo time (range 1.35–1.54 ms), shortest repetition time (range 2.64–3.12 ms), 180° flip angle, 90° saturation pre-pulse, 120 ms pre-pulse delay, typical TR 2.6 ms, typical TE 0.9 ms. Following test perfusion, a proton density weighted sequence was acquired by turning off the pre-pulse thereby minimising echo time and signal differences due to transverse decay and magnetisation relaxation times – used as a correction map to account for special inhomogeneities due to surface coils¹⁷⁹. A dual bolus protocol of Gadobutrol (Gadovist, Bayer, Berlin, Germany) at 4 ml/s followed by a 20ml saline flush was used to correct for signal saturation (dilute Gadovist 0.0075mmol/kg and neat 0.075mmol/kg, with a 25 second pause between injections)¹⁸⁰, to allow quantification of perfusion, according to published methods¹⁸¹. Gadolinium-based contrast shortens the longitudinal recovery time (T_1) by increasing relaxation rates. Stress perfusion images were acquired during pharmacological vasodilation with adenosine, 140µg/kg/min (increasing to 175 then 210µg/kg/min if no symptomatic or haemodynamic response) for at least 2 minutes with symptomatic hyperaemia (chest tightness, dyspnoea, diaphoresis) and >10% rise in heart rate. Rest images were performed approximately 10 minutes after stress imaging.

Balanced turbo field echo (gradient echo pulse sequence with a balanced gradient waveform) Modified Look-Locker Inversion recovery (MOLLI) sequences were acquired pre- and post-contrast to allow T_1 map generation and calculation of the extracellular volume (ECV) (and thus the degree of interstitial fibrosis). Partition coefficient and ECV¹⁸² appear to be the optimal non-invasive MRI T_1 measures for quantifying diffuse myocardial fibrosis. 10-15 minutes after injection of Gadovist (total dose 0.2mmol/kg), late gadolinium enhancement images were acquired with an inversion-recovery gradient-echo imaging sequence (Look-Locker) to evaluate focal myocardial scar in the same long and short-axis projections¹⁸⁰.

To measure the aortic valve area (AVA) and the left ventricular outflow tract (LVOT) area by planimetry, 7 contiguous orthogonal 4mm cine slices were taken of the aortic valve, starting 12mm upstream from the aortic valve annulus in the outflow tract and ending

METHODS

10mm downstream of the annulus in the ascending aorta. These were planned in the 3-chamber and coronal LVOT views.

Flow quantification using spoiled gradient echo by phase contrast mapping was carried out at the level of the aortic valve. In-plane flow sequence planning was obtained in the 3-chamber view with the aim of achieving a flow direction as close to the velocity encoding direction. Through-plane assessment is more accurate and negates some partial volume averaging. Initial VENC (velocity encoding) was estimated from echocardiography and repeated with a higher VENC if aliasing occurred. Flow quantification at the main pulmonary artery bifurcation level for ascending and descending aorta was also obtained. Maximal velocity from phase contrast images was estimated from the highest velocity pixel of aortic flow, by adjusting the contrast settings to highlight the brightest pixel in cine images.

2.5 Catheter Laboratory Protocol

The invasive protocol was carried out at the time of TAVI, and included paired coronary and LV physiology, paired serum sampling from the coronary sinus and aorta (trans-cardiac gradients) in the first 10 patients and an endomyocardial biopsy when possible at the end of the procedure. During the invasive assessment of hyperaemia and rapid pacing before and after TAVI in LGAS and HGAS patients, a number of invasive haemodynamic parameters were measured. Each dataset was obtained pre- and post- valve implantation, at rest, hyperaemia (by intracoronary adenosine bolus), and paced at 90bpm and 120bpm, each for 2 minutes. Table 2-2 summaries the step-by-step protocol.

Table 2-2: Step by step guide to the invasive protocol

Step	Procedure	Equipment needed
Pre	Set up	Liquid nitrogen flask, OCT, Isopentane, cork discs, tin foil, left ventricular volumes from CMR
1	ACCESS: Contralateral femoral 6F Arterial and venous sheaths Aortogram and ipsilateral puncture under fluoroscopic and angiographic guidance. Insertion of TAVI sheath. Cross the aortic valve with AL1 catheter	

METHODS

2	CORONARY: ComboWire placement in mid-LAD with longer acquisition to confirm position of coronary sinus Connect pressure first (Ethernet), then connect velocity cable. ComboWire connections to INCA (cables run top to bottom, left to right). Disable auto velocity scaling.	Guide catheter ComboWire, ComboMap Console IVUS bag
3	CORONARY SINUS: CS intubated with SL3 long sheath, then pass the pacing wire through to enable simultaneous pacing and serum sampling	SL3 sheath, pacing wire
4	LEFT VENTRICLE: Calibrate conductance catheter under water. Connect pressure cable, then volume cable. Once calibrated, insert over 0.025" wire which has been exchanged over the pigtail catheter in the left ventricle, via TAVI sheath. Rescale, record, then volume calibrate.	PV loop 7F catheter over an Amplatz Extra Stiff 0.025" 260cm J tipped wire, INCA Console
5	PRE-TAVI STRESS PROTOCOL: Pacing protocol acquisitions: rest; intra-coronary adenosine; 2mins pacing at 90bpm; 2mins pacing at 120bpm. Aortic and coronary sinus sampling at rest, after 2 minutes pacing at 90bpm, after 2 minutes pacing at 120bpm and 5 minutes post-stress Record datasets via INCA and ComboMap for each of rest, hyperaemia, 90bpm, 120bpm and removal of conductance catheter	Adenosine 40µg bolus 5ml syringes x 16 (labelled: pre-TAVI/post-TAVI; rest/90bpm/120bpm/post-stress; CS/aorta) i-STAT, charger and printer
6	REMOVAL OF KIT: Conductance catheter removed and exchanged for a pigtail catheter. Safari wire inserted. Guide catheter for changed for pigtail catheter (contralateral access).	Safari wire
7	VALVE IMPLANTATION	TAVI prosthesis
8	POST-TAVI STRESS PROTOCOL Repeat steps 2, 4 and 5 making a new file on INCA	
9	LEFT VENTRICULAR ENDOMYOCARDIAL BIOPSY: Long sheath inserted through the TAVI e-sheath and biopsies taken with the biptome	Cordis 5.5Fr Biptome and 7Fr long sheath Gallipot with saline for biopsies
10	END OF PROCEDURE Closure of femoral punctures and end of procedure	
11	TIDY UP RESULTS - Send one biopsy to histopathology to exclude amyloidosis - Snap freeze remaining samples, and store at -80°C in an HTA compliant freezer - Collate serum results taken during procedure (ABG) - Take red top serum samples to Viapath for Troponin assay, and freeze supernatant for later MyC results - Recalibrate data files, and download once filtered and cleaned	

2.5.1 Pressure Volume Loop Assessment

Real-time, *in vivo* pressure and volume measurements can be obtained from specific conductance catheters which are introduced into the left ventricle, either antegradely by

METHODS

direct apical puncture, or by retrograde catheterisation from the aorta, through the aortic valve. Each loop created by the pressure and volume relationship represents a complete cardiac cycle and describes filling, contraction, ejection and relaxation – the dynamic physiological assessment of cardiac function. A list of indices used for analysis is displayed in Table 2-4. The benefit of this technique is the generation of a three-fold load-independent ventricular contractile state relationship:

1. The Frank-Starling contractile state index (Sci), which characterises contraction from the isovolumetric contraction phase
2. The preload recruitable stroke work (PRSW), which characterises pan-cardiac cycle contractile state
3. The end systolic elastance (Ees), encapsulating contractile state during isovolumetric relaxation

The first development of cardiac functional assessment by electrical conductance, or impedance measurement of intravascular volume in humans was not until the early 1980s¹⁸³. Validation of this technique has been performed against cine computed tomography and electro-conductive balloons in animals; thus, the conductance catheter is capable of reproducing accurate global LV volumes and estimates of stroke volume as well as segmental volume calculation^{184,185}.

2.5.1.1 Properties of the Conductance Catheter

A multi-electrode catheter measured intracavitary electrical conductance, from which ventricular volumes were then calculated by taking into account several calibration factors. Continuous volume signals were generated by taking into account specific resistivity of blood and the spacing between the sensing electrodes. Conductance catheters (CD Leycom, Zoetermeer, Netherlands) are currently available in 4F or 7F with a choice of electrode spacing, and are CE marked (Figure 2-3).

Segmental volumes measured are always relative volumes. Ejection fraction and total volume by MRI volumetric assessment were used to calibrate these values by matching

METHODS

cardiac output or stroke volume derived from the volume catheter to pre-determined values from MRI.



Figure 2-3: A conductance catheter (left), the CD Leycom panel (middle), and the INCA console (right)

Total volume is calculated as $V(t) = \rho \cdot L^2 \cdot G(t)$ where ρ is blood resistivity, L is the electrode spacing, and $G(t)$ is the sum of the segmental conductance. The main module of the Cardiac Function Laboratory Modular (CFLM)-system supplies a 21.5kHz, 30 μ A current to two pairs of electrodes (or one pair if set to Single Field Ratio) to set up an intracavitary field and measures the resulting voltage gradients between the other pairs of electrodes.

2.5.1.2 INCA Console and Conduct NT Software

CD Leycom's CFLM series was used to run the software ConductNT, a Windows 16-Bit software program, which runs on a 32-Bit Windows operating system. The CFLM system includes a power cord, ethernet, volume and pressure cables, four auxiliary cables to slave data from the ComboMap to the console, and the CD Leycom conductance catheter (Figure 2-4). The Leycom INCA[®] console is an intra-cardiac function monitor which allows real-time, operator independent, beat-to-beat display, acquisition and analysis. It has a modular platform and 7 channels which compose the volume segments.

METHODS

2.5.1.3 Conductance Catheter Insertion and Calibration

7F catheters with a central lumen and 10mm spacing between 12 electrodes were passed retrogradely across the stenosed aortic valve, and across the new TAVI prosthesis following valve implantation. The valve was initially crossed with a straight wire and AL1 catheter, which was then advanced into the left ventricle and the wire exchanged for an exchange-length (260cm) 0.025" Amplatz extra stiff wire (ordered from supplychain.nhs.uk). 7F catheters allow a maximum 0.025-inch wire to pass along a central lumen and the extra stiff wire provided reasonable support to advance the conductance catheter over the wire and into the left ventricle.

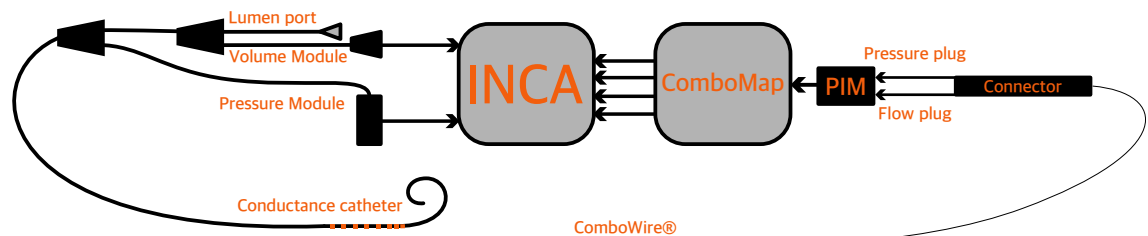


Figure 2-4: Schematic of the connections between the conductance catheter and ComboWire

The catheter was flushed with sterile saline then the distal portion of the catheter immersed in saline for approximately 10 seconds. The distal end was then connected to the pressure module, and pressure calibration performed whilst the catheter was still, lasting approximately 15 seconds. The catheter was then inserted into the left ventricle over a 0.025" super stiff Amplatz wire, verified fluoroscopically, and connected to the volume module of the Inca console, creating a circuit. Segmental loops were checked to help determine position which could be changed if necessary – ideally the catheter was coaxial with the ventricular long axis, with the pigtail tip sitting in the apex. The output was rescaled, and a baseline dataset acquired to allow volume calibration with manual input of end diastolic and end systolic volumes from MRI volumetric assessment (carried out within the previous 24 hours)¹⁸⁶.

2.5.2 Coronary Assessment

METHODS

Assessment of coronary pressure and flow during programmed physiological settings provides mechanistic insight of the interaction between cardiac contraction and coronary supply³⁵.

2.5.2.1 *Properties of the ComboWire*

Coronary pressure and flow measurements were achieved through a dual pressure and Doppler sensor-tipped 0.014-inch intracoronary wire (ComboWire®, Volcano Corp, San Diego, CA) in the left anterior descending coronary artery (Figure 2-5). This is the only available guidewire capable of acquiring simultaneous and continuous coronary artery pressure and flow data¹⁸⁷. It is a standard 185 cm long, and the pressure sensor is offset by 1.5cm from the flow sensor at the tip.

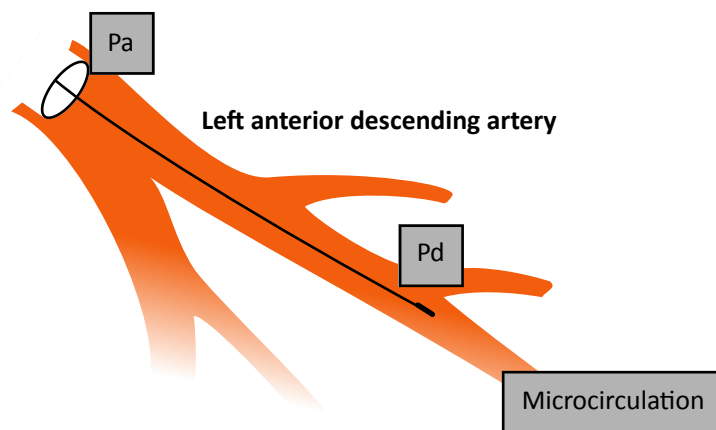


Figure 2-5: ComboWire in the left anterior descending coronary artery

Irrespective of the Doppler device used to determine CFR, it is calculated as the time-averaged peak velocity during hyperaemia (APV_h), divided by the time-averaged peak velocity at resting conditions (APV_r), assuming that the rate of flow through the artery is strictly proportional to the measured APV ¹⁸⁸. Adenosine induces coronary vasodilatation, which impacts the relationship between coronary flow velocity and volumetric flow. Flow velocity profile shapes change, and therefore this assumption can introduce potential error¹⁸⁹. The true mean flow velocity is proportional to APV , independent of the vessel diameter, with high correlation coefficients for both antegrade and retrograde perfusion where the guidewire does not appear to disturb the velocity profile¹⁸⁸. Blood flow velocity

METHODS

is determined from the Doppler frequency shift – from the difference between transmitted and returning signals:

$$V = (c * F_d) / 2 F_o \cos \theta$$

where V is flow velocity, c is the constant of velocity of sound in a medium, F_o is the transmitted frequency, $\cos \theta$ is the insonation angle cosine, and F_d the Doppler frequency¹⁹⁰.

The change in pressure from proximal (dP^+) or distal (dP^-) sources can be determined to be accelerating or decelerating waves depending on positive or negative values from the following equation:

$$dP^+ = \frac{1}{2} (dP + \rho c dU)$$

$$dP^- = \frac{1}{2} (dP - \rho c dU)$$

where ρ is the density of blood (1050 kg/m^3), dP is the change in pressure, dU the change in flow velocity, and c is the wave speed calculated using simultaneous pressure and flow, measured by the following equation¹⁹¹:

$$c = 1/\rho \sqrt{\sum dP^2 / \sum dU^2}$$

Net wave intensity (WI^{net}) is the sum of proximal (WI^+) and distal (WI^-) originating waves³³ derived from phasic changes in pressure and flow velocity:

$$WI^{\text{net}} = dP/dt \times dU/dt$$

The wave intensity for each of the 4 most prominent waves were analysed. The net wave intensity trace, WI_{net} , is the sum of WI_+ and WI_- but does not depend on a wave speed estimation.

METHODS

2.5.2.2 *The ComboMap System*

The ComboMap console (Volcano® Therapeutics, USA) processes and displays pressure and flow velocity data acquired by the ComboWire. In addition, the patient's ECG and aortic pressure (via fluid filled manometry from the guiding catheter) were slaved from the Sensis Cardiac Catheter Laboratory monitoring system (Siemens Healthcare, Erlangen, Germany). All signals were displayed in real time and adjusted as necessary. The ComboMap system input was slaved into the INCA console, as depicted in Figure 2-4.

2.5.2.3 *ComboWire Insertion*

A fluid-filled hollow guide catheter (Extra Back-Up or Judkins, 3.5 or 4mm diameter) was used to measure pressure in the ascending aorta. Pressure was transmitted through a fluid column to an external pressure transducer, to which the fluid-filled system was connected. Prior to ComboWire insertion into the guiding catheter it was initially laid flat on the catheter lab table and the modular plug inserted into the pimmette of the ComboMap (model 6800). This automatically zeroed pressure on the pressure transducer. Following this, when the ComboMap indicated that pressure had zeroed successfully, the pin plug was inserted into the ComboMap, thereby activating the Doppler flow crystal. The fluid filled manometer pressure trace was also zeroed to air via the Sensis system.

The ComboWire was then introduced through the guide catheter into the mid left anterior descending artery via an introducer needle. When the pressure sensor was visualised by fluoroscopy just beyond the tip of the guiding catheter in the left main stem, the two pressure signals were then compared, and the ComboWire signal normalised to aortic pressure. The ComboWire was then advanced to the chosen position, and the Doppler tracing assessed and adjusted by slight rotation or repositioning of the wire, and the X-ray tower elevated to minimise interference. Further optimisation was carried out on the ComboMap console, by changing the display threshold setting (adjusts the sensitivity of the greyscale pixels on the screen – usually set to 10-12) and the

METHODS

instantaneous peak velocity threshold setting (usually set to 1) which adjusts the sensitivity of the tracking blue envelope to the Doppler greyscale area.

2.5.3 Coronary Sinus Access

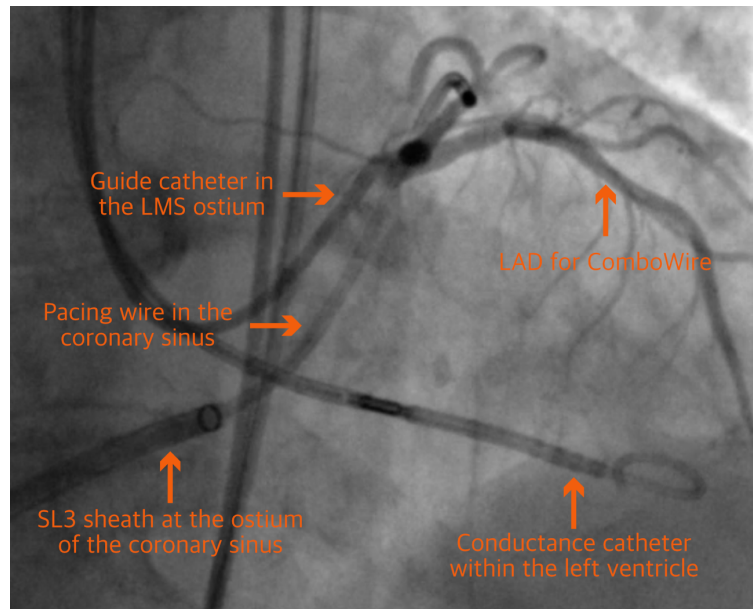


Figure 2-6: Fluoroscopic image showing the elements of the invasive protocol

On intubation of the left coronary circulation with a guide catheter, a prolonged fluoroscopic acquisition was taken with contrast to reveal the position and course of the coronary sinus (CS). Coronary sinus cannulation was achieved with a fixed curve 8 French 63cm Fast-Cath Swartz SL3 sheath (St Jude Medical, Inc.) (Figure 2-6) which was exchanged over a wire following cannulation of the femoral vein. The sheath was advanced into the right atrium, followed by withdrawal of the dilator. The tip of the sheath was then manipulated to the CS ostium. A pacing wire was advanced into the CS, with the dual ability thereafter to pace and sample from the CS. This access remained in situ for the duration of the procedure and this part of the protocol was carried out for the first 10 cases.

2.5.4 Stress Protocol

METHODS

Stress was achieved with a 40mcg bolus of intracoronary Adenosine to produce hyperaemia^{187,192}. After the average peak velocity had returned to normal, rapid pacing via the coronary sinus was initiated (or RA pacing if CS access was not required for serum sampling as in later cases), first at 90bpm for 2 minutes, then at 120bpm, after which the pacing was weaned and stopped. Pacing via the coronary sinus in patients who were sedated or under general anaesthetic, was reproducible and more physiological than right ventricular pacing. This combination of stress using adenosine and pacing provided substantial information, and avoided effects on peripheral vasculature and potentially large haemodynamic shifts in patients with AS. This protocol was performed prior to valve intervention, and immediately following valve deployment.

2.5.5 Serum Sampling and Analysis

By measuring transcardiac gradients of oxygen, we can obtain measures of myocardial oxygen delivery and extraction, which will be impacted by microvascular dysfunction^{72,193,194}. Coronary sinus and aortic blood sampling was carried out using 5ml syringes via the SL3 sheath and the coronary guide catheter, respectively. Samples were taken at rest (baseline), following 2-minutes of pacing at 90bpm, following 2-minutes of pacing at 120bpm, then 5 minutes following withdrawal of pacing. This was repeated pre- and post-TAVI for the first 10 patients.

Samples were divided into two: a few drops for the i-STAT cartridge, and the remaining blood was filled into red-topped blood tubes (gel-free) for high sensitivity Troponin-T analysis. The latter was analysed by Viapath (www.viath.co.uk) who carried out centrifugation at room temperature and aliquoting to minimise possible sampling of red blood cells. The supernatant was then collected and transferred to a Human Tissue Act compliant -80°C freezer in the Rayne Institute for later Cardiac Myosin-Binding Protein C (MyC) analysis. When ready, batched samples were prepared and 100µl of supernatant aliquoted into cryovials, labelled with a unique identifier 5-digit number, barcode and box number, and shipped to Singulex, Inc. 1701 Harbor Bay Parkway, Suite 200, Alameda, CA 94502, USA.

METHODS

Viapath emailed troponin-T results within 24 hours and a paper copy was supplied with the return of the supernatant. The i-STAT 1 analyser (Abbott Laboratories Ltd) was used in the catheter laboratory to allow immediate assessment of lactate, oxygen and pH (using CG4+ cartridges). The machine and cartridges were calibrated with TriControls at recommended intervals. All results were collated as per Table 2-3.

Table 2-3: How serum results were collated

	Aorta	Coronary Sinus
Pre-TAVI		
T=0 Rest		
T=2mins Post-2 mins 90bpm pacing		
T=4mins Post-2 mins 120bpm pacing		
T=9mins After 5 minutes of rest		
Post-TAVI		
T=0 Rest		
T=2mins Post-2 mins 90bpm pacing		
T=4mins Post-2 mins 120bpm pacing		
T=9mins After 5 minutes of rest		

2.5.6 Histological Sampling and Storage

Human Tissue Act and Consent Training was completed at Guy's Campus, King's College London, on 9th March 2016. A Material Transfer Agreement (MTA) between King's College London and Guy's and St Thomas' NHS Foundation Trust was established for the transfer of samples for the study. Proactive Gas Safety Ltd, Cryogenic Gas User Workshop was successfully completed on 19th January 2017, covering the following: gas properties and hazards; legislation of codes and practice; cylinder/vessel identification and data; associated equipment; gases storage; personal protective equipment; visual pre-use checks; practical manual handling; cryogenic vessels; emergency procedures; first aid for cold burns; and practical decanting procedures. Each biopsy sample was analysed by the hospital histopathology lab using CongoRed staining for assessment of amyloidosis.

2.6 Analysis of Invasive Parameters

2.6.1 Left Ventricular Parameters with SimpleWires

Exportation of left ventricular physiology datasets was from the INCA. First, pressure drift was checked from the file stored during the removal of the conductance catheter, and an offset added if necessary. The volume calibration was updated to the pre-TAVI baseline or “rest” file and a filter added (25Hz) to all files. Files were exported, named according to physiological setting, and edited in TextEdit to allow analysis using SimpleWires (Kings College London). The relevant .csv file was then imported to SimpleWires and beats selected for analysis (Figure 2-7). Results were saved and added to the master database for statistical analysis.

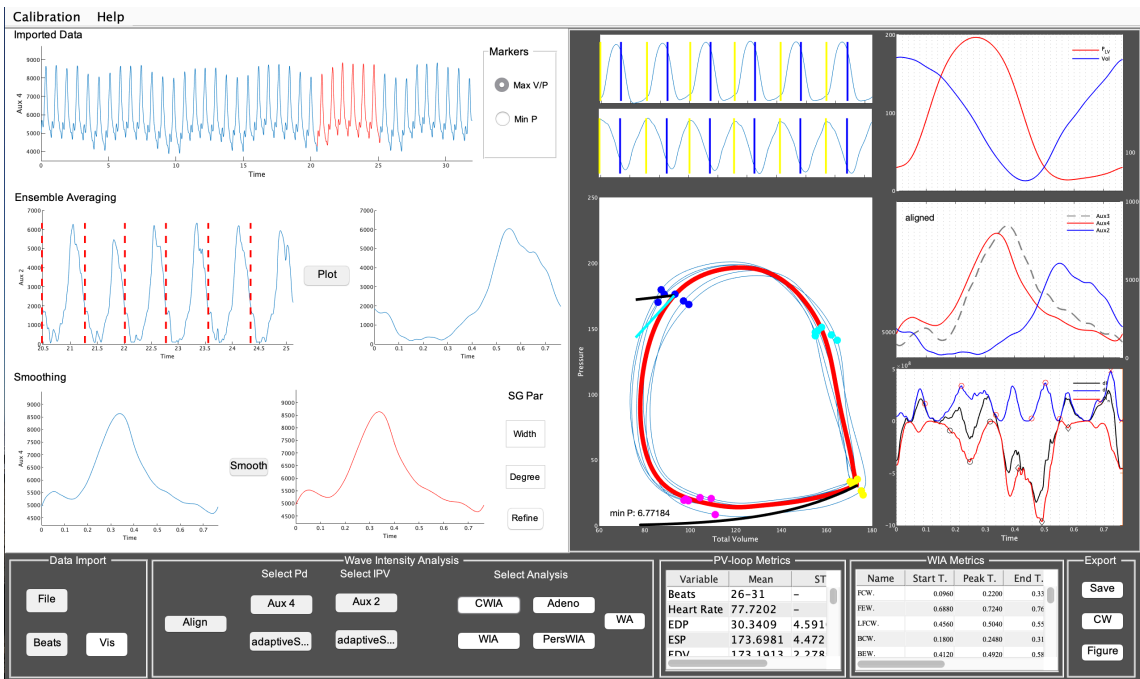


Figure 2-7: An example of a case being analysed within SimpleWires

Lusitropy, the rate and extent to which the heart relaxes during diastole, can be measured invasively as the end-diastolic pressure-volume relationship (EDPVR)¹⁹⁵. This relationship is calculated by the following:

METHODS

$$P_{ed} = \beta[e^{\alpha(V_{ed}-V_u)}-1]$$

where P_{ed} is the end diastolic pressure, V_{ed} is the end diastolic volume, and α and β are constants of the curve, derived from the myocardial mechanical properties.

2.6.2 Coronary Datasets with CardiacWaves

Coronary signals were sampled at 200 Hz and the raw data exported as .SDY files into a custom-made Study Manager platform in collaboration between Volcano Corporation and the Academic Medical Centre (Amsterdam, Netherlands) for data extraction of selected beats in the various physiological settings. This allowed assessment of all the data collected and selection of the key sections to be analyzed, which were then exported as .txt files. These text files were then loaded into CardiacWaves (Kings College London), an application written in MATLAB, specifically for performing wave intensity analysis on invasive pressure and flow signals³⁷. Briefly, a Savitzky–Golay convolution method was adopted using a polynomial filter to refine the derivatives of the intracoronary pressure and velocity signals. The selected minimum five consecutive cardiac cycles (usually many more) were gated to the ECG R wave peak, with ensemble averaging of aortic pressure, distal coronary pressure (P_d), average peak velocity (APV) and heart rate. The instantaneous peak velocity (IPV) was continually tracked from spectral recording, averaging the peak velocity (APV, cm/s). A delay was added to each of the datasets to account for the offset between pressure and Doppler sensors on the ComboWire.

2.7 Analysis of Non-Invasive Datasets

2.7.1 MRI Volumetric, Strain and Flow Analysis using CVI42

CVI⁴²® (Circle Cardiovascular Imaging Inc., Calgary, Canada, version 5.6.4) software was used to analyse the 3D cardiac volumes and left ventricular mass. This was carried out by manually contouring (by me for each scan) the endo- and epicardial borders at end-

METHODS

diastole and end-systole from cine short axis stack images, allowing calculation of the LV end diastolic and end systolic volumes, stroke volume, ejection fraction and LV mass. LV mass was measured in end-diastole and excluded papillary muscles and trabeculations. Contouring the compacted myocardium was the standard clinical practice in our institution and has been well described⁽¹⁹⁶⁾. Left atrial area was measured in the horizontal (4-chamber) long axis view¹⁹⁷ and aortic measurements were also assessed. Aortic valve area by planimetry was carried out using the aortic valve stack.

By tracking features between consecutive frames from SSFP cine acquisitions, tissue tracking is able to calculate 2D and 3D global radial, longitudinal and circumferential motion and deformation¹⁹⁸. This was carried out using the tissue tracking software on CVI42, where the short axis stack endocardial and epicardial contours were completed, the superior and inferior right ventricular insertion points marked, and combined with a 4-chamber long axis acquisition (with contours) in order to output the strain data. This was exported as a .txt file into the master data file. Flows from phase contrast sequences were assessed in the designated flow software incorporated into CVI42.

2.7.2 Quantitative MRI Perfusion Analysis using MATLAB

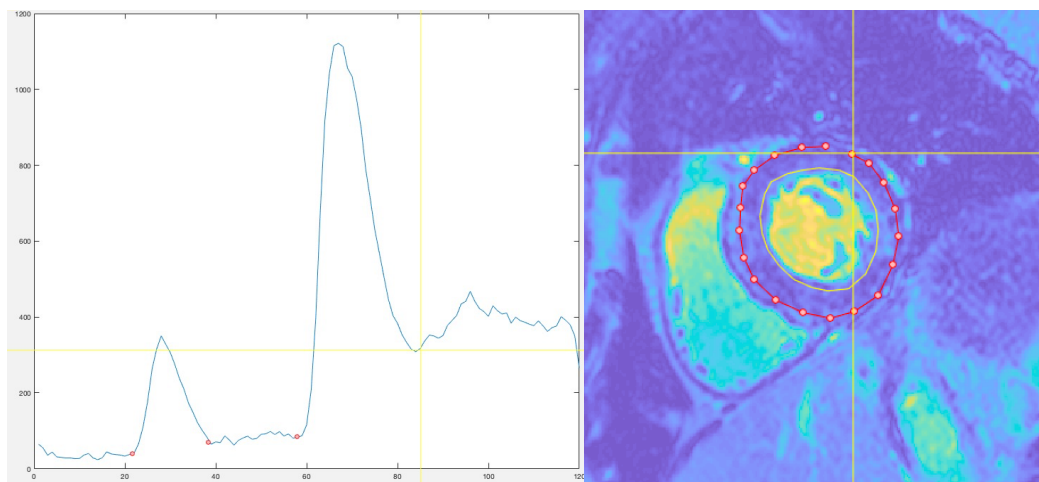


Figure 2-8: Left: signal intensity curve generated from dual bolus gadolinium sequence, Right: Manual segmentation of late gadolinium scar imaging in MATLAB

METHODS

For perfusion analysis, each MRI dataset was divided into native and post-contrast MOLLs, protein density map, stress and rest perfusion, and scar DICOM (Digital Imaging and Communications in Medicine) files. The corresponding short axis scar image relating to the positions of each of the 3-slice perfusion sequences was chosen. The DICOMDIR (DICOM directory) file was then uploaded into MATLAB and each cardiac slice manually segmented with endocardial and epicardial borders within a custom-made MATLAB tool (Figure 2-8).

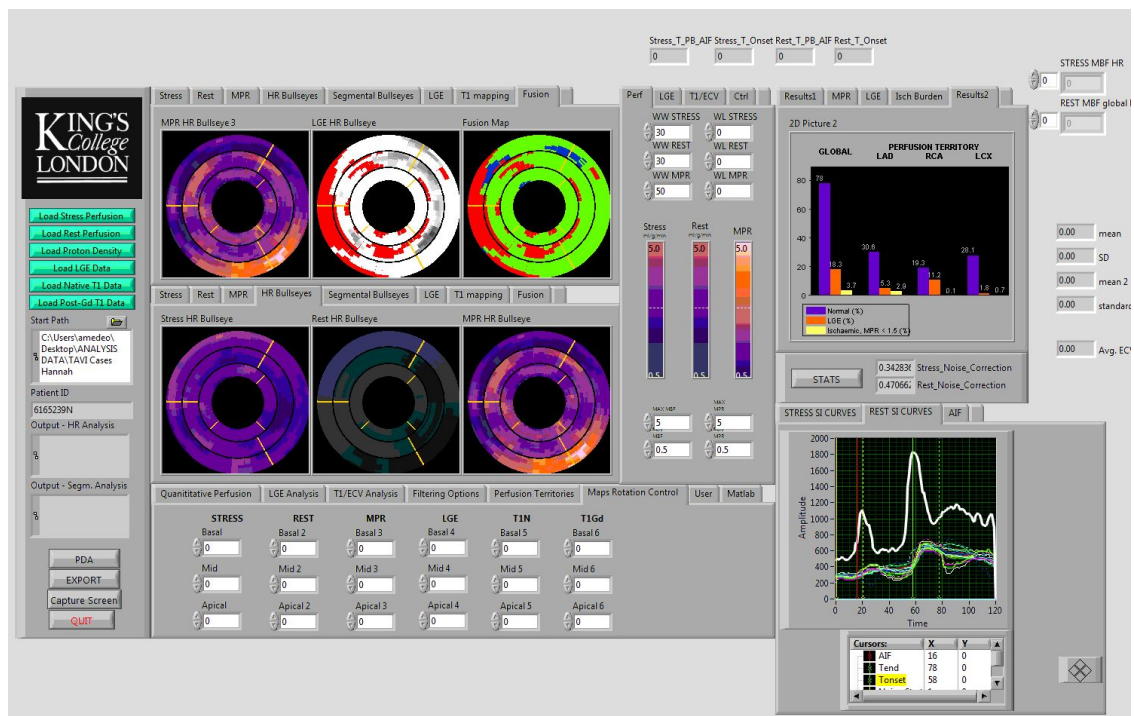


Figure 2-9: Kings College London custom designed perfusion analysis platform

An experienced MRI operator (AC), blinded to results of visual perfusion assessment and low or high gradient AS, performed quantitative analysis by Fermi-constrained deconvolution using software and methods developed and validated by Kings College London against perfusion phantom, positron emission tomography data and microspheres^{199,200}. Quantitative signal intensity analysis required a still heart during stress and rest perfusion (i.e., an adequate breath hold) for accurate myocardial contour delineation. Respiratory motion was corrected using affine image registration by maximisation of the joint correlation between consecutive dynamics within an automatically determined region of interest²⁰¹. A temporal maximum intensity projection

METHODS

was calculated to serve as a feature image for an automatic contour delineation method. The operator then manually optimised the automatically generated contours to avoid partial volume effects at the endocardial and epicardial border (Figure 2-9). Areas of subendocardial dark-rim artifact occurring at the arrival of the main bolus of contrast agent in the LV were carefully excluded from the segmentation.

Segmental quantitative perfusion analysis was performed using spatially averaged myocardial signal intensity curves according to standard cardiac segmentation. Quantitative perfusion analysis was performed by Fermi deconvolution as previously described. Myocardial blood flow (MBF) was measured in ml/min/g and MRI sequences acquired transmural MBF during hyperaemia and at rest.

2.7.3 MRI ECV Analysis

T₁ mapping by calculation of the extracellular volume is a robust, non-invasive method to quantify diffuse myocardial fibrosis which cannot be seen on late gadolinium enhancement. It avoids the need for myocardial biopsy and can calculate the myocardial contrast volume of distribution which closely reflects the fibrosis burden since collagen is aqueous and gadolinium is an extracellular tracer that can freely occupy this space²⁰².

ECV was calculated from pre-contrast (native) and post-contrast T₁ images. The images were loaded onto Osirix (Version 10.0.2, Pixmeo SARL, Switzerland), and a closed polygon covering the extent of the mid-slice myocardium traced on the scanner-generated T₁ map and a region of interest for the blood pool, producing a T₁ value. The same was carried out on post-contrast T₁ maps, as for native T₁ maps.

ECV was then calculated as¹⁸²:

$$ECV = (1 - \text{haematocrit}) \times [(1/T_{1\text{MyoPC}}) - (1/T_{1\text{MyoNative}})] / [(1/T_{1\text{BloodPC}}) - (1/T_{1\text{BloodNative}})]$$

2.7.4 Computed Tomography Calcium Scoring

METHODS

Computed tomography (CT) calcium scoring was carried out from routine standard of care pre-TAVI turboflash ECG-gated from 75-80% of the R-R interval, non-contrast enhanced, breath-hold, contiguous 3-mm axial CT slices commencing at the base of the valve. Calcium score calculation was carried out using dedicated analysis software (Aquarius iNtuition Edition Ver.4.4.11 TeraRecon) on axial slices, where particular care was taken to differentiate valvular calcium from that originating from extra-valvular structures such as the mitral valve annulus, coronary arteries or the aortic root²⁰³. The total aortic valve calcium score in AU was calculated and subsequently indexed to the body surface area.

2.7.5 Echocardiographic assessment

Left ventricular outflow tract diameter was remeasured by the same operator in the same location for each case (parasternal long-axis view from the inner edge to inner edge of the septal endocardium, and the anterior mitral leaflet in mid-systole²⁰⁴).

Relative wall thickness (RWT) was calculated as (IVSd+PWd)/LVIDd. Left ventricular mass (LVM) by echocardiographic criteria was calculated using the Devereux formula²⁰⁵ and indexed to body surface area to provide left ventricular mass index (LVMI_{ECHO}).

$$LVM (g) = 0.8 \times ([LVIDd + PWd + IVSd]^3 - [LVIDd]^3) + 0.6$$

Doppler stroke volume was estimated (LVOT_{area} × LVOT velocity-time integral) and indexed to body surface area¹⁰¹. This was used to calculate the aortic valve area with the continuity equation (stroke volume/aortic valve velocity-time integral)²⁰⁶.

2.8 Grading aortic stenosis

All patients had symptomatic severe aortic stenosis (AS) with preserved LV function and an aortic valve area ≤1cm². They were categorized into two groups – low gradient (LG) and high gradient (HG) AS. This was carried out by using the aortic valve Doppler-derived

METHODS

mean pressure gradient (MPG) from echocardiography; those with an MPG <40mmHg were classed as having low gradient aortic stenosis⁸⁸. They were not subdivided according to flow since stroke volume according to MRI was significantly higher and most patients with LGAS did not meet criteria of either normal flow (SV >35ml/m²) or low flow (SV ≤35ml/m²)⁸⁹ by both echocardiography and MRI assessment.

METHODS

2.9 Physiological Indices

The parameters used in this study are summarised below in Table 2-4.

Table 2-4: Table of Invasive Indices used in this study

PARAMETER	ABBREVIATION, (units)	CALCULATION	DESCRIPTION
<i>Derived from Pressure-Volume Loop measurements</i>			
End Diastolic Volume	EDV, (ml)		
End Systolic Volume	ESV, (ml)		
End Diastolic Pressure	EDP, (mmHg)		
End Systolic Pressure	ESP, (mmHg)		
Stroke Volume	SV, (ml)	EDV-ESV	
Ejection Fraction	EF, (%)	100 x SV/EDV	
Cardiac Output	CO, (l/min)	SV x heart rate	
Stroke Work	SW, (mmHg.ml)	SV x (Mean pressure – Filling pressure)	Area within PV loop
End Systolic Pressure Volume Relationship	ESPVR, (mmHg/ml)	Pressure:volume ratio at end systole	
End Diastolic Pressure Volume Relationship (mmHg/ml)	EDPVR, (mmHg/ml)	Pressure:volume ratio at end diastole	
Preload recruitable stroke work	PRSW, (mmHg)	SW/EDV	
Potential Energy	PE, (mmHg.ml)	Area between ESPVR and EDPVR curves left of the PV loop i.e. (0.5 x ESP ² /ESPVR)	
Pressure-Volume Area	PVA, (mmHg.ml)	SW + PE	The total mechanical energy of contraction
dP/dt ⁺	(mmHg/s)	Slope of peak maximum derivative of pressure change over time during isovolumetric contraction	
dP/dt ⁻	(mmHg/s)	Slope of peak minimum rate of pressure change over time during isovolumetric relaxation	

METHODS

<i>Starling Contractile State Index</i>	SCI, (mmHg/ml/s)	dP/dt ⁺ /EDV	
<i>Relaxation Time Constant</i>	Tau (τ), (ms)	Time for dP/dt ⁺ to be reduced by 1/e (e=the natural base of log)	
<i>Effective Arterial Elastance</i>	E _a , (mmHg/ml)	ESP/SV	Index of afterload
<i>End Systolic (maximal) Elastance</i>	E _{es} , (mmHg/ml)	The slope of ESPVR	Load-independent measure of LV contractility
<i>Ventricular–Arterial Coupling</i>	VA	E _{es} /E _a	Index of energy efficiency
<i>Valvulo-arterial Impedance</i>	Z _{va} , (mmHg/ml/m ²)	ESP/SVi	Index of global haemodynamic load
<i>Derived from coronary measurements</i>			
<i>Distal Coronary Pressure</i>	Pd, (mmHg)		
<i>Aortic Pressure</i>	Pa, (mmHg)		
<i>Instantaneous peak velocity</i>	IPV, (cm/s)	Minimum and maximum values, sampled every 5ms (200Hz)	
<i>Average peak velocity</i>	APV, (cm/s)		
<i>Velocity-time integral</i>	VTI, (cm)	Integral under the IPV curve	
<i>Coronary flow reserve</i>	CFR	Hyperaemic APV/resting APV	
<i>Microvascular Resistance (mmHg/cm/s)</i>	MR, (mmHg.s/cm)	Mean Pd/APV	
<i>Wave-free Microvascular Resistance (mmHg/cm/s)</i>	MR _{dias} , (mmHg.s/cm)	Microvascular resistance during the wave free period in diastole	
<i>Systolic Resistance</i>	SR, (mmHg.s/cm)	Pd _{systole} /V _{systole}	
<i>Augmentation Pressure (mmHg)</i>	AP, (mmHg)	P2-P1	
<i>Augmentation Index (%)</i>	AIx, (%)	AP/PP x 100	
<i>Diastolic Time Fraction</i>	DTF	Diastolic time/cardiac cycle time	
<i>Tension Time Index</i>	TTI, (mmHg.s)	Area under the curve of systole	Marker of myocardial oxygen demand
<i>Diastolic Time Index</i>	DTI, (mmHg.s)	Area under the curve of diastole	Marker of coronary perfusion
<i>Buckberg Index</i>	BI	DTI/TTI x 100	Subendocardial viability ratio
<i>Rate Pressure Product</i>	RPP, (mmHg.bpm)	BP/HR	
<i>Reflection Coefficient</i>	Γ		Measure of reflected waves

2.10 Statistical Analysis

Statistical analysis was performed using SPSS version 26.0 software (IBM SPSS Statistics, Chicago, IL, USA). Data were assessed for normality of (Gaussian) distribution both graphically with a histogram, and also by use of the Shapiro-Wilk test. Results were presented as mean \pm standard deviation when data were normally distributed, and non-normal continuous data were expressed as median with interquartile range.

Independent results were compared using Mann-Whitney U test, and the Wilcoxon signed-rank test used for paired samples. Continuous variables with normal distribution were compared with the independent and paired-samples Student T test. Repeated measures analysis of variance was not used – this was due to lack of normal distribution for some of the data, and that I was mostly interested in direct comparisons of two groups rather than between multiple groups. This does, however, come at a risk of a larger overall type I error rate. Categorical variables were presented as number and percentage and were compared using the chi-square test or Fishers exact test. Correlations between normally distributed data were performed using Pearson's correlation, whilst Spearman's correlation was used for non-parametric data. A two-sided significance level of $P < 0.05$ was considered statistically significant.

3 STUDY PATIENTS

STUDY PATIENTS

Following successful HRA, REC and R&D approval, patients were recruited between January 2017 and December 2018. Figure 3-1 summarises the screened and recruited patients who were all deemed to have severe, symptomatic aortic stenosis by the Heart Team in a large tertiary centre. All patients were in sinus rhythm with no apparent conduction disease on their resting pre-TAVI ECG. Intra-coronary adenosine was not given pre-TAVI in one patient, and another patient died from Influenza A prior to the follow-up scan. Table 3-1 summarises baseline characteristics in the 19 final patient datasets. Comparing echocardiographic and MRI left ventricular (LV) assessment, there is discrepancy between stroke volume results and therefore the sub-categorisation of low gradient aortic stenosis (LGAS). In view of this, and because of the small study numbers, subdivision into normal flow-low gradient, and low flow-low gradient AS was not used in analysis.

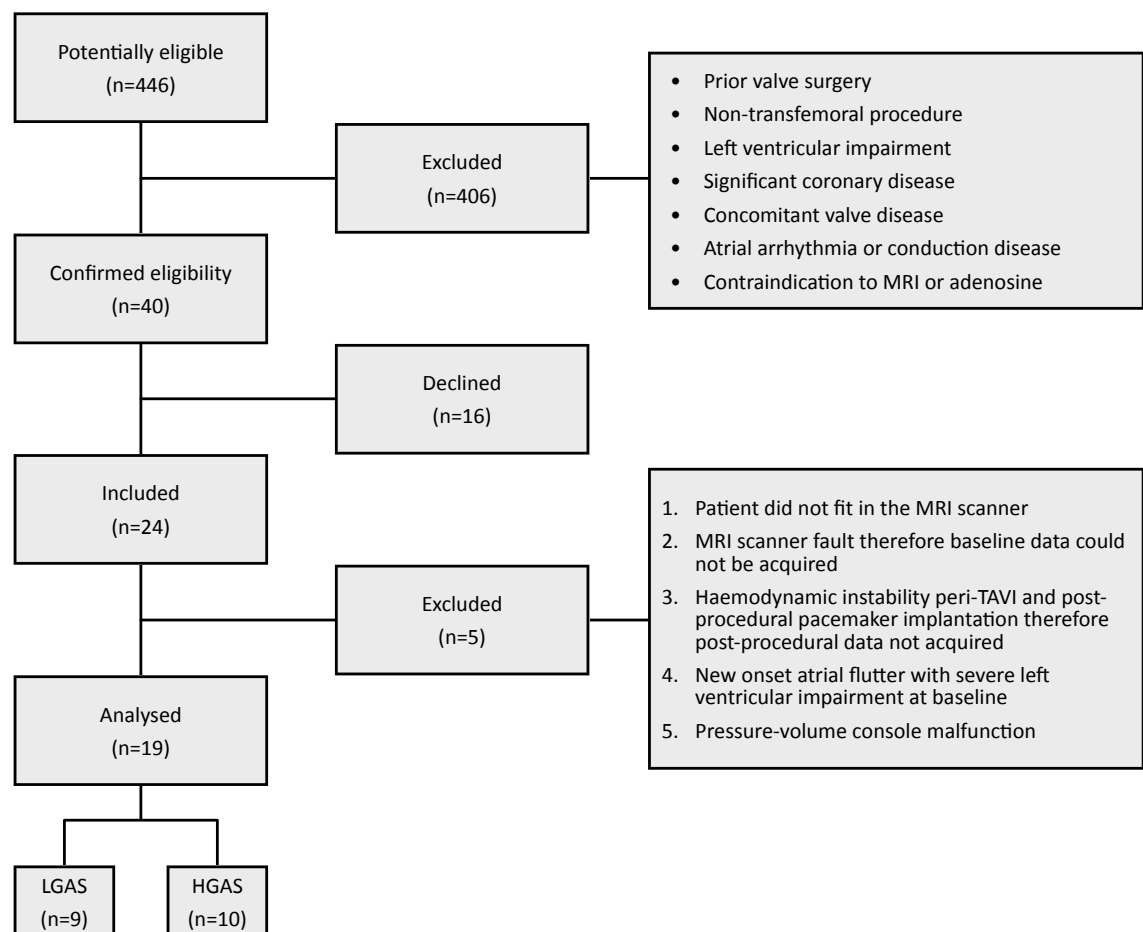


Figure 3-1: Study flow chart of patient recruitment

STUDY PATIENTS

Table 3-1: Baseline characteristics of 19 analysed patient results

Demographics								Baseline Echocardiographic Findings					Baseline MRI Findings					CT
Age	HTN	DM	COPD	CVD	Symptom	Resting HR (bpm)	Resting BP (mmHg)	MPG (mmHg)	DI	AVAi (cm ² /m ²)	SVi (ml/m ²)	LF/NF	SVi (ml/m ²)	LVEDVi (ml/m ²)	LVMi (g/m ²)	LVEF (%)	LF/NF	Calcium Score (AU)
72	-	Y	-	Y	SOB	75	112/54	27	0.235	0.366	30.0	LF	42.1	71.4	45	59	NF	1052
90	Y	Y	-	-	SOB, Syncope	66	138/97	35	0.250	0.377	18.5	LF	37.59	61.74	42.32	61	NF	2813
82	Y	Y	-	-	SOB, CP	80	165/70	33	0.256	0.554	46.9	NF	54.28	79.4	60.65	68.35	NF	1436
82	Y	-	Y	-	SOB, CP	77	133/57	35	0.260	0.571	54.4	NF	46.23	78.15	66.09	59	NF	3625
88	Y	-	-	-	SOB	77	165/68	29.8	0.359	0.508	47.6	NF	54.39	82	60.36	66.32	NF	2720
89	-	Y	Y	Y	SOB	80	158/62	22	0.361	0.333	25.8	LF	46.73	72.97	58.56	64.04	NF	1486
79	Y	Y	Y	Y	SOB	70	155/88	38	0.205	0.301	30.8	LF	27.05	38.6	49.81	70.07	LF	3745
88	Y	-	-	-	SOB	61	152/68	33	0.267	0.428	34.2	LF	44	67	64.37	64	NF	1935
90	Y	Y	-	-	SOB	70	174/69	35	0.296	0.584	56.0	NF	43.84	63.66	59.56	68.87	NF	1007
HIGH GRADIENT																		
88	-	-	-	-	SOB	77	114/53	96	0.150	0.356	56.7	NF	56.24	89.55	66.46	63	NF	2839
84	Y	Y	-	-	SOB, CP	80	158/80	47.8	0.293	0.386	49.9	NF	57.87	87.43	59.14	66.2	NF	2809
87	Y	Y	-	-	SOB	64	152/84	76	0.184	0.306	48.8	NF	63.66	97.75	90.44	65	NF	3847
76	Y	-	-	-	Syncope	74	122/53	105	0.111	0.202	40.5	NF	44.75	76.95	70.15	58	NF	2506
90	Y	-	-	-	SOB, Syncope	70	122/54	46	0.264	0.539	53.6	NF	35.79	50.06	40.81	71.5	NF	3155
88	Y	-	-	-	SOB	60	191/74	59	0.238	0.322	43.9	NF	53.53	83.5	75.3	61.6	NF	2652
85	-	-	-	Y	SOB	63	104/54	42	0.244	0.370	32.8	LF	47.79	83.72	71.26	57.09	NF	5760
90	Y	-	-	-	Syncope, CP	68	155/71	69	0.174	0.275	33.1	LF	47	82.26	66.42	57.12	NF	6352
79	-	-	Y	-	SOB	63	123/55	47	0.200	0.332	33.0	LF	44.34	74.69	62.73	59.37	NF	2787
85	-	-	-	-	SOB, CP	70	118/51	78	0.144	0.290	36.2	NF	50.49	100.81	108.35	50.29	NF	6193

Abbreviations: LG: low gradient, HG: high gradient, HTN: hypertension, DM: diabetes mellitus, COPD: chronic obstructive airways disease, CVD: cerebrovascular disease, SOB: shortness of breath, CP: chest pain, MPG: mean pressure gradient, DI: dimensionless index, AVAi: indexed aortic valve area, SVi: indexed stroke volume, LF: Low Flow, NF: Normal Flow, LVEDVi: indexed left ventricular end diastolic volume, LVMi: indexed left ventricular mass, LVEF: left ventricular ejection fraction, PLS: peak longitudinal strain, AU: Agatston units, Y: yes.

STUDY PATIENTS

Table 3-2: Baseline Characteristics: LFLG vs HGAS

Baseline Characteristics	LGAS (n=9)	HGAS (n=10)	P value
Age (years)	84±6	85±5	0.768
Male (%)	33	10	0.303
Mean aortic valve pressure gradient (mmHg)	32±5	67±22	<0.001
Indexed aortic valve area (cm ² /m ²)	0.490	0.336	0.008
Body Surface Area (m ²)	1.83±0.17	1.71±0.13	0.097
Non-invasive systolic blood pressure (mmHg)	150±19	136±27	0.198
Diabetes mellitus (%)	67	20	0.070
Hypertension (%)	78	60	0.628
Prior stroke (%)	33	10	0.303
Obstructive airways disease (%)	33	10	0.303
Haemoglobin (g/l)	125 (112,130)	124 (113,136)	0.604
eGFR (ml/min)	57±21	63±18	0.751
TAVI anaesthesia: conscious sedation	89	90	0.942
Pre-TAVI BNP (ng/l)	720 (369,983)	1355 (935,6957)	0.058
Post-TAVI BNP (ng/l)	530 (290,915)	500 (144,1457)	0.950
LV end diastolic volume index (ml/m ²)	76 (60,80)	83 (75,87)	0.010
LV mass index (g/m ²)	56.3±8.5	71.1±18.1	0.037
LV ejection fraction (%)	64.5±4.2	60.9±5.9	0.143
CT calcium score (Ag units)	2328 (1474,3655)	2982 (2686,6085)	0.028
Indexed CT calcium score (Ag/m ²)	1152 (825,1924)	1799 (1581,3383)	0.017

Error! Reference source not found. displays baseline characteristics for the two cohorts, dichotomised according to the mean aortic valve pressure gradient ($p<0.001$). Further detail regarding MRI baseline results is displayed in Table 5-2. There was no significant difference between groups with regard to age, sex, body surface area, or co-morbidities of hypertension, prior stroke, diabetes mellitus, airways disease or renal dysfunction. Not all patients had available BNP levels. LV cavity size and wall mass, along with aortic valve calcium score were significantly lower in LGAS patients.

4 ISCHAEMIA IN AORTIC STENOSIS

4.1 Introduction

In the setting of severe aortic stenosis (AS), encompassing a cluster of different phenotypes based on gradient and flow patterns, the left ventricle is a disordered tumult of supply-demand mismatch. Prolonged systole (and the relative shortening of diastolic perfusion time) due to outflow tract obstruction, and the inability to increase coronary blood flow in proportion to excess cardiac demand, subject the myocardium to stress-induced ischaemia, manifest as exertional angina, or dyspnoea in some cases.

Coronary flow reserve (CFR), the ratio of coronary average peak velocity (APV) during hyperaemia and at rest, is a measure of vasodilator capacity. This is significantly reduced in patients with AS, since most have needed to increase resting flow to compensate for increased myocardial requirement.

The mechanism whereby AS induces ischaemia was examined and the hypothesis of depressed accelerating coronary waves and higher systemic concentration of lactate and troponin in low gradient AS tested. In this chapter, I present the invasive and non-invasive determinants of ischaemia in the setting of AS, and whether any differences exist in patients with low gradient (LGAS) and high gradient AS (HGAS).

4.1.1 Invasive Physiology

The arterial bed determines pressure and flow based on resistance, compliance and inertance. This area has been extensively described and methods applied to study the pathophysiology of disease processes. The arterial waveform, as depicted in Figure 4-1, reflects the change in pressure over time (dP/dt , measured in mmHg/s) and relates to the force of LV contraction (dP/dt^+) and relaxation (dP/dt^-). The steeper the slope, the quicker the rise or fall, the greater the dP/dt , and therefore the stronger the inotropy or lusitropy²⁰⁷. The first derivative of aortic pressure (dP/dt^+) is slowed by AS²⁰⁸ (Figure 4-2) – this slurred systolic upstroke is known as *pulsus tardus*²⁰⁹. There is a delay in peak systole (*pulsus tardus*), and arterial pressure may be small in amplitude (*pulsus parvus*).

ISCHAEMIA IN AORTIC STENOSIS

During upstroke, the anacrotic notch corresponds to reflected waves from poorly compliant vessels – the position of the anacrotic notch on the arterial upstroke is not correlated with the severity of AS²⁰⁸. The dicrotic notch is often indiscernible in AS.

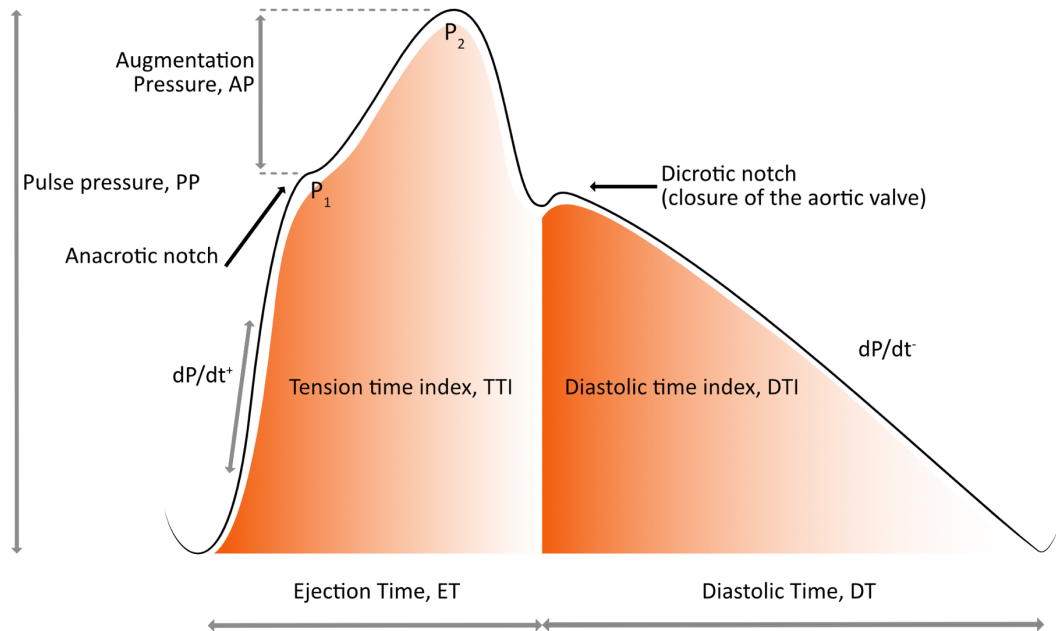


Figure 4-1: The aortic waveform and associated derivations

Left ventricular ejection time (ET) is measured from the upstroke of the arterial tracing until the trough of the dicrotic notch, and diastolic time (DT) accounts for the remainder of the cardiac cycle. The percentage of the pulse pressure formed by the augmentation pressure (AP, difference between early [P1] and late [P2] pressures) is known as the augmentation index and is a marker of pulsatile afterload. Increased augmentation index is indicative of arterial stiffness²¹⁰, along with a diminished reflected wave (the dicrotic notch).

The area under the curve (AUC) of systole is known as the tension time index (TTI) and the AUC of diastole known as the diastolic time index (DTI). The TTI relates to myocardial oxygen demand²¹¹, and DTI to coronary perfusion. The Buckberg Index (BI) is the ratio of demand and supply, and also known as the subendocardial viability ratio²¹². It has been shown to correlate well with the ratio of subepicardial to subendocardial blood flow, and

ISCHAEMIA IN AORTIC STENOSIS

represents an index of subendocardial viability²¹³. A lower BI indicates an increased risk of subendocardial ischaemia and can be used as a determinant of such, and valvuloplasty has previously been shown to increase baseline BI²¹⁴.

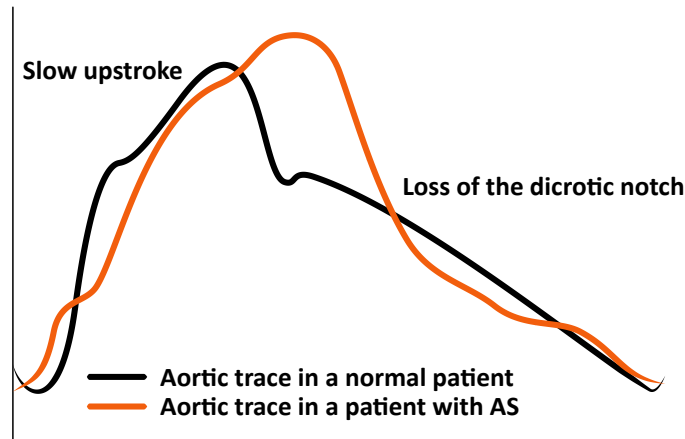


Figure 4-2: Differences in aortic waveform in normal and aortic stenosis

Impaired CFR in AS is likely to result from both increased basal flow and blunted hyperaemic flow, related to capillary rarefaction, mechanical forces, and reduced diastolic time fraction. It has been shown that CFR does not improve immediately after relief of valve obstruction³⁵ but improves after 1 year⁷⁸. Other studies have also demonstrated improved subendocardial blood flow at 2 weeks⁴⁹, CFR at 6 months⁷⁶ and myocardial perfusion reserve index (MPRI) at 8 months⁴⁵ following valve replacement.

4.1.2 Wave intensity analysis

Coronary blood flow is unique (Figure 4-3). It is intensely coupled with the myocardium and cardiac cycle and as a result it is not simply driven down a pressure gradient toward a passive capillary bed but pushed and pulled into and from the distal microvasculature²¹⁵. Wave intensity assesses the rate of energy per unit area transferred by fluid waves. It allows mechanistic insight into this coupling between cardiac contraction and coronary supply and is typically applied both for the separation of measured waves into forward and backward travelling components, and for the interpretation of the timing and nature (compression/expansion) of wave reflections²¹⁶.

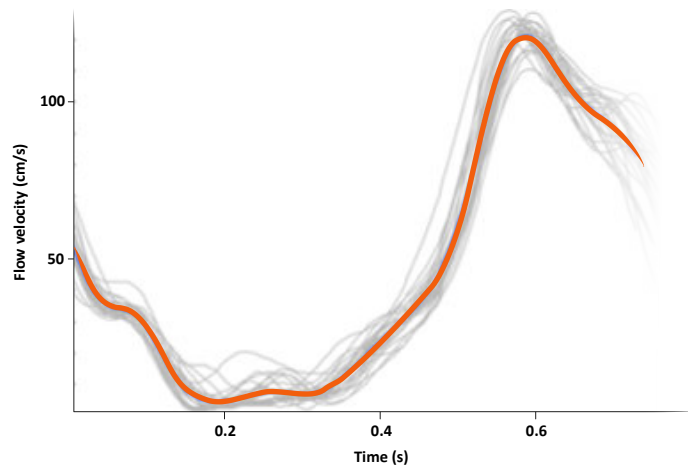


Figure 4-3: A typical flow velocity waveform at rest in a patient with severe AS. There is almost entirely diminished flow during systole.

Wave intensity has been extensively studied in healthy hearts and in an array of disease processes – AS¹⁹, transcatheter aortic valve implantation (TAVI)^{34,35,60}, hypertrophic cardiomyopathy³⁶, left ventricular hypertrophy (LVH)³³, prediction of myocardial viability following acute coronary syndromes³⁷, dyssynchronous heart failure³⁸, intra-aortic balloon pump therapy²¹⁷, warm-up³⁹, nitroglycerin⁴⁰, mental stress⁴¹ and cold stress²¹⁸.

Lumley *et al*¹⁹ studied WIA in patients with AS in comparison to normal hearts and found, as expected, reduced forward travelling waves (both FCW and FEW), but, with both hyperaemia and exercise, a greater increase in FEW in patients with AS. Patients with AS rely more on coronary flow related to BEW which has a significantly higher contribution to overall WI in comparison to that in normal hearts.

4.1.3 Other Invasive Indices of Ischaemia

The overall proportion of waves that accelerate and decelerate flow can be calculated:

$$\text{Accelerating wave proportion (\%)}: (FCW + BEW)/(FCW + FEW + BEW + BCW)$$

$$\text{Decelerating wave proportion (\%)}: (FEW + BCW)/(FCW + FEW + BEW + BCW)$$

The accelerating wave proportion is known as the coronary perfusion efficiency index

(PE)¹⁹, a metric to quantify accelerating waves by the magnitude of the areas under the curve (AUCs) of the component waves.

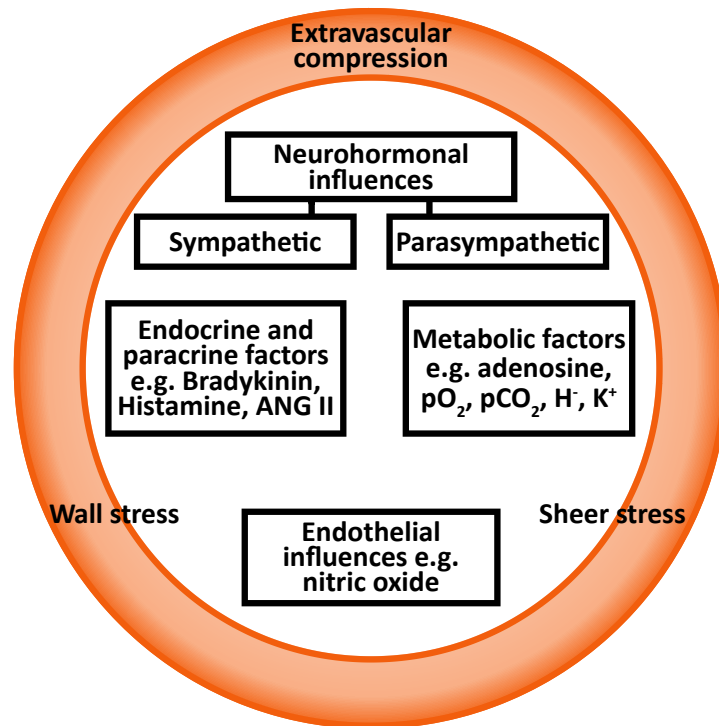


Figure 4-4: Considerations relating to microvascular resistance and tone

Wave intensity analysis also enables identification of microvascular resistance (MR) during the wave-free period in diastole (MR_{dias}). During this part of the cardiac cycle, intra-myocardial compressive forces are at their lowest, and this may more closely reflect vascular tone²¹⁹. MR is defined as the ratio between distal coronary pressure and flow velocity, and hyperaemic MR (hMR) reflects this ratio during hyperaemia²²⁰. An hMR threshold of ≥ 2.5 mmHg/cm/s is optimal for predicting microvascular dysfunction determined by CFR and MPRI²²¹.

4.1.4 Non-Invasive Indices of Ischaemia

Microvascular ischaemia is one of the hallmarks of AS, and can be diagnosed using non-invasive imaging modalities, including positron emission tomography (PET)⁴⁶, and first-pass perfusion cardiovascular magnetic resonance (CMR)⁷⁷. CMR is a powerful tool in its ability to provide information on cardiac volumes and function, fibrosis and ischaemia.

ISCHAEMIA IN AORTIC STENOSIS

Myocardial perfusion reserve index (MPRI, the ratio of stress perfusion myocardial blood flow to resting perfusion myocardial blood flow) has an inverse relationship with left ventricular hypertrophy and the presence of late gadolinium enhancement, and a positive correlation with aortic valve area⁴⁵. Transmural left ventricular myocardial perfusion is a relative crude measure of MBF since large differences exist between the subepicardium and the subendocardium. Important considerations may be glossed over if we purely assess the global transmural perfusion as MPRI.

It is assumed that serum from the coronary sinus reflects venous cardiac metabolism. Previous studies have demonstrated normal coronary sinus lactate at rest in patients with AS, but under metabolic stress, a decrease in lactate extraction or increase in lactate production^{72,193}. Under increased myocardial requirements, the coronary circulation is incapable of fully matching increased demand. This is commonly the case in patients with coronary artery disease or severe AS, despite compensation at rest – an inability to meet increased metabolic demand²²². Measurement of trans-cardiac release of biomarkers at rest and during pharmacological and haemodynamic stress is an attempt to determine ischaemic abnormalities.

Troponin is a component of thin filaments (along with actin and tropomyosin) and is the protein to which calcium binds to accomplish contraction and relaxation. Cardiac injury in the form of myocyte death can be detected by highly sensitive and specific cardiac biomarkers. In the setting of AS, plasma Troponin-I levels are associated with advanced hypertrophy and replacement fibrosis and predict aortic valve intervention and cardiovascular death¹³⁷. In a large cohort of patients with AS, another highly sensitive marker of myocardial injury, cMyC, has also been shown to correlate with left ventricular mass, fibrosis volume and extracellular volume and associated with all-cause mortality¹⁷⁴.

Valvuloplasty has previously been shown to reduce myocardial oxygen consumption and demand, decreasing aorto-coronary sinus oxygen content difference, and reduce lactate productions under stress conditions²¹⁴. Lactate values below 10% indicate abnormally

reduced extraction, or production (if a negative value) by the myocardium, signalling anaerobic glycolysis due to myocardial hypoxia.

4.2 Results

4.2.1 Aortic and Coronary Physiology in AS

The effects of hyperaemia and pacing from baseline measurements, along with the impact of TAVI on these respective physiological settings are displayed in Table 4-1, Table 4-2 and Table 4-3.

Coronary VTI and APV increased, and MVR decreased both pre- and post-TAVI during hyperaemia, as expected. Pre-TAVI, hyperaemia and rapid pacing induced a fall in BI, an effect which was not observed following TAVI. Pre- and post-TAVI, rapid pacing lowered systolic BP, coronary VTI, TTI, DTI, DTF and shortened ET.

During resting state and hyperaemia, TAVI induced a drop in coronary VTI and APV. Under conditions of rapid pacing, TAVI induced a significant increase in BI ($p=0.008$), diastolic time fraction ($p=0.004$), DTI ($p=0.055$), shortening of the ejection time ($p=0.020$) along with a decrease in TTI ($p=0.045$). TAVI also caused an increase in MR at baseline ($p=0.001$).

ISCHAEMIA IN AORTIC STENOSIS

Table 4-1: The haemodynamic impact of hyperaemia pre- and post-TAVI from all paired datasets

	Pre-TAVI			Post-TAVI		
	<i>Rest</i>	<i>Hyperaemia</i>		<i>Rest</i>	<i>Hyperaemia</i>	
<i>Heart rate (bpm)</i>	78 (68,85)	80 (73,90)	P=0.073	76 (67,85)	80 (73,87)	NS
<i>sBP_{Ao} (mmHg)</i>	117 (102,134)	123 (104,149)	NS	123 (113,131)	133 (108,170)	NS
<i>VTI_{coro} (cm)</i>	19 (15,22)	24 (20,32)	P<0.001	13 (10,16)	22 (16,30)	P<0.001
<i>APV_{coro} (cm/s)</i>	23 (19,27)	30 (26,42)	P<0.001	17 (15,22)	28 (20,34)	P<0.001
<i>BI</i>	0.75±0.25	0.61±0.22	P=0.020	0.71±0.19	0.74±0.38	NS
<i>ET (s)</i>	0.40±0.07	0.43±0.06	NS	0.38±0.06	0.42±0.14	NS
<i>DTF</i>	0.49±0.10	0.43±0.11	P=0.059	0.50±0.08	0.47±0.15	NS
<i>TTI (mmHg.s)</i>	37 (29,44)	39 (32,46)	NS	35 (31,40)	40 (30,55)	NS
<i>DTI (mmHg.s)</i>	26±8	26±12	NS	25±6	32±23	NS
<i>MR (mmHg.s/cm)</i>	3.1 (2.5,4.2)	2.2 (1.7,3.4)	P=0.001	4.2 (3.4,5.4)	2.4 (2.0,3.3)	P<0.001
<i>MR_{dias} (mmHg.s/cm)</i>	1.7 (1.2,2.5)	1.2 (0.8,2.0)	P=0.014	2.3 (1.6,3.1)	1.2 (1.0,2.3)	P<0.001

Table 4-2: The haemodynamic impact of pacing pre- and post-TAVI from all paired datasets

	Pre-TAVI			Post-TAVI		
	<i>Rest</i>	<i>Pacing</i>		<i>Rest</i>	<i>Pacing</i>	
<i>Heart rate (bpm)</i>	78 (68,85)	126 (124,129)	P<0.001	76 (67,85)	126 (124,130)	P<0.001
<i>sBP_{Ao} (mmHg)</i>	117 (102,134)	107 (85,128)	P=0.008	123 (113,131)	100 (83,126)	P<0.001
<i>VTI_{coro} (cm)</i>	19 (15,22)	11 (8,14)	P<0.001	13 (10,16)	9 (7,10)	P<0.001
<i>APV_{coro} (cm/s)</i>	23 (19,27)	21 (16,30)	NS	17 (15,22)	18 (15,21)	NS
<i>BI</i>	0.68 (0.56,0.93)	0.41 (0.25,0.58)	P<0.001	0.72±0.19	0.70±0.40	NS
<i>ET (s)</i>	0.41±0.07	0.32±0.05	P<0.001	0.38±0.06	0.27±0.07	P<0.001
<i>DTF</i>	0.51 (0.44,0.54)	0.32 (0.22,0.40)	P<0.001	0.50±0.08	0.44±0.15	P=0.036
<i>TTI (mmHg.s)</i>	37 (29,44)	30 (20,34)	P<0.001	35 (31,40)	22 (17,30)	P<0.001
<i>DTI (mmHg.s)</i>	27±11	11±4	P<0.001	26±6	14±5	P<0.001
<i>MR (mmHg.s/cm)</i>	3.1 (2.5,4.2)	3.3 (2.5,4.9)	P=0.096	4.2 (3.4,5.4)	4.4 (3.2,4.8)	NS
<i>MR_{dias} (mmHg.s/cm)</i>	1.7 (1.2,2.5)	2.5 (1.8,3.9)	P=0.001	2.3 (1.6,3.1)	3.7 (2.4,4.7)	P=0.003

ISCHAEMIA IN AORTIC STENOSIS

Table 4-3: The haemodynamic impact of TAVI during three physiological states from all paired datasets

	Baseline			Hyperaemia			Pacing		
	<i>Pre-TAVI</i>	<i>Post-TAVI</i>		<i>Pre-TAVI</i>	<i>Post-TAVI</i>		<i>Pre-TAVI</i>	<i>Post-TAVI</i>	
<i>Heart rate (bpm)</i>	78 (68,85)	76 (67,85)	NS	80 (73,90)	80 (73,87)	NS	126 (124,129)	126 (124,130)	NS
<i>sBP_{Ao} (mmHg)</i>	117 (102,134)	123 (113,131)	NS	123 (104,149)	133 (108,170)	NS	107 (85,128)	100 (83,126)	NS
<i>VTI_{coro} (cm)</i>	18 (15,22)	13 (10,16)	P=0.001	24 (20,32)	20 (15,26)	P=0.018	11 (8,14)	9 (7,10)	NS
<i>APV_{coro} (cm/s)</i>	23 (18,28)	17 (14,22)	P=0.012	30 (26,42)	28 (19,32)	P=0.024	21 (16,30)	18 (15,21)	NS
<i>BI</i>	0.74±0.25	0.72±0.19	NS	0.62±0.22	0.75±0.39	NS	0.41 (0.25,0.58)	0.56 (0.47,0.98)	P=0.008
<i>ET (s)</i>	0.41±0.07	0.38±0.06	NS	0.43±0.06	0.42±0.15	NS	0.32±0.05→	0.27±0.07	P=0.020
<i>DTF</i>	0.48±0.09	0.50±0.08	NS	0.44±0.10	0.47±0.15	NS	0.32 (0.22,0.40)	0.43 (0.38,0.54)	P=0.004
<i>TTI (mmHg.s)</i>	37 (29,44)	35 (31,40)	NS	39 (32,46)	40 (30,55)	NS	30 (20,34)	22 (17,30)	P=0.045
<i>DTI (mmHg.s)</i>	27±11→	26±6	NS	25±11	32±23	NS	11±4	14±5	P=0.055
<i>MR (mmHg.s/cm)</i>	3.1 (2.5,4.2)	4.2 (3.4,5.4)	P=0.001	2.2 (1.7,3.4)	2.4 (2.0,3.3)	NS	3.3 (2.5,4.9)	4.4 (3.2,4.8)	NS
<i>MR_{dias} (mmHg.s/cm)</i>	1.7 (1.2,2.5)	2.3 (1.6,3.1)	P=0.003	1.2 (0.8,2.0)	1.2 (1.0,2.3)	NS	2.5 (1.8,3.9)	3.7 (2.4,4.7)	P=0.055

Table 4-4: Coronary and aortic haemodynamic indices in LGAS and HGAS cohorts. Results displayed when P<0.010 for LGAS then HGAS with SD or IQR in brackets.

	Pre-TAVI		Post-TAVI		Pre-TAVI		Post-TAVI	
	REST				HYPERAEMIA			
HR (bpm)		NS		NS		NS		NS
sBP _{Ao} (mmHg)		NS		NS		NS		NS
VTI _{coro} (cm)	16(12,18)/21(18/29)	P=0.006		NS		NS	18±7/27±13	P=0.087
APV _{coro} (cm/s)	20(15,23)/26(22,32)	P=0.022		NS		NS		NS
BI		NS		NS		NS		NS
ET (s)	0.36(0.34,0.39)/0.44(0.38,0.49)	P=0.022		NS		NS		NS
DTF	0.53(0.49,0.56)/0.45(0.36,0.54)	P=0.053		NS		NS		NS
TTI (mmHg.s)		NS		NS		NS		NS
DTI (mmHg.s)		NS		NS	29(21,43)/20(14,32)	P=0.094		NS
MR (mmHg.s/cm)	3.9±1.2/2.9±1.0	P=0.070		NS		NS		NS
MR _{dias} (mmHg.s/cm)	2.5±0.9/1.5±0.6	P=0.012	3.1(1.8,3.9)/2.1(1.5,2.5)	P=0.065		NS	2.1±1.0/1.1±0.4	P=0.025
HMR (mmHg.s/cm)						NS	3.2(2.3,3.6)/2.1(1.9,3.0)	P=0.095

ISCHAEMIA IN AORTIC STENOSIS

Results concerning differences between LGAS and HGAS groups are displayed in Table 4-4. Coronary VTI and APV were lower in LGAS patients and ejection time significantly shorter ($p=0.022$). Following TAVI during hyperaemia, diastolic MR was higher in LGAS patients. There were no differences observed between groups during rapid pacing both pre-TAVI and post-TAVI.

4.2.2 Subendocardial Viability

The BI fell with hyperaemia ($p=0.020$, Table 4-1) and rapid pacing ($p<0.001$, Table 4-2) pre-TAVI, yet when rapid pacing before and after TAVI were compared, BI increased ($p=0.008$, Table 4-3). From rest pre-TAVI and post-TAVI, the relative increase in TTI in LGAS in comparison to a decrease in HGAS ($+12\pm13\%$ vs $-12\pm16\%$, $p=0.002$), reflects a relative decrease in BI ($-11\pm20\%$ vs $+24\pm48\%$, $p=0.058$), and raises the suspicion of increased susceptibility to ischaemia and myocardial oxygen supply-demand mismatch in LGAS. This predisposition to ischaemia was further supported by a lack of change in DTF post-TAVI in LGAS but an increase in HGAS (-1% $[-19,+4]$ vs $+11\%$ $[0,29]$, $p=0.053$). Ejection time remained similar in LGAS but was significantly shortened in HGAS patients ($+3\pm11\%$ vs $-14\pm11\%$, $p=0.003$).

4.2.3 Coronary Flow Reserve

CFR was assessed immediately before, and immediately following TAVI. It did not change significantly following TAVI (overall 1.42 ± 0.44 to 1.52 ± 0.41 , $p=0.460$). There was no difference between the pre-TAVI CFR (1.49 ± 0.53 vs 1.3 ± 0.35 , $p=0.522$) and post-TAVI CFR (1.48 ± 0.35 vs 1.61 ± 0.47 , $p=0.473$) in low gradient and high gradient cohorts, respectively (Figure 4-5), or their delta change ($p=0.546$).

There was significant correlation between pre-TAVI CFR and resting EDP ($R=-0.494$, $p=0.044$), global MPR ($R=-0.497$, $p=0.036$), Tau ($R=-0.588$, $p=0.013$) and microvascular resistance (pancardiac MR $R=-0.549$, $p=0.018$, diastolic MR $R=-0.641$, $p=0.004$ and hyperaemic MR $R=-0.657$, $p=0.003$).

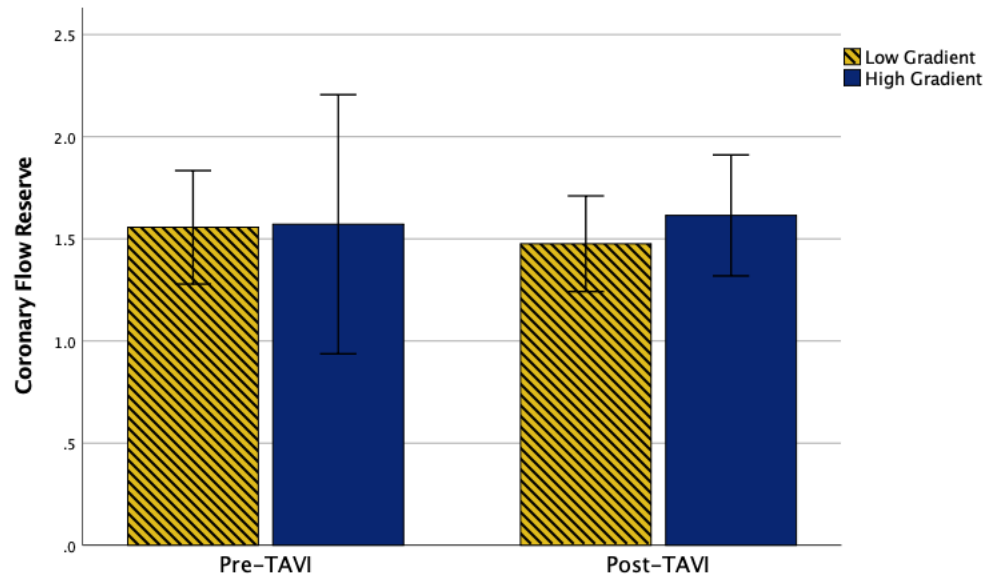


Figure 4-5: CFR results

4.2.4 Microvascular Resistance

Both the pancardiac and diastolic coronary MR were calculated. There was a significant reduction in pancardiac and diastolic MR from rest during hyperaemia pre-TAVI ($p=0.001$ and $p=0.014$, respectively) and post-TAVI ($p<0.001$ for both) (Figure 4-6), with no difference in the delta change pre-TAVI from rest between groups ($p=0.387$). There was no difference between hMR pre- and post-TAVI ($2.2 [1.7,3.4]$ vs $2.4 [2.0,3.3]$, $p=0.154$), nor between groups pre-TAVI (2.65 ± 0.76 in LGAS vs 2.33 ± 1.03 in HGAS, $p=0.462$) or post-TAVI ($3.2 [2.3,3.5]$ vs $2.1 [2.0,3.0]$, $p=0.095$). Following intervention, wave-free hyperaemic microvascular resistance was higher in LGAS patients ($p=0.025$), suggesting underlying endothelial dysfunction.

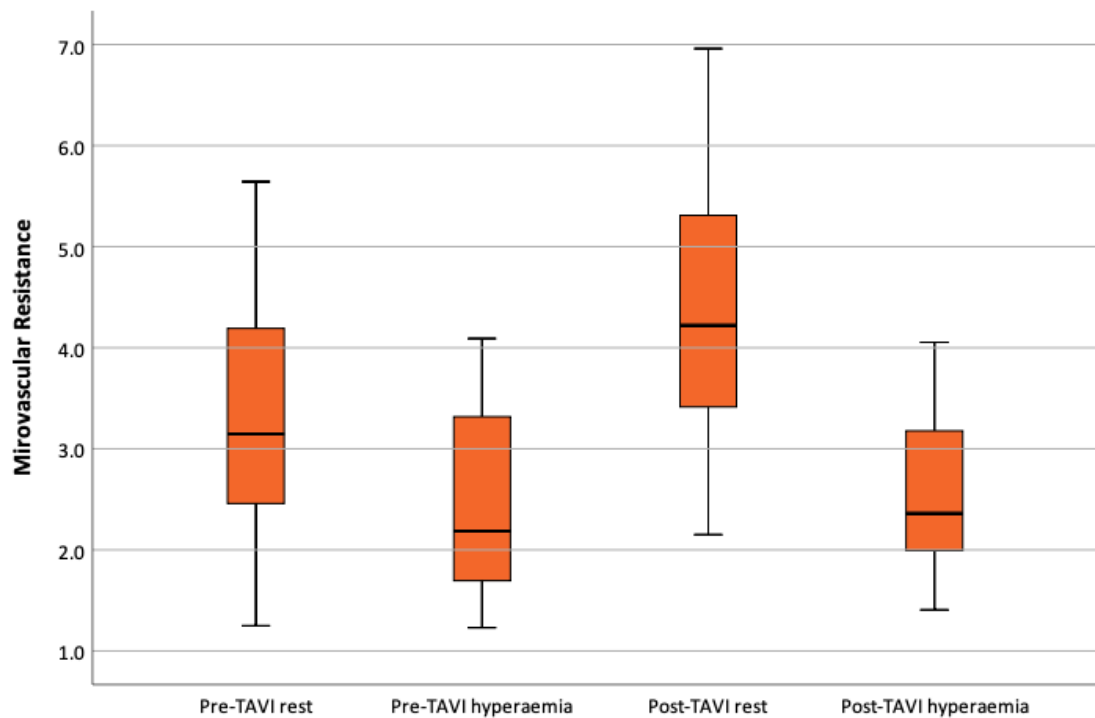


Figure 4-6: Pan-cardiac microvascular resistance pre- and post-TAVI

4.2.5 Wave Intensity Analysis during hyperaemia, pacing and following TAVI

Results for all patients are displayed in Table 4-5, Table 4-6 and Table 4-7. Before TAVI, hyperaemia caused an increase in accelerating FCW and BEW, and decelerating BCW. There was an overall increase in the proportion of accelerating waves ($p=0.024$). Post-TAVI, the impact of hyperaemia was certainly less impressive, with minimal statistical significance in changes in WIA aside from increased BCW, and greater area under forward travelling ($p=0.023$) and above backward travelling ($p=0.018$) waves.

Pre- and post-TAVI, rapid pacing at 120bpm caused a reduction in forward travelling waves ($p<0.001$ and $p=0.003$, respectively). The most dramatic effect was with decelerating waves: there was a reduction in FEW pre-TAVI (possibly purely related to reduced forward flow in the aorta and not observed post-TAVI after relief of outflow tract obstruction) but a sustained increase in BCW, culminating in a greater proportion of decelerating waves both pre- and post-TAVI ($p=0.005$ and $p=0.007$, respectively).

ISCHAEMIA IN AORTIC STENOSIS

The main differences when assessing the effect of TAVI were more profound during hyperaemia. The BEW fell sharply and there was a huge drop in accelerating waves which accounted for a smaller proportion of coronary flow ($p=0.001$), related almost entirely to the fall in backward travelling waves. Even comparing pre- and post-TAVI during rapid pacing, the proportion of accelerating waves dropped after intervention.

Pre-TAVI, BEW during hyperaemia correlated with DTI ($R=0.581$, $p=0.011$), aortic Alx ($R=-0.488$, $p=0.040$), aortic AP ($R=-0.564$, $p=0.015$), stroke work ($R=-0.691$, $p=0.002$), pressure volume area ($R=-0.772$, $p<0.001$) and with dP/dt (from pressure-volume loop datasets) ($r=0.581$, $p=0.014$).

ISCHAEMIA IN AORTIC STENOSIS

Table 4-5: Hyperaemic wave intensity analysis results pre- and post-TAVI from all paired datasets

	Pre-TAVI (n=18)			Post-TAVI (n=19)		
	<i>Rest</i>	<i>Hyperaemia</i>		<i>Rest</i>	<i>Hyperaemia</i>	
ACCELERATING WAVES						
<i>FCW (WI^{net}) (W.m⁻²s⁻² x 10⁴)</i>	5.8 (3.0,8.7)	6.3 (5.2,12.4)	P=0.008	6.2 (3.0,9.6)	6.7 (4.0,10.6)	NS
<i>FCW (WI⁺) (W.m⁻²s⁻² x 10⁴)</i>	6.5 (4.0,9.9)	8.1 (6.0,12.9)	P=0.007	7.2 (4.3,10.9)	8.6 (4.9,12.8)	NS
<i>FCW area (%)</i>	27 (22,35)	29 (23,41)	NS	23 (20,38)	25 (23,36)	NS
<i>BEW (WI^{net}) (W.m⁻²s⁻² x 10⁴)</i>	2.2 (0.86,8.9)	6.0 (2.3,13.4)	P=0.025	2.0 (0.8,4.4)	2.5 (0.8,4.7)	NS
<i>BEW (WI⁺) (W.m⁻²s⁻² x 10⁴)</i>	5.2 (2.3,13.7)	9.5 (4.6,17.6)	P=0.005	4.0 (1.8,6.8)	3.6 (1.5,7.4)	NS
<i>BEW area (%)</i>	17 (8,23)	21 (13,32)	P=0.024	10 (4,20)	7 (5,15)	P=0.087
<i>Acc waves (%)</i>	45 (37,59)	52 (38,63)	P=0.024	33 (27,42)	33 (25,41)	NS
DECELERATING WAVES						
<i>FEW (WI^{net}) (W.m⁻²s⁻² x 10⁴)</i>	2.9 (1.2,7.0)	3.3 (1.8,9.1)	NS	4.9 (2.7,8.7)	6.1 (4.1,11.1)	NS
<i>FEW (WI⁺) (W.m⁻²s⁻² x 10⁴)</i>	6.5 (4.4,8.4)	6.9 (4.9,11.6)	NS	7.2 (3.5,9.5)	8.7 (5.6,12.8)	P=0.087
<i>FEW area (%)</i>	26 (19,33)	28 (19,38)	NS	28 (21,35)	33 (28,39)	NS
<i>BCW (WI^{net}) (W.m⁻²s⁻² x 10⁴)</i>	8.0 (3.4,11.7)	9.3 (5.1,16.0)	P=0.010	5.9 (4.7,10.8)	10.0 (5.6,14.8)	P=0.018
<i>BCW (WI⁺) (W.m⁻²s⁻² x 10⁴)</i>	8.9 (5.5,12.5)	10.0 (6.6,17.3)	P=0.012	8.2 (6.3,11.2)	12.0 (7.1,14.9)	P=0.004
<i>BCW area (%)</i>	29 (19,39)	26 (18,37)	NS	39 (28,47)	41 (26,54)	NS
<i>Dec waves (%)</i>	55 (41,63)	48 (37,62)	P=0.024	67 (20,38)	67 (59,75)	NS
OTHER						
<i>Area under WI⁺</i>	1.3 (1.0,1.7)	1.6 (1.1,2.0)	P=0.024	1.2 (0.9,2.2)	1.5 (1.1,2.5)	P=0.023
<i>Area above WI⁻</i>	1.8 (1.1,2.3)	2.4 (1.4,3.2)	P=0.001	1.3 (0.9,2.2)	1.7 (1.3,2.2)	P=0.018

ISCHAEMIA IN AORTIC STENOSIS

Table 4-6: Rapid pacing wave intensity analysis results pre- and post-TAVI from all paired datasets

	Pre-TAVI (n=19)			Post-TAVI (n=19)		
	<i>Rest</i>	<i>Pacing</i>		<i>Rest</i>	<i>Pacing</i>	
ACCELERATING WAVES						
<i>FCW (WI^{net}) (W.m⁻²s⁻² x 10⁴)</i>	5.8 (3.0,8.7)	2.3 (0.9-4.6)	P=0.036	6.2 (3.0,9.6)	2.3 (1.1,4.9)	P=0.011
<i>FCW (WI⁺) (W.m⁻²s⁻² x 10⁴)</i>	6.5 (4.0,9.9)	4.8 (2.0,8.2)	NS	7.2 (4.3,10.9)	4.2 (2.3,7.6)	NS
<i>FCW area (%)</i>	27 (22,35)	19 (14,36)	NS	23 (20,38)	21 (13,29)	NS
<i>BEW (WI^{net}) (W.m⁻²s⁻² x 10⁴)</i>	2.2 (0.86,8.9)	3.4 (2.2,6.6)	NS	2.0 (0.8,4.4)	2.8 (0.6,5.0)	NS
<i>BEW (WI⁺) (W.m⁻²s⁻² x 10⁴)</i>	5.2 (2.3,13.7)	4.5 (3.2,9.5)	NS	4.0 (1.8,6.8)	3.8 (1.6,5.7)	NS
<i>BEW area (%)</i>	17 (8,23)	17 (10,22)	NS	10 (4,20)	10 (7,16)	NS
<i>Acc waves (%)</i>	45 (37,59)	33 (20,42)	P=0.005	33 (27,42)	24 (18,31)	P=0.007
DECELERATING WAVES						
<i>FEW (WI^{net}) (W.m⁻²s⁻² x 10⁴)</i>	2.9 (1.2,7.0)	2.4 (0.5,5.2)	NS	4.9 (2.7,8.7)	3.1 (2.0,6.7)	NS
<i>FEW (WI⁺) (W.m⁻²s⁻² x 10⁴)</i>	6.5 (4.4,8.4)	4.9 (2.0,7.4)	P=0.045	7.2 (3.5,9.5)	4.6 (2.4,8.2)	NS
<i>FEW area (%)</i>	26 (19,33)	33 (22,45)	P=0.006	28 (21,35)	40 (22,53)	P=0.087
<i>BCW (WI^{net}) (W.m⁻²s⁻² x 10⁴)</i>	8.0 (3.4,11.7)	9.6 (6.8,17.8)	P=0.029	5.9 (4.7,10.8)	11.7 (8.4,20.3)	P=0.049
<i>BCW (WI⁺) (W.m⁻²s⁻² x 10⁴)</i>	8.9 (5.5,12.5)	11.6 (7.7,18.3)	P=0.040	8.2 (6.3,11.2)	12.5 (10.0,21.0)	P=0.045
<i>BCW area (%)</i>	29 (19,39)	45 (32,53)	P=0.001	39 (28,47)	54 (42,62)	P=0.003
<i>Dec waves (%)</i>	55 (41,63)	67 (58,80)	P=0.005	67 (20,38)	76 (69,82)	P=0.007
OTHER						
<i>Area under WI⁺</i>	1.3 (1.0,1.7)	0.8 (0.3,1.1)	P<0.001	1.2 (0.9,2.2)	0.7 (0.5,1.0)	P=0.003
<i>Area above WI⁻</i>	1.8 (1.1,2.3)	1.4 (0.8,1.9)	NS	1.3 (0.9,2.2)	1.5 (0.9,2.2)	NS

ISCHAEMIA IN AORTIC STENOSIS

Table 4-7: The impact of TAVI (pre- vs post) on coronary wave intensity analysis results from all paired datasets

	Baseline (n=19)			Hyperaemia (n=18)			Pacing (n=19)		
	<i>Pre-TAVI</i>	<i>Post-TAVI</i>		<i>Pre-TAVI</i>	<i>Post-TAVI</i>		<i>Pre-TAVI</i>	<i>Post-TAVI</i>	
ACCELERATING WAVES									
<i>FCW (WI^{net}) (W.m⁻²s⁻² x 10⁴)</i>	5.8 (3.0,8.7)	6.2 (3.0,9.6)	NS	6.3 (5.2,12.4)	6.7 (4.0,10.6)	NS	2.3 (0.9-4.6)	2.3 (1.1,4.9)	NS
<i>FCW (WI⁺) (W.m⁻²s⁻² x 10⁴)</i>	6.5 (4.0,9.9)	7.2 (4.3,10.9)	NS	8.1 (6.0,12.9)	8.6 (4.9,12.8)	NS	4.8 (2.0,8.2)	4.2 (2.3,7.6)	NS
<i>FCW area (%)</i>	27 (22,35)	23 (20,38)	NS	29 (23,41)	25 (23,36)	NS	19 (14,36)	21 (13,29)	NS
<i>BEW (WI^{net}) (W.m⁻²s⁻² x 10⁴)</i>	2.2 (0.86,8.9)	2.0 (0.8,4.4)	NS	6.0 (2.3,13.4)	2.5 (0.8,4.7)	P<0.001	3.4 (2.2,6.6)	2.8 (0.6,5.0)	NS
<i>BEW (WI⁺) (W.m⁻²s⁻² x 10⁴)</i>	5.2 (2.3,13.7)	4.0 (1.8,6.8)	P=0.096	9.5 (4.6,17.6)	3.6 (1.5,7.4)	P<0.001	4.5 (3.2,9.5)	3.8 (1.6,5.7)	NS
<i>BEW area (%)</i>	17 (8,23)	10 (4,20)	P=0.032	21 (13,32)	7 (5,15)	P<0.001	17 (10,22)	10 (7,16)	NS
<i>Acc waves (%)</i>	45 (37,59)	33 (27,42)	P=0.002	52 (38,63)	33 (25,41)	P=0.001	33 (20,42)	24 (18,31)	P=0.018
DECELERATING WAVES									
<i>FEW (WI^{net}) (W.m⁻²s⁻² x 10⁴)</i>	2.9 (1.2,7.0)	4.9 (2.7,8.7)	P=0.051	3.3 (1.8,9.1)	6.1 (4.1,11.1)	NS	2.4 (0.5,5.2)	3.1 (2.0,6.7)	NS
<i>FEW (WI⁺) (W.m⁻²s⁻² x 10⁴)</i>	6.5 (4.4,8.4)	7.2 (3.5,9.5)	NS	6.9 (4.9,11.6)	8.7 (5.6,12.8)	NS	4.9 (2.0,7.4)	4.6 (2.4,8.2)	NS
<i>FEW area (%)</i>	26 (19,33)	28 (21,35)	NS	28 (19,38)	33 (28,39)	NS	33 (22,45)	40 (22,53)	NS
<i>BCW (WI^{net}) (W.m⁻²s⁻² x 10⁴)</i>	8.0 (3.4,11.7)	5.9 (4.7,10.8)	NS	9.3 (5.1,16.0)	10.0 (5.6,14.8)	NS	9.6 (6.8,17.8)	11.7 (8.4,20.3)	NS
<i>BCW (WI⁺) (W.m⁻²s⁻² x 10⁴)</i>	8.9 (5.5,12.5)	8.2 (6.3,11.2)	NS	10.0 (6.6,17.3)	12.0 (7.1,14.9)	P=0.005	11.6 (7.7,18.3)	12.5 (10.0,21.0)	NS
<i>BCW area (%)</i>	29 (19,39)	39 (28,47)	P=0.016	26 (18,37)	41 (26,54)	P<0.001	45 (32,53)	54 (42,62)	P=0.016
<i>Dec waves (%)</i>	55 (41,63)	67 (20,38)	P=0.002	48 (37,62)	67 (59,75)	P=0.001	67 (58,80)	76 (69,82)	P=0.018
OTHER									
<i>Area under WI⁺</i>	1.3 (1.0,1.7)	1.2 (0.9,2.2)	NS	1.6 (1.1,2.0)	1.5 (1.1,2.5)	NS	0.8 (0.3,1.1)	0.7 (0.5,1.0)	NS
<i>Area above WI⁻</i>	1.8 (1.1,2.3)	1.3 (0.9,2.2)	P=0.045	2.4 (1.4,3.2)	1.7 (1.3,2.2)	P=0.012	1.4 (0.8,1.9)	1.5 (0.9,2.2)	NS

ISCHAEMIA IN AORTIC STENOSIS

Table 4-8: Pre-TAVI coronary wave intensity analysis results in LGAS and HGAS cohorts. Results displayed when $P < 0.010$ for LGAS then HGAS with SD or IQR in brackets.

REST			HYPERAEMIA		RAPID PACING	
ACCELERATING WAVES						
FCW (WI^{net}) ($W.m^{-2}s^{-2} \times 10^4$)		NS		NS		NS
FCW (WI^+) ($W.m^{-2}s^{-2} \times 10^4$)		NS		NS		NS
FCW area (%)	32(23,38)/27(10,28)	P=0.022	31(24,40)/24(21,34)	P=0.063		NS
BEW (WI^{net}) ($W.m^{-2}s^{-2} \times 10^4$)	-0.8(-1.8,-0.6)/-2.2(-9.5,-1.5)	P=0.070	-3.5(-7.6,-1.7)/-6.3(-16.0,-4.2)	P=0.014	-2.8(-4.2,-1.3)/-4.6(-7.3,-1.9)	P=0.095
BEW (WI^+) ($W.m^{-2}s^{-2} \times 10^4$)	-2.7(-3.8,-1.9)/-6.4(-18.5,-3.7)	P=0.006	-5.9(-11.6,-3.2)/-17.7(-23.3,-7.1)	P=0.008	-3.3(-5.7,-2.1)/-5.7(-15.0,-3.3)	P=0.028
BEW area (%)	7.3(6.1,11.8)/18.2(10.2,39.9)	P=0.013	13(7,16)/32(15,52)	P=0.011		NS
Acc waves (%)		NS		NS		NS
DECELERATING WAVES						
FEW (WI^{net}) ($W.m^{-2}s^{-2} \times 10^4$)	6.2(3.7,11.2)/2.5(1.7,5.7)	P=0.021		NS		NS
FEW (WI^+) ($W.m^{-2}s^{-2} \times 10^4$)		NS		NS		NS
FEW area (%)		NS	39(28,41)/25(23,35)	P=0.024		NS
BCW (WI^{net}) ($W.m^{-2}s^{-2} \times 10^4$)		NS		NS		NS
BCW (WI^+) ($W.m^{-2}s^{-2} \times 10^4$)		NS		NS		NS
BCW area (%)	36(29,46)/22(16,31)	P=0.079		NS		NS
Dec waves (%)		NS		NS		NS
Area under WI^+		NS		NS		NS
Area above WI^-	1.3(1.0,2.4)/2.1(1.5,3.6)	P=0.002		NS		NS

4.2.6 Wave Intensity Analysis in LGAS vs HGAS

Results are displayed in Table 4-8. At baseline pre-TAVI, LGAS was associated with larger decelerating FEW, and smaller accelerating BEW waves. Backward travelling waves were reduced in LGAS patient ($p=0.002$). Before TAVI during hyperaemia, the BEW was significantly smaller in LGAS, and post-TAVI the only difference during hyperaemia was reduced FCW in LGAS patients ($6.6 [4.2,9.7]$ vs $9.8 [5.4,17.8]$, $p=0.035$). Following TAVI, baseline rest measurements revealed a trend towards reduced overall backward travelling waves in LGAS patients ($1.1 [0.7,1.9]$ vs $1.8 [1.2,2.5]$, $p=0.079$). In addition, the change in BEW from rest with hyperaemia was notable in that it decreased in LGAS patients but increased in HGAS patients ($-63\% [-69,+23]$ vs $55\% [-22,+174]$, $p=0.022$). Comparing hyperaemic results pre-TAVI and post-TAVI, BEW fell in both cohorts (Table 4-7) but the effect was less profound in LGAS patients ($-23\pm 70\%$ vs $-71\pm 123\%$, $p=0.077$).

4.2.7 Coronary Perfusion Efficiency

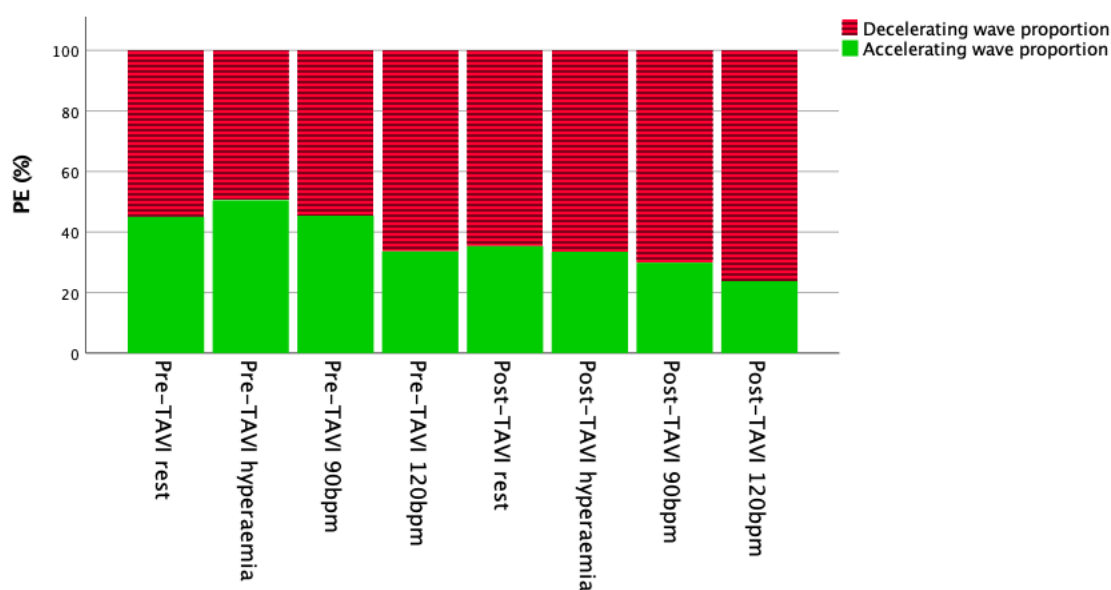


Figure 4-7: Coronary perfusion efficiency

In this study, improved PE was observed during hyperaemia pre-TAVI ($p=0.024$), but rapid pacing induced a significant fall in PE from resting measurements ($p=0.005$) (Figure 4-7). TAVI caused a significant drop at rest ($p=0.001$), hyperaemia (pre- to post-TAVI, $p<0.001$),

ISCHAEMIA IN AORTIC STENOSIS

and during rapid pacing at 120bpm (pre- to post-TAVI, $p=0.016$). Following TAVI, hyperaemia made no difference but rapid pacing demonstrated reduced PE from post-TAVI baseline ($p=0.007$). Comparing relative change of PE in LGAS and HGAS cohorts, following TAVI, rest to hyperaemia induced a decrease in PE in LGAS but an increase in HGAS patients ($-17\pm 18\%$ vs $+13\pm 33\%$, $p=0.028$).

4.2.8 Myocardial Perfusion Reserve Index

Cardiac MRI was used to calculate MPRI. Patients with LGAS exhibited a more profound rise in heart rate with IV adenosine during stress perfusion imaging (93 ± 11 vs 83 ± 10 bpm, $p=0.038$). Global MPRI increased following TAVI ($2.1 [1.8,2.3]$ to $2.4 [2.3,2.8]$, $p=0.029$). Before TAVI, there was a trend towards reduced MPRI in LGAS patients ($1.88 [1.63,2.13]$ vs $2.41 [1.97,2.84]$, $p=0.090$) (Figure 4-8), but no difference between groups post-TAVI (2.35 ± 0.24 vs 2.55 ± 0.68 , $p=0.711$).

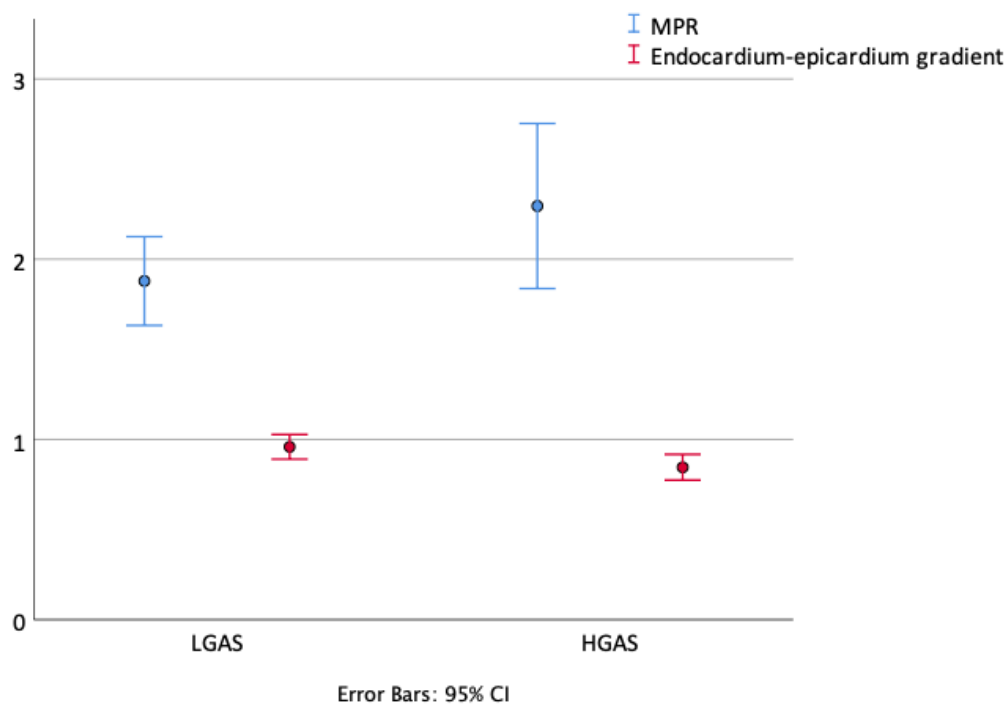


Figure 4-8: Pre-TAVI MPR and endocardium-epicardium gradient results for LGAS and HGAS patients

4.2.9 Endocardium-Epicardium Gradients

Endocardium-epicardium gradients did not change following TAVI (0.94 [0.81,0.98] to 0.95 [0.80,1.02], $p=0.694$) but pre-TAVI stress endocardium-epicardium gradient closely correlated with left ventricular indexed stroke volume ($R=-0.519$, $p=0.023$). Pre-TAVI, there was a less significant gradient in LGAS patients (0.98 [0.88,1.03] vs 0.83 [0.76,0.94], $p=0.014$) (Figure 4-8) but following TAVI, there was no difference between groups (0.95 [0.87,1.02] vs 0.93 [0.73,0.99], $p=0.389$). Interestingly, in this study, there was no correlation between endocardial-epicardial gradients and MPRI either before ($r=0.101$, $p=0.682$) or following ($R=-0.147$, $p=0.560$) TAVI. There was also no significant correlation between endocardium-epicardium gradients and end diastolic or systolic pressures ($r=-0.234$, $p=0.349$).

4.2.10 Serum Biomarkers

Differences in serum concentrations of Troponin T, cardiac myosin binding protein C (cMyC), lactate and oxygen were assessed between the aortic root and coronary sinus. Transcardiac biomarker release was defined as coronary sinus (CS) concentration minus the aortic concentration.

Table 4-9: Results from aortic and coronary sinus serum sampling

	Pre-TAVI	P value	Post-TAVI	P value
Aortic Troponin T (ng/l)				
<i>Rest → 90bpm</i>	92±74 → 100±82	0.023	203±163 → 218±168	0.039
<i>Rest → 120bpm</i>	77±58 → 85±64	0.019	203±163 → 208±161	NS
<i>Rest → post-stress</i>	98±75 → 117±85	0.015	203±163 → 218±163	NS
<i>Pre- → post-TAVI</i>	74±61 → 203±163	0.007		
Troponin Transcardiac Release				
<i>Rest → 90bpm</i>	19±43 → 13±30	NS	25±43 → 2±12	0.095
<i>Rest → 120bpm</i>	7±8 → 3±5	NS	25±43 → 14±29	NS
<i>Rest → post-stress</i>	19±43 → 11±22	NS	25±43 → 35±103	NS
<i>Pre- → post-TAVI</i>	7±8 → 25±43	NS		
Aortic cMyC (pg/ml)				
<i>Rest → 90bpm</i>	310±358 → 355±376	0.070	857±1015 → 971±1058	0.075

ISCHAEMIA IN AORTIC STENOSIS

Rest → 120bpm	272±363 → 334±409	0.057	857±1015 → 945±1101	NS
Rest → post-stress	310±358 → 403± 386	0.050	857±1015 → 936±1144	NS
Pre- → post-TAVI	272±363 → 897±1077	0.049		
Aortic Lactate (mmol/l)				
Rest → 90bpm	0.476±0.196 → 0.599±0.227	0.004	0.524±0.203 → 0.663±0.294	0.002
Rest → 120bpm	0.509±0.202 → 0.677±0.218	0.001	0.524±0.203 → 0.752±0.333	0.007
Rest → post-stress	0.484±0.204 → 0.701±0.319	0.005	0.518±0.214 → 0.791±0.331	0.004
Pre- → post-TAVI	0.488±0.202 → 0.524±0.203	NS		

Key: NS - non-significant

Results are displayed in Table 4-9. There was no statistical difference in any oxygen or lactate extraction values (calculated as $Extraction = [Ao-CS]/Ao \times 100$) or cMyC transcardiac release. In some cases, the coronary sinus sheath may have sampled from the right atrium rather than directly from the coronary sinus, representing the challenge in this technique, resulting in unreliable results. Post-intervention, interpretation was muddled by TAVI. There was no difference between LGAS and HGAS groups for any of the values.

4.3 Discussion and summary

At baseline, a shorter ejection time in LGAS patients would suggest that AS is less severe as blood is briskly ejected through the aortic valve and systole is completed sooner. Despite this, there is a relative increase in TTI and decrease in BI in LGAS patients post-TAVI and hyperaemia caused impaired (rather than improved) perfusion efficiency in LGAS patients. This suggests a pathological response to stressors and intervention with distorted cardiac-coronary coupling, rendering the heart vulnerable to resting ischaemia. Blunted microvascular-originating accelerating coronary waves, both a lack of shortening of the ET, and lack of lengthening of the DTF following TAVI, and raised microvascular resistance, all suggests an adverse response to TAVI.

In all patients, improved BI during pacing post-TAVI alludes to improved subendocardial perfusion during stress following valve intervention. This correlates with previous work demonstrating an increase in BI up to seven days post-TAVI from pre-TAVI

ISCHAEMIA IN AORTIC STENOSIS

measurements²²³. However, physiological assessment in the immediate aftermath of TAVI may represent, at least in part, ventricular stunning. BEW decline post-TAVI has already been demonstrated, but with a fall in LVMI at 12 months there is an accompanying increase in BEW fraction²²⁴.

The results of this study indicate that patients with LGAS and unobstructed coronary arteries have a distinct profile of coronary flow when compared to that of HGAS patients. The hypothesis of depressed accelerating coronary waves in LGAS patients was supported by the findings, but not the hypothesised higher systemic concentration of lactate and troponin in this cohort. Despite lower LV mass, pressure and volumes in the LGAS cohort, there was no significant difference between MRI perfusion assessment or serum markers of ischaemia between groups at baseline, perhaps revealing a disproportionate degree of myocardial oxygen supply-demand mismatch in LGAS patients despite markers of less severe AS.

5 CONTRACTILITY, LUSITROPY AND HYPERTROPHY IN AORTIC STENOSIS

5.1 Introduction

Aortic stenosis (AS) induces progressive left ventricular hypertrophy in an effort to reduce wall stress from chronic high afterload. This adaptive process continues to contribute to symptomatology and impaired cardiac reserve post-valve intervention and takes several months to regress. There is wide individual variation in the ventricular remodelling response to AS. Four left ventricular adaptive phenotypes in hypertensive patients have previously been identified on the basis of echocardiographic measurements²²⁵.

- Normal (normal indexed LV mass (LVMI) and mass to volume ratio (M/V)
- Concentric remodelling with normal LVMI but elevated M/V
- Concentric LV hypertrophy (LVH), associated with a raised LVMI but normal indexed end-diastolic volume (EDV)
- Eccentric LVH with high LVMI and EDV

This has been expanded on by Dweck *et al* who categorised patients with AS into six groups, by CMR criteria²²⁶ (Table 5-1).

Table 5-1: Cardiac remodelling phenotypes in aortic stenosis

	LVMI	LVEDV	M/V	Asymmetric wall thickness
<i>Normal</i>	↔	↔	↔	
<i>Concentric remodelling</i>	↔	↓	↑	
<i>Asymmetric remodelling</i>	↔	↓	↑	✓
<i>Concentric Hypertrophy</i>	↑	↔	↑	
<i>Asymmetric hypertrophy</i>	↑	↔	↑	✓
<i>Eccentric hypertrophy</i>	↑	↑	↔	

5.1.1 Invasive Assessment of Myocardial Mechanics

There is a complex interplay between preload, afterload and ventricular mechanics. Lusitropy, the rate and extent to which the heart relaxes during diastole, can be measured invasively as the end-diastolic pressure-volume relationship (EDPVR) (Figure 5-1, green line, ESPVR is the blue line). The ease with which blood enters and fills the ventricle during

CONTRACTILITY, LUSITROPY AND HYPERTROPHY IN AORTIC STENOSIS

diastole is related to the compliance or stiffness of the ventricular wall²²⁷. Compliance is the reciprocal of the EDPVR slope: the change in volume resulting from a change in pressure²²⁸. The EDPVR slope is shallow at low pressures, when compliance is greatest. Elastance, the reciprocal of compliance, is high in the setting of myocardial stiffness (a leftward shifted EDPVR signifies a stiff and noncompliant ventricle).

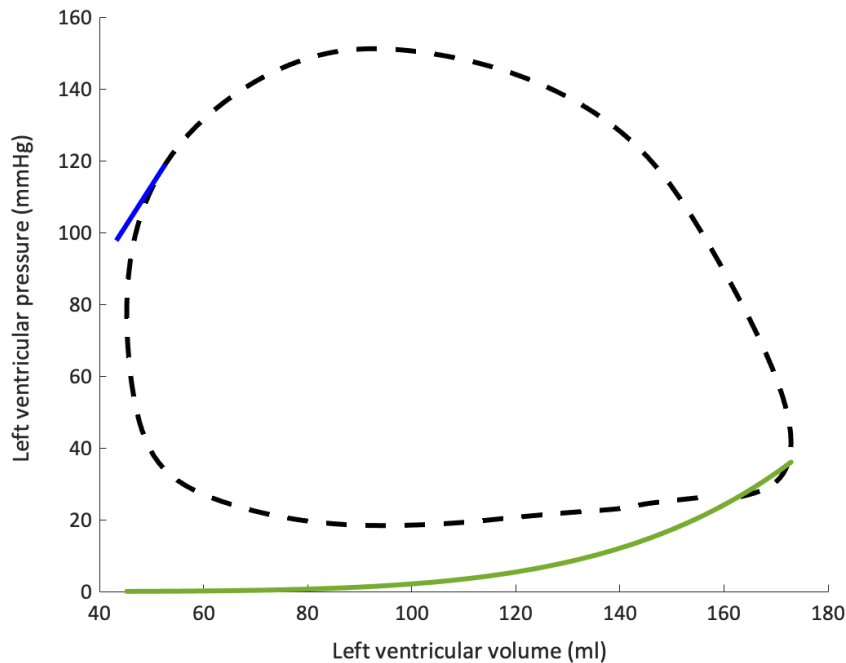


Figure 5-1: The end-diastolic and end-systolic pressure volume relationship in a patient with AS

Cardiac relaxation relates to the renin–angiotensin and endothelin systems²²⁹, muscle bulk²³⁰, capillary rarefaction and collagen content²³¹. Rate of relaxation, as measured by the exponential time constant, τ , is sensitive to ischaemia and dependent on heart rate. It is pathologically prolonged when tachycardia does not allow complete relaxation between beats and the pressure-volume loop progressively rises above the baseline EDPVR.

In an elastic vessel of changing dimension, the conservation of mass and energy require that pressure and flow waves must generate reflected waves. The amount of reflection is expressed in the reflection coefficient (Γ)²³², calculated from each harmonic, followed by derivation of the Fourier components of the forward and backward pressure and flow waves. Understandably, it is altered by peripheral resistance^{233,234}.

Change in Augmentation index, Alx, is a robust predictor of left ventricular mass regression in hypertensive patients following therapy²³⁵ (see Figure 4-1 and Table 2-4). It has been shown to independently correlate with the extent of coronary artery disease, left ventricular hypertrophy, aortic wall structure, cardiovascular events and all-cause mortality and is determined by chronotropic rather than inotropic effects²³⁶. Arterial wave reflection may contribute to the process leading to aortic valve calcification, as postulated after a previous correlation between Γ and aortic valve calcification²³⁷.

5.1.2 Non-Invasive Assessment of Myocardial Mechanics

Echocardiographic (tissue Doppler and mitral valve inflow Doppler signals) and cardiac magnetic resonance imaging (CMR) tissue tracking software can also be used to examine relaxation of the myocardium. By using tissue tracking technology, this cardiac motion allows the assessment of displacements and velocity, and also deformation, i.e., strain and strain rates. The latter provides a relatively load-independent quantitative evaluation of the myocardium and can be a sensitive marker of subclinical dysfunction. Patients with preserved LV systolic function and AS, with an echocardiographic derived global longitudinal strain of $\leq -14\%$, have a significantly higher survival than those with reduced strain²³⁸.

The presence of cardiac amyloidosis is increasingly recognised as a common incidental finding in AS and may confound results²³⁹⁻²⁴¹. Amyloid can be formed from a large number of precursor proteins. Amyloidosis denotes the deposition of amyloid proteins in the extracellular space, and this infiltration and accumulation causes organ dysfunction. The most common forms of protein producing cardiac amyloidosis are immunoglobulin-derived light chains (AL) and transthyretin (TTR). TTR amyloidosis may arise from wild-type (normal) TTR, or more commonly from a genetic mutation of the transthyretin protein gene. AL amyloidosis is the more serious form and is a haematological disorder, similar to multiple myeloma, where abnormal plasma cells overproduce lambda or kappa light chains.

Myocardial tissue histology is the current gold standard for detection of cardiac amyloidosis – stained using Congo Red where deposits of amyloid appear pale red but show apple-green birefringence under cross-polarised light. CMR has a high diagnostic accuracy for amyloidosis²⁴² and the non-invasive nature of this technique is more favourable. Amyloidosis typically produces a progressive subendocardial to transmural late gadolinium enhancement with difficulty nulling the myocardium on phase-sensitive inversion recovery imaging. This infiltrative disease can significantly alter the cardiac mechanics and is an important factor when considering the LV in the setting of AS.

Valvulo-arterial impedance, Z_{va} , is considered a measure of global afterload and is calculated as the sum of the systolic arterial pressure and mean aortic valve pressure gradient divided by the indexed stroke volume. Non-invasively, the ESP is assumed to be the sum of the mean aortic valve pressure gradient (MPG) and the systolic arterial pressure (SAP). Z_{va} is therefore a measure of both the valvular load (by MPG) and arterial load (SAP) – how much a structure resists motion when subjected to a given force. It represents the cost in pressure (mmHg) per systemic millilitre of blood indexed for body size pumped by the left ventricle during systole and is increased in patients with AS. Non-invasively, $>3.5\text{mmHg/ml/m}^2$ is considered to correlate with moderate AS, whereas $>4.5\text{mmHg/ml/m}^2$ is in the severe range²⁴³. Thoracic aorta calcification burden correlates with increased Z_{va} and unfavourable outcomes in patients with AS²⁴⁴. Patients with LGAS typically have higher LV global load²⁴⁵ and Z_{va} can be used to predict adverse outcomes in AS⁹².

Low gradient AS (LGAS) is often associated with a characteristic small left ventricular cavity and concentric remodelling, resulting in diastolic dysfunction, poor filling and a low-flow state. I sought to determine the remodelling patterns, contractility and lusitropy and their effects on flow and gradient in patients with AS and preserved LV systolic function. The hypothesis of more florid evidence of restriction in LGAS was tested.

5.2 Results

5.2.1 Cardiac Magnetic Resonance Imaging Assessment

Baseline results are displayed in Table 5-2.

Table 5-2: Pre-TAVI baseline characteristics and cardiac magnetic resonance findings

	LGAS (n=9)	HGAS (n=10)	P value
<i>Age (years)</i>	84±6	85±5	NS
<i>Body Surface Area (m²)</i>	1.83±0.17	1.71±0.13	0.097
<i>Hypertension (%)</i>	78	60	NS
<i>Mean aortic valve pressure gradient (mmHg)</i>	32±5	67±22	<0.001
<i>Resting heart rate (bpm)</i>	72.9±6.6	68.7±6.3	NS
<i>Non-invasive systolic blood pressure (mmHg)</i>	150±19	136±27	NS
<i>LV end diastolic volume (ml)</i>	125±26	141±26	NS
<i>LV end diastolic volume index (ml/m²)</i>	68±13	83±14	0.035
<i>LV end systolic volume (ml)</i>	45±12	56±16	NS
<i>LV end systolic volume index (ml/m²)</i>	25±6	32±9	0.032
<i>LV ejection fraction (%)</i>	65±4	61±6	NS
<i>Stroke volume (ml)</i>	80.5±17	85±15	NS
<i>Indexed stroke volume (ml/m²)</i>	44±8	50±8	NS
<i>Effective volume (ml/min)</i>	3645±1644	2709±1462	NS
<i>LV mass (g)</i>	97±16	121±31	0.035
<i>LV mass index (g/m²)</i>	56±8	71±18	0.017
<i>Mass:volume ratio</i>	0.80±0.21	0.85±0.11	NS
<i>Regurgitant fraction (%)</i>	12±21	18±16	NS

5.2.2 Left Ventricular Mass

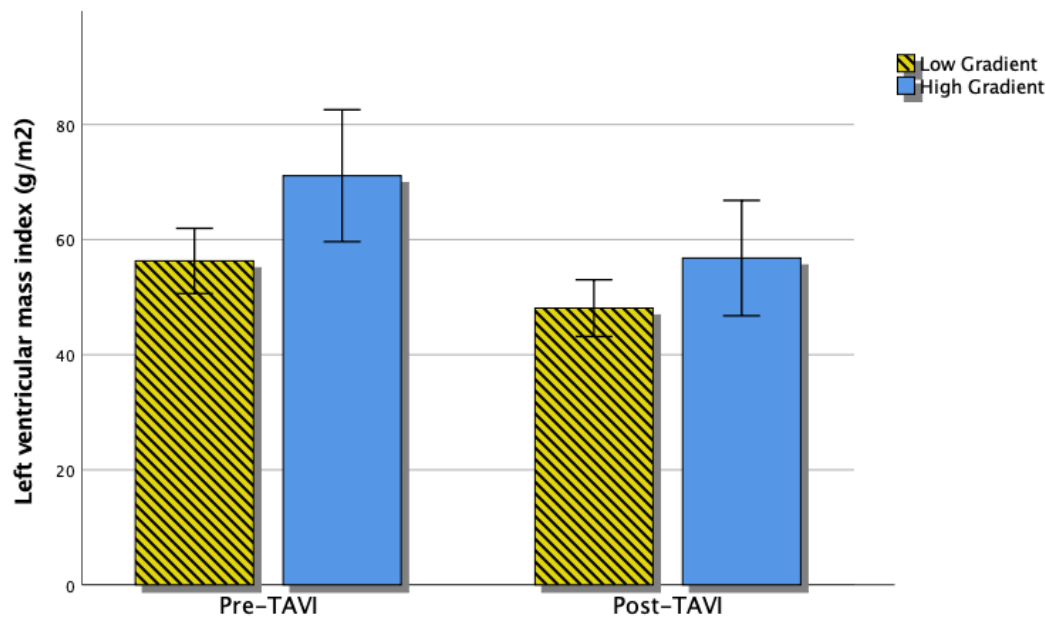


Figure 5-2: LVMI in LGAS vs HGAS

LGAS patients had smaller baseline LV sizes and lower mass index (Figure 5-2), although there was no difference in mass/volume ratio (M/V). Left ventricular mass index by MRI (LVMI_{MRI}) correlated significantly with mean aortic valve pressure gradient (MPG) from Doppler echocardiography ($r=0.625$, $p=0.004$, Figure 5-3), indexed calcium score ($R=0.477$, $p=0.039$), SVi ($R=0.586$, $p=0.008$) and indexed aortic valve area ($r=-0.498$, $p=0.030$). There was no significant difference in the change in M/V following TAVI between groups (LGAS -0.030 ± 0.1778 , HGAS -0.092 ± 0.111 , $p=0.406$).

CONTRACTILITY, LUSITROPY AND HYPERTROPHY IN AORTIC STENOSIS

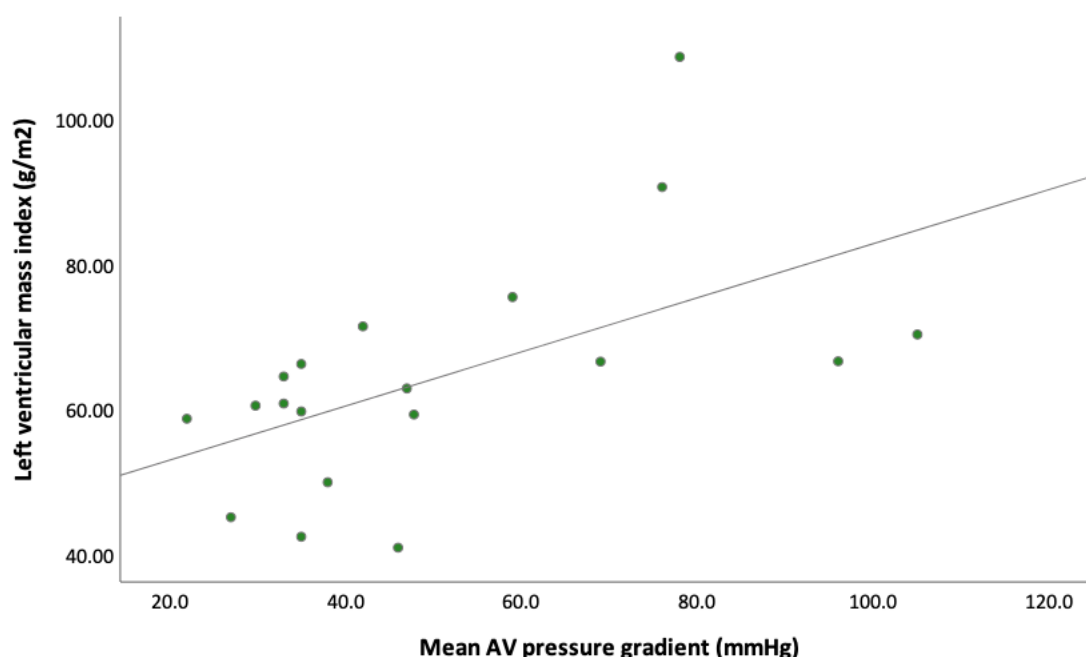


Figure 5-3: Correlation between MPG and LVMI

Following TAVI, significant remodelling occurred within a few months (Table 5-3). Pressure-loading was relieved: left ventricular and left atrial volumes and left ventricular muscle mass reduce; and ejection fraction and forward flow increase. Preferential reduction in LV hypertrophy over LV cavity size reduction was reflected in reduced M/V.

Table 5-3: Paired (pre- and post-TAVI) MRI results in all patients (18 pairs), values are presented as the mean \pm SD or median with interquartile range as appropriate

	Pre	Post	P value
Resting heart rate (bpm)	74 \pm 7	70 \pm 9	NS
Resting systolic blood pressure (mmHg)	141 \pm 24	139 \pm 24	NS
Resting diastolic blood pressure (mmHg)	66 \pm 14	61 \pm 8	NS
LV end diastolic volume (ml)	135 \pm 27	124 \pm 28	0.009
LV end diastolic volume index (ml/m ²)	77 \pm 15	70 \pm 15	0.013
LV end systolic volume (ml)	51 \pm 14	42 \pm 14	0.003
LV end systolic volume index (ml/m ²)	29 \pm 8	23 \pm 7	0.003
LV ejection fraction (%)	62 \pm 5	67 \pm 6	0.006
Stroke volume (ml)	83 \pm 15	83 \pm 17	NS
Indexed stroke volume (ml/m ²)	47 \pm 9	47 \pm 10	NS
LV mass (g)	108 (97,119)	91 (78,105)	0.001
LV mass index (g/m ²)	63 (59,70)	51 (44,56)	<0.001

CONTRACTILITY, LUSITROPY AND HYPERTROPHY IN AORTIC STENOSIS

<i>Mass:volume ratio</i>	0.83±0.17	0.76±0.12	0.023
<i>Indexed LA Volume (ml/m²)</i>	15±4	14±4	0.030
<i>Indexed RA volume (ml/m²)</i>	10±2	10±2	NS
<i>Total forward volume (ml)</i>	48±17	67±13	0.001
<i>Effective volume (l)</i>	3.1±1.6	4.5±1.0	0.001

5.2.3 Tissue Tracking

Table 5-4: Strain MRI results in all patients (18 pairs), values are presented as the mean ± SD or median with interquartile range as appropriate

	Pre	Post	P value
RADIAL 3D STRAIN			
<i>Peak strain (%)</i>	51 (41,62)	67 (54,85)	0.006
<i>Peak systolic strain rate (1/s)</i>	4.0 (2.7,5.8)	6.0 (5.6,7.0)	0.005
<i>Peak diastolic strain rate (1/s)</i>	-3.8 (-4.7,-2.6)	-5.0 (-7,-3)	0.065
<i>Peak displacement (mm)</i>	6.3 (5.5,7.0)	7.4 (7.0,8.2)	0.003
<i>Peak systolic velocity (mm/s)</i>	48 (43,67)	69 (55,79)	0.001
<i>Peak diastolic velocity (mm/s)</i>	-40 (-58,-35)	-54 (-71,-45)	0.034
CIRCUMFERENTIAL 3D STRAIN			
<i>Peak strain (%)</i>	-16±3 (-18,-13)	-20 (-21,-17)	0.010
<i>Peak systolic strain rate (1/s)</i>	-1.36 (-1.59,-0.95)	-1.7 (-2.1,-1.3)	0.006
<i>Peak diastolic strain rate (1/s)</i>	1.2 (0.9,0.4)	1.4 (1.3,1.7)	0.008
<i>Peak displacement (mm)</i>	-0.13 (-0.17,+0.18)	0.06 (-0.19,+0.20)	NS
<i>Peak systolic velocity (mm/s)</i>	-1.28 (-2.98,+2.18)	1.9 (-2.0,+2.8)	NS
<i>Peak diastolic velocity (mm/s)</i>	-0.5 (-2.9,+1.7)	1.5 (-3.2,+2.5)	NS
LONGITUDINAL 3D STRAIN			
<i>Peak strain (%)</i>	-12 (-14,-10)	-15 (-18,-13)	0.013
<i>Peak systolic strain rate (1/s)</i>	-1.02 (-1.37,-0.74)	-1.2 (-1.5,-0.8)	NS
<i>Peak diastolic strain rate (1/s)</i>	0.90 (0.65,1.15)	1.2 (0.9,1.6)	NS
<i>Peak displacement (mm)</i>	3.8 (2.6,4.4)	4.8 (3.5,6.4)	0.016
<i>Peak systolic velocity (mm/s)</i>	37 (11,47)	55 (32,69)	0.016
<i>Peak diastolic velocity (mm/s)</i>	-52 (-72,-24)	-45 (-52,-34)	NS

Following TAVI, there was statistically significant improvement in peak radial, circumferential and longitudinal strain, radial and circumferential strain rate, radial and

CONTRACTILITY, LUSITROPY AND HYPERTROPHY IN AORTIC STENOSIS

longitudinal peak displacement and systolic velocity (mm/s), and radial diastolic velocity (Table 5-4).

5.2.4 Remodeling Patterns between Cohorts

Baseline strain data (Table 5-5**Error! Reference source not found.**) revealed that both cohorts had significant but similarly reduced global longitudinal strain (GLS). There was no significant difference following intervention in the delta change between groups. Circumferential time to peak strain was reduced in LGAS patients (330ms [277,373] vs 400ms [358,430], $p=0.034$), and there was a trend towards reduced radial time to peak strain in this group (315 [260,372] vs 365ms [333,392], $p=0.062$). There were also differences in peak circumferential displacement (-0.14 ± 0.03 vs $+0.05\pm0.23$ mm, $p=0.028$) and diastolic velocity (1.3 ± 2.1 vs -2.1 ± 2.3 mm/s, $p=0.005$).

LVMl_{MRI} correlated with peak radial ($R=-0.540$, $p=0.021$) and peak circumferential strain ($R=0.476$, $p=0.046$) but not longitudinal strain ($R=0.150$, $p=0.553$). LVEDVi also correlated with peak radial ($R=-0.606$, $p=0.008$), and peak circumferential strain ($R=0.550$, $p=0.018$) but not peak longitudinal strain.

Table 5-5: LGAS vs HGAS pre-TAVI CMR strain results

	LGAS (n=9)	HGAS (n=10)	P value
Global 3D peak radial strain (%)	55±12	48±17	NS
Global 3D peak circumferential strain (%)	-17±2	-15±3	NS
Global 3D peak longitudinal strain (%)	-13 (-14,-12)	-10 (-13,-10)	NS
3D peak radial displacement (mm)	6.3±0.8	6.3±1.1	NS
3D peak circumferential displacement (mm)	-0.14±0.03	+0.05±0.23	0.028
3D peak longitudinal displacement (mm)	4.4±1.9	3.3±1.4	NS
3D peak diastolic radial velocity (mm/s)	-44±14	-46±16	NS
3D peak diastolic circumferential velocity (mm/s)	+1.25±2.12	-2.13±2.3	0.005
3D peak diastolic longitudinal velocity (mm/s)	-57±28	-45±29	NS

Table 5-6 presents the follow-up MRI results separated into low or high gradient cohorts, and Table 5-7**Error! Reference source not found.** presents the relative change in MRI parameters. There were no significant differences between cohorts noted in these results.

CONTRACTILITY, LUSITROPY AND HYPERTROPHY IN AORTIC STENOSIS

Table 5-6: LGAS vs HGAS follow-up cardiac magnetic resonance scan results

	LGAS (n=8)	HGAS (n=10)	P value
<i>Non-invasive systolic blood pressure (mmHg)</i>	132±28	144±21	NS
<i>LV end diastolic volume (ml)</i>	123±33	125±25	NS
<i>LV end diastolic volume index (ml/m²)</i>	67±16	73±14	NS
<i>LV end systolic volume (ml)</i>	40±17	42±12	NS
<i>LV end systolic volume index (ml/m²)</i>	22±8	25±6	NS
<i>LV ejection fraction (%)</i>	68±6	66±6	NS
<i>Stroke volume (ml)</i>	83±17	83±17	NS
<i>Indexed stroke volume (ml/m²)</i>	45±10	48±10	NS
<i>Effective volume (ml/min)</i>	4436±1547	4290±937	NS
<i>LV mass (g)</i>	89±15	97±27	NS
<i>LV mass index (g/m²)</i>	49 (41,54)	54 (44,66)	NS
<i>Mass:volume ratio</i>	0.70 (0.64,0.86)	0.76 (0.68,0.86)	NS
<i>Regurgitant fraction (%)</i>	6 (2,8)	18 (5,30)	NS
<i>Global 3D peak radial strain (%)</i>	67±15	72±31	NS
<i>Global 3D peak circumferential strain (%)</i>	-20±3	-18±3	NS
<i>Global 3D peak longitudinal strain (%)</i>	-16±2	-13±5	NS
<i>Peak displacement radial (mm)</i>	7.3±1.1	7.6±1.7	NS
<i>Peak displacement circumferential (mm)</i>	0.05±0.17	-0.02±0.22	NS
<i>Peak displacement longitudinal (mm)</i>	5.6±1.2	4.4±1.7	NS
<i>Peak diastolic velocity radial (mm/s)</i>	-59±21	-53±17	NS
<i>Peak diastolic velocity circumferential (mm/s)</i>	0.47±3.3	-0.42±3.2	NS
<i>Peak diastolic velocity longitudinal (mm/s)</i>	-55±24	-38±15	0.084

Table 5-7: LGAS vs HGAS change in MRI parameters following intervention

	LGAS (n=8)	HGAS (n=10)	P value
<i>Resting heart rate (%)</i>	-3±8	2±18	NS
<i>Resting systolic blood pressure (%)</i>	-10±12	8±17	0.019
<i>Resting diastolic blood pressure (%)</i>	-13±15	1±21	NS
<i>LV end diastolic volume (%)</i>	-5±11	-14±14	NS
<i>LV end diastolic volume index (%)</i>	-4±11	-14±15	NS
<i>LV end systolic volume (%)</i>	-26±42	-32±25	NS
<i>LV end systolic volume index (%)</i>	-24±41	33±26	NS
<i>LV ejection fraction (%)</i>	5±12	8±7	NS
<i>Stroke volume (%)</i>	1±13	-3±14	NS
<i>Indexed stroke volume (%)</i>	0 (-0.1,+0.1)	0 (-0.2,+0.1)	NS
<i>LV mass (%)</i>	-11±18	-26±20	NS
<i>LV mass index (%)</i>	-17±13	-27±21	NS
<i>Mass:volume ratio (%)</i>	-3±18	-9±11	NS
<i>Global 3D peak radial strain (%)</i>	24±34	59±43	0.093
<i>Global 3D peak circumferential strain (%)</i>	19±20	24±30	NS
<i>Global 3D peak longitudinal strain (%)</i>	22 (2,49)	17 (-14,+42)	NS
<i>Peak displacement radial (%)</i>	18±22	24±23	NS
<i>Peak displacement circumferential (%)</i>	-177 (-227,-143)	-12 (-195,+20)	0.052
<i>Peak displacement longitudinal (%)</i>	59 (-3,+116)	29 (-12,+142)	NS
<i>Peak diastolic velocity radial (%)</i>	48±79	19±32	NS
<i>Peak diastolic velocity circumferential (%)</i>	-152±188	-24±111	NS
<i>Peak diastolic velocity longitudinal (%)</i>	16 (-44,+141)	-23 (-37,+109)	NS

5.2.5 Echocardiography for Left Ventricular Assessment

Indexed stroke volume from the participants included in this study was calculated as 47.2 ± 8.5 ml by MRI (SVI_{MRI}), and 40.7 ± 11.2 ml by echocardiography (SVI_{ECHO}), null hypothesis $p=0.014$; correlation $r=0.452$, $p=0.052$. I observed that the LVOT areas derived from echocardiography correlated with gated computed tomography measurements ($r=0.480$, $p=0.037$) but were significantly smaller (2.99 ± 0.65 vs 4.10 ± 0.78 cm², $p<0.001$).

There was no correlation between echocardiographic derived relative wall thickness (RWT) and MRI-derived LVMI ($r=-0.016$, $p=0.949$) but there was significant correlation between LVMI derived from MRI and ECHO ($r=0.584$, $p=0.009$). Despite a correlation between $LVMI_{MRI}$ and AV Calcium Score ($R=0.477$, $p=0.039$), none was found with $LVMI_{ECHO}$ ($r=0.13$, $p=0.591$). There was also no correlation between E:A Doppler Mitral valve inflow and $LVMI_{MRI}$ ($r=-0.240$, $p=0.323$) or $LVMI_{ECHO}$ ($r=-0.099$, $p=0.686$). In keeping, despite significant correlation between LVMI and tissue tracked strain markers, there was no correlation between RWT or $LVMI_{ECHO}$ and radial, circumferential or longitudinal strain.

5.2.6 Valvulo-Arterial Impedance

Invasive Zva was assessed for each physiological setting pre- and post-TAVI with updated stroke volumes and blood pressure. It increased from baseline pre-TAVI with pacing ($p=0.001$), and from baseline post-TAVI with pacing ($p=0.038$). Zva during hyperaemia and rapid pacing fell post-TAVI when compared to before intervention ($p=0.031$ and 0.030 , respectively), and also during hyperaemia from baseline post-TAVI ($p=0.021$) (Table 7-2, Table 7-3, and Table 7-4).

At baseline, there was no difference between the invasive Zva between LGAS and HGAS cohorts in this study (

CONTRACTILITY, LUSITROPY AND HYPERTROPHY IN AORTIC STENOSIS

Table 7-5). There was, however, significant correlation between Zva_{ECHO} and SV_{IMRI} ($R=-0.532$, $p=0.019$), and also with hyperaemic invasive pre-TAVI Zva and $LVMI_{IMRI}$ ($R=0.505$, $p=0.029$) and AVA_i ($R=-0.757$, $p<0.001$).

5.2.7 Pressure-Volume Loop Assessment of the Left Ventricle

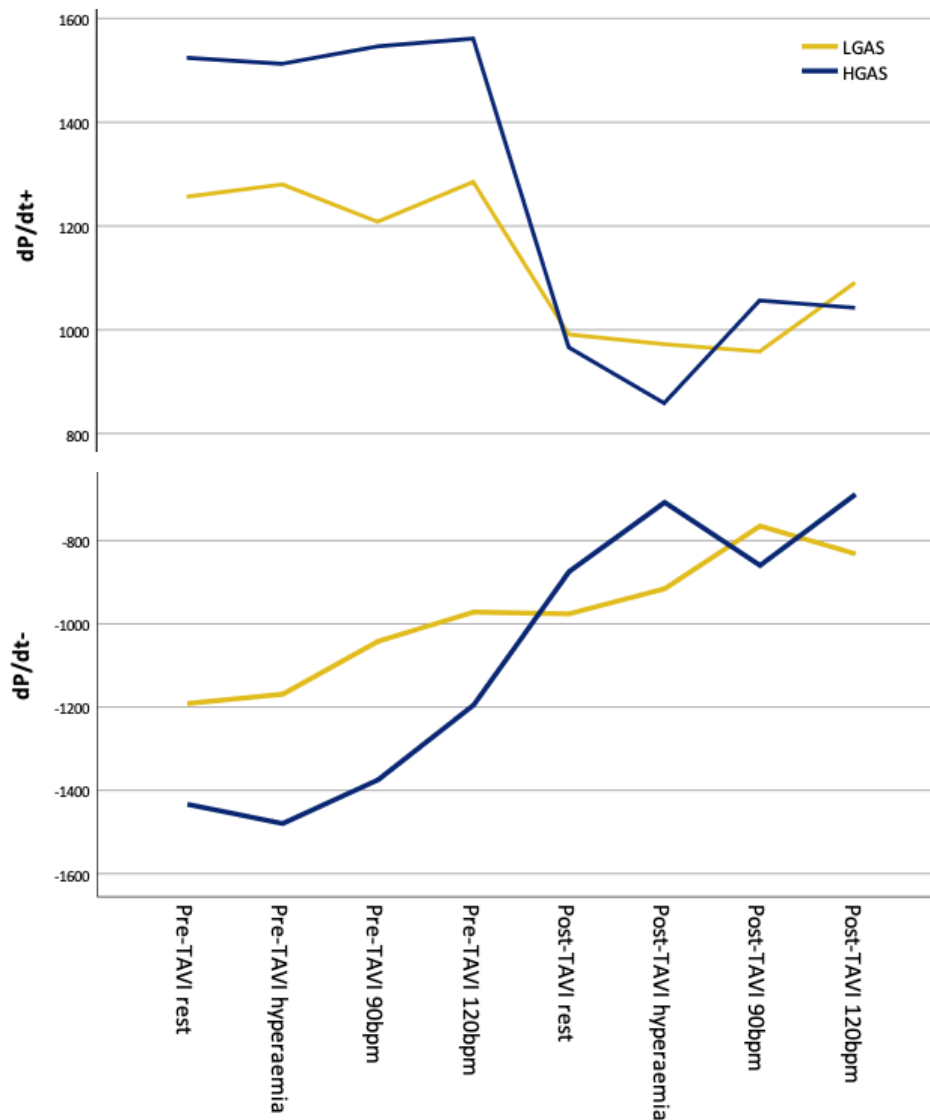


Figure 5-4: Maximum and minimum dP/dt in LGAS and HGAS patients

Pressure–volume loop (PVL) analysis is considered the gold standard for the investigation of myocardial haemodynamics. Results are displayed in Table 5-8, Table 5-9 and Table 5-10 and this topic will also be explored in more detail in Chapter 7.

Prior to TAVI, hyperaemia induced minimal effect on the myocardium, however post-TAVI, a significant reduction in both dP/dt⁻ and dP/dt⁺ was observed with hyperaemia. Both before and after intervention, pacing had a pronounced effect on the reduction of

CONTRACTILITY, LUSITROPY AND HYPERTROPHY IN AORTIC STENOSIS

dP/dt^- ($p<0.0001$). TAVI induced significant reduction in ESPVR, dP/dt^- and dP/dt^+ at rest, with hyperaemia and with pacing.

When assessing the correlation between the resting haemodynamic measurements of minimum and maximum dP/dt , ESPVR, EDPVR, and strain as derived from tissue tracking MRI cine images, only 3D radial strain and ESPVR ($r=0.686$, $p=0.002$) were significant associates. $LVMl_{ECHO}$ did not correlate with dP/dt^+ , dP/dt^- , EDPVR or ESPVR and $LVMl_{MRI}$ correlated only loosely with ESPVR ($r=-0.432$, $p=0.073$) and EDPVR ($r=-0.430$, $p=0.083$) and not with dP/dt^+ or dP/dt^- .

In LGAS patients, I observed reduced baseline dP/dt^- (-1066 [$-1494, -974$] vs -1439 [$-1652, -1153$], $p=0.050$) and dP/dt^+ (1267 [$1047, 1408$] vs 1533 [$1259, 1812$], $p=0.031$) (Figure 5-4). In addition, there was a trend toward reduced values during hyperaemia before TAVI for dP/dt^- ($p=0.074$).

Post-TAVI, the relative change from pre-TAVI resting ESP ($-9\pm 19\%$ vs $-34\pm 11\%$, $p=0.004$), dP/dt^+ ($-19\pm 15\%$ vs $-37\pm 9\%$, $p=0.013$) and dP/dt^- ($-17\pm 19\%$ vs $-39\pm 15\%$, $p=0.015$) was significantly less profound in LGAS when compared to HGAS patients. In addition, from resting state post-TAVI, hyperaemia also induced a less pronounced effect in the LGAS cohort concerning dP/dt^+ (-1% [$-6, +2$] vs -6% [$-12, -4$], $p=0.014$), and dP/dt^- (-3% [$-11, +1$] vs -10% [$-18, -6$], $p=0.024$). Post-TAVI with rapid pacing, ESP fell less significantly in LGAS patients ($-16\pm 11\%$ vs $-27\pm 10\%$, $p=0.037$).

CONTRACTILITY, LUSITROPY AND HYPERTROPHY IN AORTIC STENOSIS

Table 5-8: Invasive results from induced hyperaemia in all paired datasets

	Pre-TAVI			Post-TAVI		
	<i>Rest</i>	<i>Hyperaemia</i>		<i>Rest</i>	<i>Hyperaemia</i>	
<i>HR (bpm)</i>	78 (68,85)	80 (73,90)	P=0.073	76 (67,85)	80 (73,87)	NS
<i>sBP_{Ao} (mmHg)</i>	117 (102,134)	123 (104,149)	NS	123 (113,131)	133 (108,170)	NS
<i>Alx_{Ao} (%)</i>	70 (46,99)	71 (61,98)	NS	57 (29,68)	71 (47,99)	NS
<i>Alx_{coro} (%)</i>	71 (55,75)	67 (52,75)	NS	37 (25,50)	42 (30,53)	NS
<i>AP_{coro} (mmHg)</i>	40±17	42±14	NS	26±24	32±21	NS
<i>TTI (mmHg.s)</i>	37 (29,44)	39 (32,46)	NS	35 (31,40)	40 (30,55)	NS
<i>DTI (mmHg.s)</i>	26±8	26±12	NS	25±6	32±23	NS
<i>Γ</i>	1.15±0.23	1.20±0.21	NS	1.04±0.25	1.11±0.28	NS
<i>dP/dt+ (mmHg/s)</i>	1397 (1156,1563)	1430 (1106,1558)	NS	960 (833,1095)	864 (742,1036)	P=0.002
<i>dP/dt- (mmHg/s)</i>	-1297 (-1595,-1065)	-1309 (-1577,-999)	NS	-834 (-1071,-715)	-742 (-900,-657)	P<0.001
<i>EDPVR (mmHg/ml)</i>	0.14 (0.10,0.17)	0.13 (0.09,0.16)	P=0.051	0.13 (0.79,0.20))	0.13 (0.07,0.24)	NS
<i>ESPVR (mmHg/ml)</i>	3.15 (2.37,3.87)	2.76 (2.25,3.66)	NS	2.12 (1.73,2.60)	2.12 (1.69,2.55)	NS
<i>RPP (mmHg.bpm)</i>	8536 (7367,11087)	9906 (7415,12518)	P=0.090	9808 (8166,10605)	11078 (9096,13707)	P=0.045

CONTRACTILITY, LUSITROPY AND HYPERTROPHY IN AORTIC STENOSIS

Table 5-9: Invasive results from pacing in all paired datasets

	Pre-TAVI			Post-TAVI		
	<i>Rest</i>	<i>Pacing</i>		<i>Rest</i>	<i>Pacing</i>	
<i>HR (bpm)</i>	78 (68,85)	126 (124,129)	P<0.001	76 (67,85)	126 (124,130)	P<0.001
<i>sBP_{Ao} (mmHg)</i>	117 (102,134)	107 (85,128)	P=0.008	123 (113,131)	100 (83,126)	P<0.001
<i>Alx_{Ao} (%)</i>	70 (46,99)	90 (49,104)	NS	57 (29,68)	43 (27,99)	NS
<i>Alx_{coro} (%)</i>	71 (55,75)	64 (59,81)	NS	37 (25,50)	60 (24,92)	NS
<i>AP_{coro} (mmHg)</i>	42±18	28±14	P=0.012	26±24	27±18	NS
<i>TTI (mmHg.s)</i>	37 (29,44)	30 (20,34)	P<0.001	35 (31,40)	22 (17,30)	P<0.001
<i>DTI (mmHg.s)</i>	27±11	11±4	P<0.001	26±6	14±5	P<0.001
<i>Γ</i>	1.14±0.23	1.37±0.24	P<0.001	1.04±0.25	1.31±0.16	P=0.002
<i>dP/dt+ (mmHg/s)</i>	1397 (1156,1563)	1405 (1078,1781)	NS	960 (833,1095)	1023 (860,1270)	NS
<i>dP/dt- (mmHg/s)</i>	-1297 (-1595,-1065)	-1029 (-1424,-750)	P<0.001	-834 (-1071,-715)	-679 (-905,-514)	P<0.001
<i>EDPVR (mmHg/ml)</i>	0.14 (0.10,0.17)	0.17 (0.10,0.28)	NS	0.13 (0.08,0.20)	0.14 (0.08,0.23)	NS
<i>ESPVR (mmHg/ml)</i>	3.15 (2.37,3.87)	2.66 (2.23,4.05)	NS	2.12 (1.73,2.60)	1.71 (1.37,2.38)	P=0.018
<i>RPP (mmHg.bpm)</i>	8536 (7367,11087)	13682 (10679,15621)	P<0.001	9808 (8166,10605)	12094 (10795,15867)	P<0.001

CONTRACTILITY, LUSITROPY AND HYPERTROPHY IN AORTIC STENOSIS

Table 5-10: The impact of TAVI (pre- vs post) on cardiac mechanics during three physiological settings in all paired datasets

	Baseline			Hyperaemia			Pacing		
	Pre-TAVI	Post-TAVI		Pre-TAVI	Post-TAVI		Pre-TAVI	Post-TAVI	
HR (bpm)	78 (68,85)	76 (67,85)	NS	80 (73,90)	80 (73,87)	NS	126 (124,129)	126 (124,130)	NS
sBP _{AO} (mmHg)	117 (102,134)	123 (113,131)	NS	123 (104,149)	133 (108,170)	NS	107 (85,128)	100 (83,126)	NS
AIx _{AO} (%)	70 (46,99)	57 (29,68)	P=0.023	71 (61,98)	71 (47,99)	NS	90 (49,104)	43 (27,99)	P=0.096
AIx _{coro} (%)	71 (55,75)	37 (25,50)	P=0.001	67 (52,75)	42 (30,53)	P<0.001	64 (59,81)	60 (24,92)	NS
AP _{coro} (mmHg)	42±18	26±24	P=0.026	42±14	29±14	P<0.001	28±14→	27±18	NS
TTI (mmHg.s)	37 (29,44)	35 (31,40)	NS	39 (32,46)	40 (30,55)	NS	30 (20,34)	22 (17,30)	P=0.045
DTI (mmHg.s)	27±11	26±6	NS	25±11	32±23	NS	11±4	14±5	P=0.055
Γ	1.14±0.23	1.04±0.25	NS	1.20±0.21	1.12±0.28	NS	1.37±0.24	1.31±0.16	NS
dP/dt+ (mmHg/s)	1397 (1156,1563)	960 (833,1095)	P<0.001	1430 (1106,1558)	864 (742,1036)	P<0.001	1405 (1078,1781)	1023 (860,270)	P<0.001
dP/dt- (mmHg/s)	-1297 (-1595,-1065)	-834 (-1071,-715)	P<0.001	-1309 (-1577,-999)	-741 (-900,-657)	P<0.001	-1029 (-1424,-750)	-679 (-905,-514)	P=0.001
EDPVR (mmHg/ml)	0.14 (0.10,0.17)	0.13 (0.09,0.20)	NS	0.13 (0.09,0.16)	0.13 (0.07,0.24)	NS	0.17 (0.10,0.28)	0.14 (0.08,0.23)	NS
ESPVR (mmHg/ml)	3.15 (2.37,3.87)	2.12 (1.73,2.60)	P<0.001	2.76 (2.25,3.66)	2.12 (1.69,2.55)	P=0.001	2.66 (2.23,4.05)	1.71 (1.37,2.38)	P<0.001
RPP (mmHg.bpm)	8536 (7367,11087)	9808 (8166,10605)	NS	9906 (7415,12518)	11078 (9096,13707)	NS	13682 (10679,15621)	12094 (10795,15867)	NS

5.2.8 Reflection Coefficient and Augmentation Index

Γ increased from baseline with pacing both pre- and post-TAVI (Table 5-9). TAVI caused the coronary Alx to fall at rest and during hyperaemia, presumably related to reduced systemic vascular resistance following valve intervention.

These variables were also different between study groups (Table 5-11). Both coronary and aortic Alx, coronary AP and Γ were significantly lower in LGAS at rest and during hyperaemia pre-TAVI. Post-TAVI, the observation of reduced aortic Alx and coronary AP in LGAS patients was sustained during hyperaemia. There were no statistically significant differences observed between cohorts during rapid pacing. In this study, there was no association between the arterial wave reflection with either the aortic valve calcium score or indexed calcium score.

CONTRACTILITY, LUSITROPY AND HYPERTROPHY IN AORTIC STENOSIS

Table 5-11: Invasive results in LGAS and HGAS cohorts for resting and hyperaemic states. Results displayed when P<0.010 for LGAS then HGAS with SD or IQR in brackets.

	Pre-TAVI		Post-TAVI	Pre-TAVI		Post-TAVI
	REST			HYPERAEMIA		
<i>HR (bpm)</i>		NS	NS		NS	NS
<i>sBP_{Ao} (mmHg)</i>		NS	NS		NS	NS
<i>AIx_{Ao} (%)</i>	57 (28,72)/91 (55,102)	P=0.010	NS	65 (35,71)/88 (76,102)	P=0.014	49 (28,71)/99 (61,106) P=0.022
<i>AIx_{coro} (%)</i>	55 (30,73)/74 (66,87)	P=0.028	NS	65 (40,70)/74 (65,85)	P=0.040	20 (14,29)/32 (20,53) P=0.095
<i>AP_{coro} (mmHg)</i>	26 (18,47)/49 (38,54)	P=0.035	NS	36 (28,43)/45 (38,53)	P=0.063	39 (20,43)/45 (34,64) P=0.022
<i>TTI (mmHg.s)</i>		NS	NS		NS	NS
<i>DTI (mmHg.s)</i>		NS	NS	29 (21,43)/20 (14,32)	P=0.094	NS
<i>Γ</i>	0.99 (0.85,1.08)/1.33 (1.12,1.45)	P=0.028	NS	1.12 (0.88,1.25)/1.33 (1.20,1.42)	P=0.014	NS
<i>RPP (mmHg.bpm)</i>		NS	NS		NS	NS

5.2.9 Tissue and Serum Results

In this study, of the ten endomyocardial biopsy samples, no cases of amyloidosis were detected. In addition, there was no evidence of amyloidosis in any case with CMR.

The role of cardiac biomarkers in stratifying the risk and timing of intervention is key, especially when symptoms are confounded by comorbidities. Neurohormonal activation, stimulating the release of enzymes such as troponin and N-terminal pro-B natriuretic peptide (NT-proBNP) correlates well with symptom-free survival and allows monitoring using a simple blood test. NT-proBNP levels at baseline were 720ng/l (369,983) in LGAS patients and 1355ng/l (935,6957) in HGAS patients ($p=0.058$) and reduced following TAVI when both cohorts were analysed together (897 [566,1559] to 500 [174,1209], $p=0.011$). However, BNP change was less profound in LGAS patients when compared with HGAS (+16% [-55,+37] vs -73% [-89,-42], $p=0.020$).

Baseline NT-proBNP levels correlated closely with the indexed aortic valve area ($R=-0.527$, $p=0.025$), LVMI ($R=0.550$, $p=0.018$), backward expansion wave ($R=-0.821$, $p<0.001$), peak radial strain ($R=-0.819$, $p<0.001$), and microvascular resistance (pancardiac MR $R=-0.496$, $p=0.036$ and diastolic MR $R=-0.480$, $p=0.044$).

5.3 Discussion and summary

Significant remodelling occurred within a few months of valve intervention. LV size, mass and mass:volume ratio reduced. Poor correlation existed between measures of stroke volume, aortic valve area and left ventricular mass when measured by echocardiography and MRI or CT and echocardiography is known to underestimate stroke volume²⁴⁶. Left ventricular outflow tract (LVOT) diameter is an important measurement in stroke volume calculation by echocardiography, yet this calculation does not take into consideration its elliptical shape and it is frequently inaccurately measured. In this study, LVOT measurement by echocardiography was lower than comparative gated computed tomography resulting in a significant impact on stroke volume calculation. Stroke volume

CONTRACTILITY, LUSITROPY AND HYPERTROPHY IN AORTIC STENOSIS

as calculated by echocardiography was also significantly lower than that calculated by MRI.

There was no significant difference in Z_{va} between cohorts, contrary to previous work. Baseline Alx and Γ measurements were significantly lower in LGAS patients, perhaps related to lower LVMI or reduced vascular load, however these differences from HGAS patients were eliminated immediately following TAVI. There were minimal differences in strain parameters between cohorts but minimum and maximum dP/dt were lower in LGAS patients as was the change in LV end systolic pressure post-TAVI.

GLS is closely related to all-cause mortality²³⁸ and both cohorts exhibited reduced strain. Whilst LGAS is typically associated with reduced GLS in comparison to HGAS⁸¹ which was not found in this study, the HGAS recruits in this study were at the “critical” end of severe AS and likely to feature profound subclinical LV dysfunction. Low-flow in the setting of AS has been linked with higher levels of miRNA1 and miRNA21 when compared to other subgroups of AS, the latter found to correlate with reduced global longitudinal strain²⁴⁷.

These data are supportive of LGAS exhibiting reduced LV contractility and similarly reduced strain in comparison to HGAS patients despite reduced LVMI. LV remodelling did however respond to TAVI in a similar way to HGAS patients.

6 MYOCARDIAL FIBROSIS IN AORTIC STENOSIS

6.1 Introduction

“...Factors other than the functional state of the myocardium may be responsible for substantial alterations in ventricular end-diastolic pressure”

Herbert J Levine, 1972²²⁷

Fibrosis is a maladaptive response to damaged myocardium. It can be macroscopically identifiable and is detected as late gadolinium enhancement on cardiac magnetic resonance. This replacement fibrosis is irreversible, whereas earlier diffuse interstitial fibrosis may be reversible, detected by cardiac magnetic resonance T₁ mapping techniques. Interstitial fibrosis appears as fine strands of collagenous connective tissue encircling and separating individual muscle fibres. In another form, perivascular fibrosis is expansion of the amount of fibrosis in adventitia of intramyocardial arteries and veins¹²⁸. Interstitial, and replacement fibrosis in the sub-endocardium, and midwall of the left ventricle have been demonstrated in patients with aortic stenosis (AS) and normal coronary arteries^{88,127,133,136,138,140,143}. The result is stiffened, impaired myocardium with clinical sequelae of heart failure and increased mortality. This chapter will focus on the pathophysiology of fibrosis in AS, and findings from cardiac magnetic resonance imaging and histological assessment of patients undergoing trans-catheter aortic valve implantation to challenge the hypothesis of a greater proportion and distinct distribution of myocardial fibrosis in low gradient aortic stenosis.

6.1.1 Pathogenesis of Fibrosis

Pressure overload from AS results in compensatory hypertrophy, a response to increased biomechanical stress but this later becomes pathological and results in apoptosis and necrosis, and fibrosis. Cardiomyocyte width and subendocardial collagen content increase²⁴⁸. Myocardial extracellular matrix (ECM) provides a dynamic balance of proteins and signaling molecules to maintain an appropriate scaffold for cardiac structure and provide a link between intracellular cytoskeletal proteins and intercellular proteins. The myocardial cells are supported by it, which consists of a macromolecular network of

MYOCARDIAL FIBROSIS IN AORTIC STENOSIS

fibres with intricate 3D organisation that largely determines the structural and functional integrity of the heart²⁴⁹. This matrix is composed of collagen, pericellular matrix components (fibronectin and proteoglycans), basement membrane components (laminin and collagen type IV), proteases and growth factors²⁵⁰.

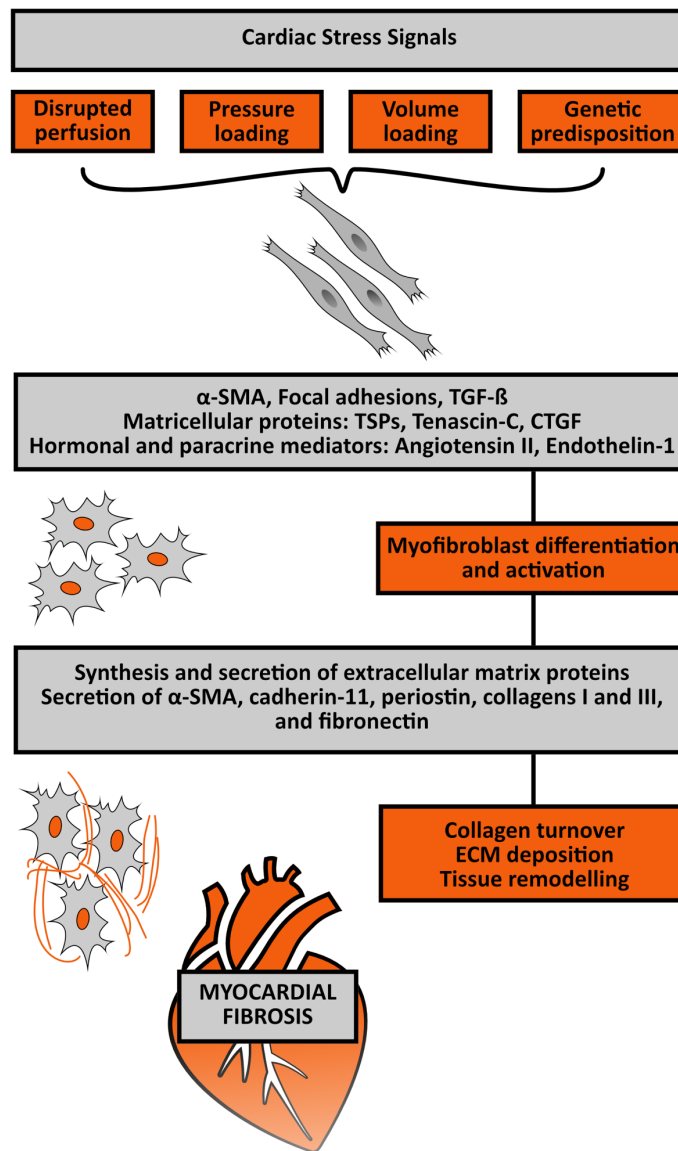


Figure 6-1: Schematic diagram of the pathogenesis of fibrosis

Many different pathophysiological stimuli can insult the myocardium, inducing a cascade which ultimately results in fibrosis by stimulating cardiac myofibroblasts to mediate excessive deposition of connective tissue in the interstitial space. Instigators include myocarditis, ischaemia and infarction, pressure overload from hypertension or AS,

MYOCARDIAL FIBROSIS IN AORTIC STENOSIS

diabetes mellitus, chronic renal impairment, non-ischaemic dilated cardiomyopathy, hypertrophic cardiomyopathy, toxic cardiomyopathies, sarcoidosis, and infiltrative disease such as amyloidosis and Anderson-Fabry disease.

In response to insult, cardiac myofibroblasts are activated by mechanical conductor signals and signaling molecules (including TGF- β , endothelin-1, fibroblast growth factor and cytokines), become proliferative and invasive, increasing secretion of ECM-degrading matrix metalloproteinases (MMPs) and collagen turnover (Figure 6-1). Cardiac remodelling ensues, including myocyte hypertrophy, apoptosis, necrosis, fibroblast proliferation, increased fibrillar collagen and fibrosis²⁵¹. Early response of MMP activation and regulation of tissue inhibitors of metalloproteinases (TIMPs) allow repair but later become maladaptive with clinical impact. Whilst MMPs, which control ECM degradation, do not normally exist in the ECM, they are upregulated in pathological settings, and TGF- β can suppress their activity and enhance activity of TIMPs²⁵².

Two main cell types are found in the heart, cardiac myocytes and mesenchymal cells (cardiac fibroblasts and myofibroblasts). Pro-fibrotic signaling factors cause quiescent cardiac fibroblasts to differentiate into myofibroblasts and proliferate, inducing ECM deposition. During this process they express α -smooth muscle actin (SMA), and synthesise and secrete fibrillar collagen types I and III²⁵³ and fibronectin. A cycle of increasing ECM ensues, with positive feedback from myofibroblasts which release profibrotic signaling factors, such as TGF- β 1 and Wnt, which further promote myofibroblast differentiation and ECM deposition. Typically, fibrosis is accompanied by apoptosis and necrosis, and its formation is related to complex spatial and temporal remodeling of the myocardium and controlled by a plethora of signaling cascades. These intra- and intercellular pathways include inflammatory, pro-fibrotic, and migratory mediators²⁵⁴.

Several critical contributors are involved. TGF- β stimulates α -SMA-rich myofibroblast formation²⁵⁵, and α -SMA is a powerful marker of myofibroblastic cells and negatively regulated by γ -interferon²⁵⁶. TGF- β is mediated via fibronectin to induce α -SMA and

MYOCARDIAL FIBROSIS IN AORTIC STENOSIS

collagen formation, and also stimulates connective tissue growth factor (CTGF)²⁵⁷. CTGF is an essential mediator in TGF- β induced tissue remodeling and fibrosis²⁵⁸ and it correlates with fibronectin and collagen types I and III in the setting of ischaemia. Inhibition of both CTGF and TGF- β 1 has been shown to prevent myocardial fibrosis in animal models^{258,259}.

The renin-angiotensin-aldosterone system is involved in regulating myocardial fibrosis and circulating angiotensin II is thought to affect gene expression. Blockade of angiotensin II type-1 receptors has been shown to normalise the ratio of collagen I (providing rigidity and stiffness) to collagen III (providing elasticity) since this is usually imbalanced (collagen I increases more than III), leading to increased wall tension²⁶⁰.

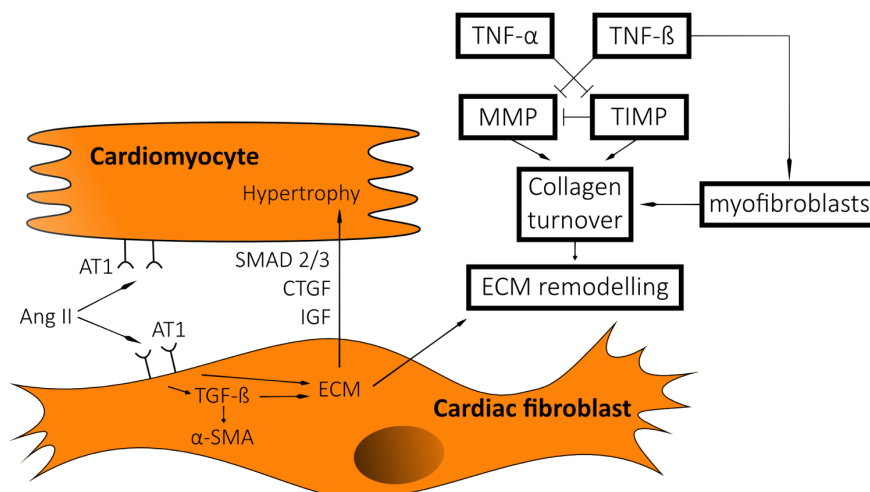


Figure 6-2: Molecular signaling involved between cardiac fibroblasts and cardiomyocytes

Inflammatory cells also play a vital role in the response to pathological stimulus. Monocytes differentiate into macrophages, travel to the area of damage and carry out proteolytic activity and secrete pro-inflammatory mediators. These cells can regulate the balance of MMPs and TIMPs²⁶¹.

6.1.2 Fibrosis in AS

MYOCARDIAL FIBROSIS IN AORTIC STENOSIS

Increasing pressure overload in AS results in left ventricular myocyte hypertrophy and the proliferation (or hyperplasia) of connective tissue cells²⁶². The tensile stress of the myocardium reflects the mechanical properties of its integrated muscle and interstitial connective tissues, and with increased stiffness, ventricular filling requires more energy, leading to increased ventricular filling pressures and symptoms of heart failure. As the myocardium responds to pressure overload, reduced density of cardiac muscle nuclei signifies hypertrophy rather than hyperplasia, and there is a proportionate increase in connective tissue (muscle cell % of myocardium remains steady at 75-81% irrespective of left ventricular mass) – that commensurate connective tissue increase is a component of cardiac enlargement^{228,263}.

The mRNA expression of MMPs and TIMPs along with their protein levels has been investigated in patients with AS undergoing aortic valve replacement, with findings of significantly greater levels of MMP-2 and an overall balance shifted towards MMP inhibition, thereby favouring collagen accumulation²⁶⁴.

Cellular adhesion molecules are expressed on vascular endothelium and on immune and inflammatory cells and are involved the migration of cells to areas of inflammation, transmigration of lymphocytes, and in immune effector functions. The molecules intercellular adhesion molecule 1 (ICAM-1), vascular cell adhesion molecule 1 (VCAM-1), and E-selectin are expressed on vascular endothelium and serve as ligands for counter-receptors on circulating inflammatory cells. Serum levels of these molecules are elevated in patients with AS²⁶⁵ and this upregulation may indicate underlying microvascular inflammation and macrophage activation.

PECAM-1 (CD31) staining is known to be a highly sensitive endothelial marker and can be used to measure blood vessel density in myocardium. A higher percentage of blood vessels in the total myocardium correlates with reduced LV ejection fraction, higher E/e', blunted global longitudinal strain, greater LVMI and smaller aortic valve area²⁶⁶.

6.1.3 Interstitial and Replacement Fibrosis in Aortic Stenosis

MYOCARDIAL FIBROSIS IN AORTIC STENOSIS

Chelates of gadolinium, a ferromagnetic metal, are used routinely as contrast media for cardiac magnetic resonance imaging (CMR), having been first applied in 1984²⁶⁷. They are safe for clinical use since chelated gadolinium compounds are renally excreted, although rarely may cause nephrogenic systemic fibrosis in patients with severe renal impairment. Scarred tissue passively accumulates more contrast agent, thereby shortening the T_1 value in comparison to healthy myocardium, visible on inversion recovery sequences. Delayed imaging to detect this gadolinium hold up in the extracellular expansion (late gadolinium enhancement, LGE) provides detailed information on diseased myocardium, and is an independent and powerful predictor of death and cardiovascular risk. Utilisation of this tissue characterisation is arguably the most pertinent use for CMR. Once established, fibrosis progresses but is arrested (not reversed) by aortic valve intervention^{268,269}. LGE is sensitive in detecting replacement fibrosis, however it is insensitive in the detection of diffuse fibrosis.

Native longitudinal relaxation time (T_1) is increased with the expansion of the interstitial space, for example with oedema, fibrosis, infarction, and protein infiltration (and shortened with fat and iron deposition) and can be used in the detection of interstitial fibrosis. T_1 is measured in CMR by creating T_1 mapping sequences and T_1 mapping describes the pixel-wise quantification of the relaxation time, mapped to enable tissue characterisation. Extracellular volume (ECV) using pre- and post-contrast myocardial and blood pool T_1 values was then calculated as outlined in Section 2.7.3 – this has been shown to correlate more closely with outcomes when compared with native T_1 alone²⁷⁰.

6.2 Results

6.2.1 LGE results

I found that three out of nine patients with LGAS exhibited subendocardial late gadolinium enhancement, and two patients out of ten with HGAS demonstrated mid-wall enhancement (Figure 6-3) – there was no crossover. Focal fibrosis did not change when assessed on follow-up CMR post-TAVI.

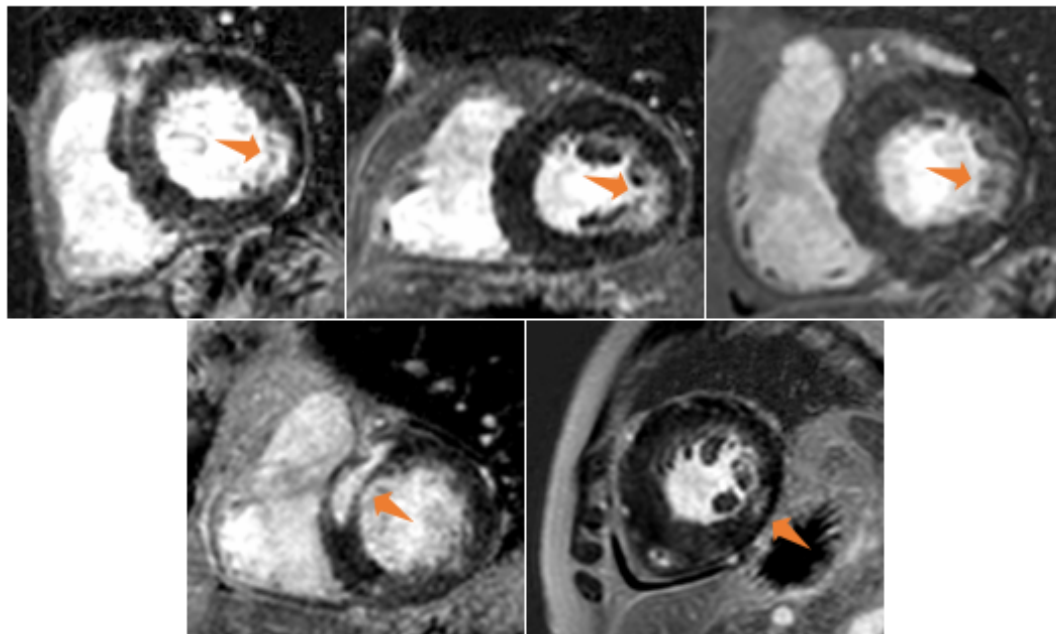


Figure 6-3: Late gadolinium demonstrating replacement fibrosis. Top panel: three patients with LGAS featuring subendocardial fibrosis; Bottom panel: Midwall fibrosis in two patients with HGAS (there was no crossover in this pattern of LGE)

6.2.2 T₁ Mapping for Interstitial Fibrosis

ECV did not change following intervention (0.299 ± 0.044 to 0.292 ± 0.024 , $p=0.533$). This was despite a fall in LVMI by 17% (64 to 53 g/m^2 , $p<0.001$) and a similar reduction in matrix volume (the product of LV mass and ECV) by 18% (33.2 ± 9.9 to $27.2 \pm 6.8 \text{ ml/m}^2$, $p=0.002$) (Table 6-1). These changes in LV mass and matrix volume are in keeping with previously published data demonstrating a 19% and 22% reduction, respectively, one year after aortic valve replacement²⁶⁹.

Table 6-1: LGAS and HGAS results for myocardial components

	LGAS	HGAS	P value
Myocardial mass			
ALL (g)	108.0 (96.8,118.7)	→ 90.9 (78.4,104.7)	0.001
Pre-TAVI (g)	97.3±16.4	120.9±30.6	0.051
Post-TAVI myocardial mass (g)	88.5±15.4	97.3±27.4	NS
Change following intervention (%)	-11±18	-26±20	NS
Left ventricular mass index			
ALL (g/m ²)	62.7 (58.6,70.2)	→ 51.0 (44.1,55.8)	<0.001
Pre-TAVI (g/m ²)	56.3±8.5	71.1±18.1	0.037

MYOCARDIAL FIBROSIS IN AORTIC STENOSIS

<i>Post-TAVI (g/m²)</i>	48.1±7.0	56.8±15.8	NS
<i>Change following intervention (%)</i>	-17±13	-27±21	NS
Extracellular volume			
<i>ALL (%)</i>		29.9±4.4 → 29.2±2.4	NS
<i>Pre-TAVI (%)</i>	30.3±4.9	29.4±3.8	NS
<i>Post-TAVI (%)</i>	29.1±2.4	29.3±2.5	NS
<i>Change following intervention (%)</i>	-2±16	0.4±11	NS
Matrix volume			
<i>ALL (ml/m²)</i>		33.2±9.9 → 27.2±6.8	0.002
<i>Pre-TAVI (ml/m²)</i>	29.9±8.4	35.7±10.4	NS
<i>Post-TAVI (ml/m²)</i>	25.6±3.9	28.5±8.5	NS
<i>Change following intervention (%)</i>	-8±30	-19±13	NS
Native T1			
<i>ALL (ms)</i>		1158±67 → 1182±54	0.089
<i>Pre-TAVI (ms)</i>	1158±75	1166±64	NS
<i>Post-TAVI (ms)</i>	1168±63	1194±46	NS
<i>Change following intervention (%)</i>	2±3	3±6	NS

There was no difference between LGAS and HGAS groups for pre-TAVI native T₁, ECV and matrix volume. There was also no difference for these values post-TAVI and relative change post-intervention.

Significant correlations existed between baseline matrix volume and LVMI_{MRI} (R=0.619, p=0.005), resting diastolic microvascular resistance (R=-0.482, p=0.036), LVEDVi (R=0.710, p=0.001), LVESVi (R=0.648, p=0.003), SVi (R=0.614, p=0.006), CO (R=0.528, p=0.020) and global radial strain (R=-0.578, p=0.012). Native pre-TAVI T1 was associated with the relative change in endocardial-epicardial gradient (r=0.471, p=0.049) following intervention, and with resting diastolic microvascular resistance (R=-0.483, p=0.036). In addition, the change in native T1 following TAVI was associated with baseline BNP level (R=-0.716, p=0.001), ejection fraction (R=0.599, p=0.009) and radial strain (R=0.576, p=0.016). There was no significant correlation between global MPRI and LVMI, indexed stroke volume, or indexed end systolic and diastolic volumes.

6.2.3 Aortic Valve Calcification and Correlations

The normal aortic valve is a complex functional unit which ensures seamless kinetic energy transfer from the ventricle to the aorta. Aortic valve calcification is not simply a degenerative process. The initial cause is often linked to altered mechanical loading, but tissue remodelling is perpetuated by inflammation and fibrosis. Calcific AS

MYOCARDIAL FIBROSIS IN AORTIC STENOSIS

pathophysiology can be divided into two distinct phases – initiation and propagation. The former has a similar profile to that of atherosclerosis, from endothelial insult/activation to inflammation with risk factors including male gender, body mass index, smoking, hypertension, and deranged lipid profile⁴³.

In this study, patients with LGAS had a lower calcium score compared to HGAS patients (1935 [1244,3219] vs 2997 [2753,5868], $p=0.028$) and also when indexed to body surface area (720 [550,1821] vs 1649 [1544,1799], $p=0.017$). There was significant correlation between indexed calcium score and indexed aortic valve area ($R=-0.516$, $p=0.024$), mean aortic valve pressure gradient ($R=0.614$, $p=0.006$), peak pressure gradient ($R=0.610$, $p=0.006$), baseline indexed LV end systolic volume ($R=0.540$, $p=0.017$), and $LVMl_{MRI}$ ($R=0.477$, $p=0.039$). There was no correlation between calcium score values and stroke volume calculated either by MRI or echocardiography.

6.3 Summary

Hermann *et al*⁸⁸ demonstrated that patients with a low transvalvular gradient present with more advanced myocardial fibrosis, typically at the subendocardium. As discussed in section 1.7.2, longitudinal subendocardial fibres are vulnerable to ischaemia and left ventricular pressure overload and may not be reflected by global ejection fraction. Left ventricular pressure was lower in LGAS patients (see

Table 7-5), yet the pattern of subendocardial fibrosis as assessed by us was more prominent. Midwall fibrosis has been clearly described¹³³ and carries significant risk and is the pattern of fibrosis typically associated with HGAS as seen in this study.

There was no difference in the burden of interstitial fibrosis between patients with LGAS and HGAS. This was despite lower LVMI in patients with LGAS and reduced contractility. Patients with LGAS had reduced aortic valve calcification, correlating with LVMI, and valve gradients, but not stroke volume. Left ventricular mass regression following aortic valve intervention can be driven by ECM regression alone (reduction in ECV), by cellular regression alone (ECV increases), or by proportional regression in cellular and matrix compartments (ECV remains the same)²⁶⁹, as observed in this study in both cohorts. Our hypothesis that LGAS would demonstrate higher levels of interstitial fibrosis is not supported by these findings. AS may be a secondary condition in these patients, with an underlying primary ventricular myopathy yet this is not explained by LV mass regression, and a lack of differentiation between cohorts post-intervention. Further histological assessment to correlate ECV to collagen volume fraction would be beneficial in the assessment of fibrosis phenotyping.

7 CARDIAC-CORONARY COUPLING PRE- AND POST-TAVI

7.1 Introduction

“If it were possible to correlate the family of ventricular function curves under varying conditions with simultaneously obtained ventricular pressure-volume curves, a comprehensive view of the physical determinants of cardiac action would be at hand”

Sarnoff & Berglund 1954²⁷¹

Left ventricular (LV) contraction influences the arterial systolic pressure upstroke in a complex interplay of contractility, aortic valve flow, arterial peripheral resistance, diastolic pressure, and the pattern of LV electrical activation. Cardiac-coronary coupling is the term used to describe the intertwined relationship which comes from simultaneous crosstalk between excitation-contraction, coronary blood flow and ventricular mechanical properties.

This chapter focuses on the interaction of coronary and cardiac performance and efficiency, and their quantification by physiological assessment before and after transcatheter aortic valve implantation (TAVI) using left ventricular pressure-volume loops and coronary pressure and flow. This complex relationship has been described in previous chapters, but here, I will focus on acute modifications of coronary and LV performance and interaction, testing further hypothesised patterns of impaired coronary flow and left ventricular myopathy in low gradient patients.

7.1.1 The Cardiomyocyte

Cardiomyocytes are the individual functional units of cardiac muscle, providing the contractile power of the heart. Cardiac muscle is striated due to alternating thick and thin filaments composed of myosin and actin, respectively. Cardiomyocytes contain these contractile protein filaments known collectively as myofibrils, as repeating sections of sarcomeres, the basic unit of contractile muscle. Sarcomeres are connected to a plasma membrane, a sarcolemma, by transverse (T)-tubules, which speed up the rate of

depolarisation within the sarcomere. Contraction and relaxation is made possible by myosin and actin adenosine triphosphate binding, allowing the two proteins to slide past each other – thin over thick filaments.

7.1.2 Cardiac Excitation-Contraction Coupling

Excitation-contraction coupling embodies the process of converting electrical stimulus (excitation) to a mechanical response (contraction). Action potentials, induced by the pacemaker cells in the sinoatrial and atrioventricular nodes, are conducted to cardiomyocytes through gap junctions. When between sarcomeres in the sarcolemma, it travels into T-tubes, depolarising the cell membrane (Figure 7-1).

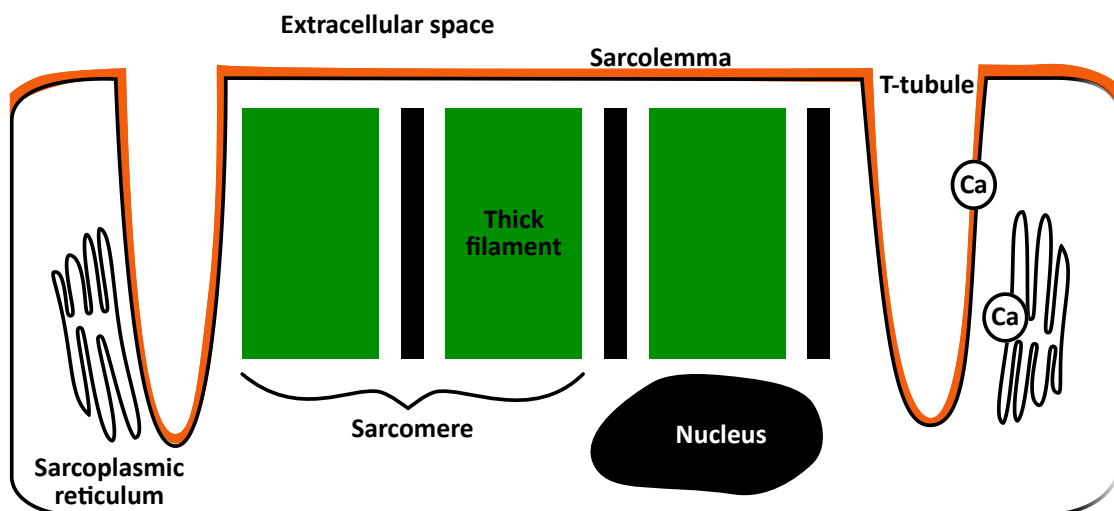


Figure 7-1: Figure demonstrating the cardiac excitation-contraction on a cellular level

Cell membrane calcium channel receptors respond to the action potential to open and allow calcium influx, which subsequently causes sarcoplasmic reticulum to release further calcium. Thin filaments are composed of troponin, tropomyosin and actin, together forming a regulatory protein complex. Resulting high levels of intracellular calcium binds to troponin-C in the regulatory complex and resulting changes in the structure of this complex triggers exposure of actin through Troponin-I, allowing myosin ATPase located on the myosin head to bind to actin, which is pulled towards the centre of the sarcomere, contracting the muscle. Intracellular calcium is then removed by the

sarcoplasmic reticulum, and with this reduction in concentration, the regulatory protein complex returns to its original structure, breaking the actin-myosin connection and ending contraction.

7.1.3 Preload and Afterload

Preload refers to the degree of tension on the cardiac myocytes when they begin to contract, and afterload is the load against which the muscle exerts its contractile force. End diastolic pressure relates to preload and is a measure of sarcomere length. Changes in preload dramatically affect ventricular dimensions and stroke volume by the Frank-Starling mechanism – the greater the heart muscle is stretched during filling, the greater the force of contraction and the greater the stroke volume, within physiologic limits. By contrast, if preload decreases, stroke volume drops.

Table 7-1: Influences of variables on parameters of ventricular function²⁷²

	Contractility sensitive	Diastolic function sensitive	Afterload independent	Size (body, heart) independent	Valve function independent
PRSW	✓	✓	✓	✓	✓
EF	✓	-	-	✓	-
Ees	✓	-	✓	-	✓

Preload recruitable stroke work (PRSW) is determined by the linear regression of stroke work with the end-diastolic volume. The slope of the PRSW is an index for evaluating the overall ventricular function that is independent of the afterload, preload, and ventricle size (Table 7-1).

Starling's contractility index (SCI), the slope of the relationship between dp/dt^+ and EDV upon preload reduction, is more sensitive to changes in contractility than end-systolic elastance (Ees) and PRSW.

The PVA is the area between the EDPVR and ESPVR as a function of EDP and is independent of afterload. A previous study demonstrated a highly significant linear correlation with myocardial oxygen consumption²⁷³.

The time constant of isovolumetric relaxation, Tau, has previously been shown to increase with progressive left ventricular dysfunction and pulmonary hypertension in the setting of aortic stenosis. It positively correlates with EDV, ESV, LV mass index, pulmonary capillary wedge pressure and EDP, and negatively with ejection fraction and dP/dt ²⁷⁴.

7.1.4 Ventricular-Arterial Coupling

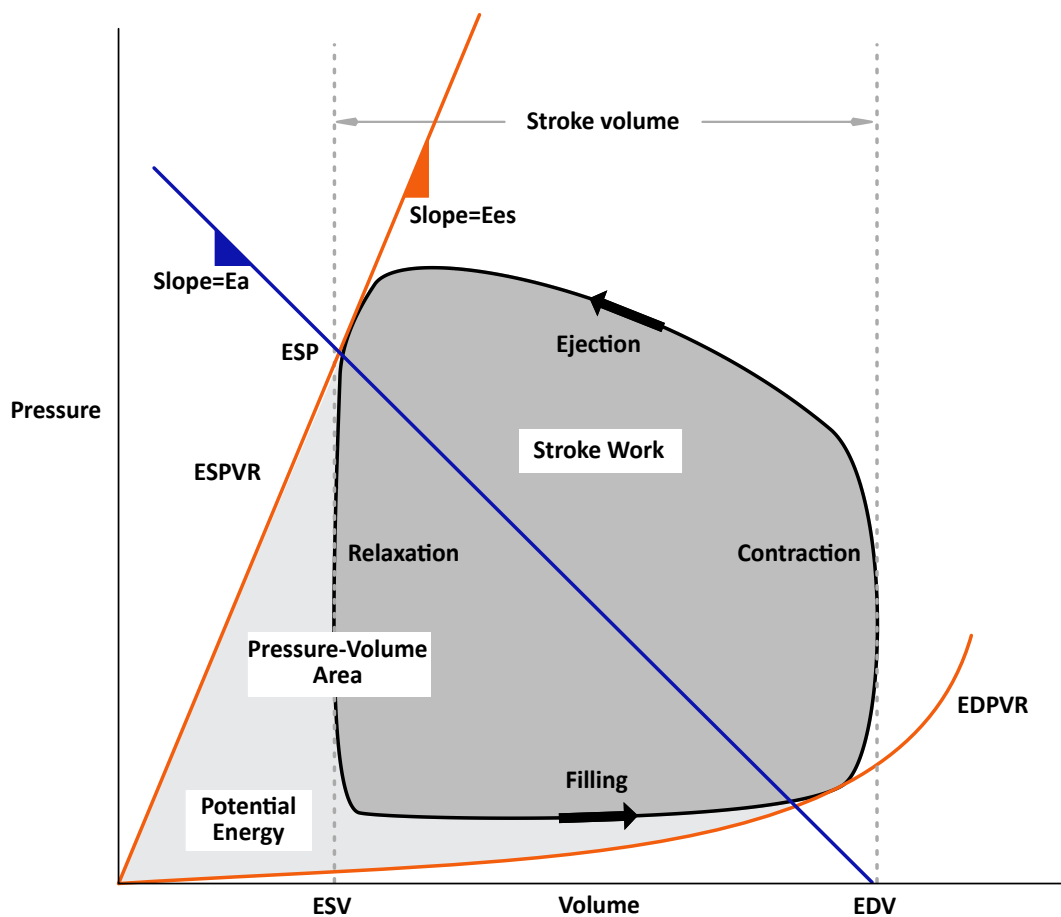


Figure 7-2: Haemodynamic indices used in pressure-volume loop datasets

Ventricular-arterial coupling (VA) is measured as the ratio between effective arterial elastance (E_a), an index of afterload, and end systolic elastance (E_{es}), a load-independent index of contractility (Figure 7-2). E_a is an integrative index incorporating the principal elements of arterial load including peripheral vascular resistance, total arterial

compliance, characteristic impedance and systolic and diastolic time intervals²⁷⁵. VA is therefore a measure of the interaction between the LV and the arterial system and can be used to assess acute modifications of LV performance. Increasing VA coupling signifies increased end systolic LV stiffness, which may be mediated by enhanced myocardial contractility. VA has been shown to fall post-TAVI, along with Zva – this is in relation to increased systemic arterial compliance and reduced systemic vascular resistance²⁷⁵.

7.2 Results

In all patients, both before and after TAVI, the PRSW fell from baseline with rapid pacing ($p<0.001$) and when comparing rest measurements, hyperaemia and rapid pacing, like for like, before and after TAVI, all PRSW values reduced ($p<0.001$) (Table 7-3 and Table 7-4). Pre-TAVI, there was reduced PRSW in LGAS patients ($p=0.013$) indicating reduced myocardial contractility (

Table 7-5). Stroke work at baseline closely correlated with dP/dt ($R=-0.661$, $p=0.003$), and peak radial and circumferential strain ($R=-0.510$, $p=0.037$, and $R=0.535$, $p=0.027$, respectively). PRSW also closely correlated with resting dP/dt ($R=-0.658$, $p=0.003$) and ESPVR ($R=0.480$, $p=0.044$). There was also a link between resting dP/dt and PVA ($R=-0.606$, $p=0.008$).

SCI increased with rapid pacing, pre- and post-TAVI, and TAVI induced a reduction in SCI during like-for-like conditions of rest, hyperaemia and rapid pacing ($p<0.001$). There was a close correlation between SCI and ESPVR ($R=0.847$, $p<0.001$).

CARDIAC-CORONARY COUPLING PRE- AND POST-TAVI

Table 7-2: The effect of hyperaemia on full pressure-volume loop results in all paired datasets

	Pre-TAVI (n=17)			Post-TAVI (n=18)		
	<i>Rest</i>	<i>Hyperaemia</i>		<i>Rest</i>	<i>Hyperaemia</i>	
<i>SV (ml)</i>	77 (66,96)	84 (65,95)	NS	82 (62,92)	85 (59,89)	NS
<i>EDP (mmHg)</i>	17 (12,27)	19 (13,26)	NS	17 (10,26)	18 (8,27)	NS
<i>ESP (mmHg)</i>	151 (126,172)	149 (125,168)	NS	110 (104-126)	101 (95,121)	P=0.003
<i>EDV (ml)</i>	135 (104,152)	133 (107,159)	NS	132 (108,148)	126 (101,147)	NS
<i>ESV (ml)</i>	50 (38,56)	49 (40,66)	NS	55 (46,58)	53 (39,64)	NS
<i>EF (%)</i>	61 (56,68)	60 (53,68)	NS	62 (55,66)	63 (52,69)	P=0.074
<i>CO (l/min)</i>	5.4 (4.3,6.5)	5.3 (4.3,7.3)	NS	6.0 (4.0,7.1)	5.5 (3.7,6.8)	NS
<i>Ea (mmHg/ml)</i>	1.9 (1.6,2.5)	1.7 (1.4,2.6)	NS	1.5 (1.2,1.8)	1.44 (1.09,1.94)	P=0.021
<i>Ees (mmHg/ml)</i>	3.0 (2.4,3.9)	2.7 (2.2,3.6)	NS	2.0 (1.7,2.6)	2.1 (1.7,2.5)	NS
<i>VA</i>	0.63 (0.48,0.79)	0.66 (0.48,0.90)	NS	0.63 (0.51,0.84)	0.60 (0.46,0.92)	P=0.048
<i>SCI (mmHg/ml/s)</i>	10.2 (8.1,14.8)	10.5 (7.9,13.2)	P=0.071	7.9 (6.1,10.0)	7.9 (5.8,9.4)	NS
<i>Tau (ms)</i>	40 (36,53)	41 (37,58)	NS	52 (37,423)	89 (40,415)	P=0.067
<i>dP/dt+ (mmHg/s)</i>	1397 (1156,1563)	1430 (1106,1558)	NS	960 (833,1095)	864 (742,1036)	P=0.002
<i>dP/dt- (mmHg/s)</i>	-1297 (-1595,-1065)	-1309 (-1577,-999)	NS	-834 (-1071,-715)	-742 (-900,-657)	P<0.001
<i>EDPVR (mmHg/ml)</i>	0.14 (0.10,0.17)	0.13 (0.09,0.16)	P=0.051	0.13 (0.79,0.20)	0.13 (0.07,0.24)	NS
<i>ESPVR (mmHg/ml)</i>	3.15 (2.37,3.87)	2.76 (2.25,3.66)	NS	2.12 (1.73,2.60)	2.12 (1.69,2.55)	NS
<i>PVA (mmHg.ml)</i>	15961 (13050,21389)	15149 (12954,20714)	NS	11254 (8818,14518)	9707 (7612,13349)	P<0.001
<i>SW (ml.mmHg)</i>	12804 (9602,15221)	12336 (9356,15868)	NS	8220 (5989,10703)	7439 (4323,9459)	P=0.043
<i>PRSW (mmHg)</i>	100 (87,109)	90 (81,107)	NS	59 (53,68)	57 (49,65)	NS
<i>Zva (mmHg/ml/m²)</i>	3.46 (2.72,4.20)	3.12 (2.41,4.30)	NS	2.74 (2.21,3.20)	2.56 (1.90,3.49)	P=0.021

CARDIAC-CORONARY COUPLING PRE- AND POST-TAVI

Table 7-3: The effect of pacing on full pressure-volume loop results in all paired datasets

	Pre-TAVI (n=18)			Post-TAVI (n=18)		
	<i>Rest</i>	<i>Pacing</i>		<i>Rest</i>	<i>Pacing</i>	
<i>SV (ml)</i>	77 (66,96)	56 (41,68)	P<0.001	82 (62,92)	48 (34,66)	P<0.001
<i>EDP (mmHg)</i>	17 (12,27)	16 (12,26)	NS	17 (10,26)	15 (8,20)	P=0.060
<i>ESP (mmHg)</i>	151 (126,172)	130 (106,169)	P=0.003	110 (104,126)	90 (72,102)	P<0.001
<i>EDV (ml)</i>	135 (104,152)	101 (81,120)	P=0.001	132 (108,148)	100 (80,111)	P<0.001
<i>ESV (ml)</i>	50 (38,56)	49 (33,64)	NS	55 (46,58)	49 (43,60)	P=0.067
<i>EF (%)</i>	61 (56,68)	54 (44,65)	P=0.004	62 (55,66)	52 (40,62)	P=0.008
<i>CO (l/min)</i>	5.4 (4.3,6.5)	6.7 (4.8,8.2)	P=0.004	6.0 (4.0,7.1)	5.8 (4.1,8.1)	NS
<i>Ea (mmHg/ml)</i>	1.9 (1.6,2.5)	2.6 (1.9,3.0)	P=0.001	1.5 (1.2,1.8)	2.0 (1.4,2.3)	P=0.043
<i>Ees (mmHg/ml)</i>	3.0 (2.4,2.9)	2.7 (2.2,4.0)	NS	2.0 (1.7,2.6)	1.7 (1.4,2.4)	P=0.099
<i>VA</i>	0.63 (0.48,0.79)	0.85 (0.55,1.26)	P=0.003	0.63 (0.51,0.84)	0.94 (0.60,1.49)	P=0.008
<i>SCI (mmHg/ml/s)</i>	10.2 (8.1,14.8)	14.0 (10.5,15.8)	P=0.002	7.9 (6.1,10.0)	10.7 (8.1,14.2)	P<0.001
<i>Tau (ms)</i>	40 (36,53)	44 (36,69)	NS	52 (37,423)	68 (41,219)	NS
<i>dP/dt+ (mmHg/s)</i>	1397 (1156,1563)	1405 (1078,1781)	NS	960 (833,1095)	1023 (860,1270)	NS
<i>dP/dt- (mmHg/s)</i>	-1297 (-1595,-1065)	-1029 (-1424,-750)	P<0.001	-834 (-1071,-715)	-679 (-905,-514)	P<0.001
<i>EDPVr (mmHg/ml)</i>	0.14 (0.10,0.17)	0.17 (0.10,0.28)	NS	0.13 (0.08,0.20)	0.14 (0.08,0.23)	NS
<i>ESPVR (mmHg/ml)</i>	3.15 (2.37,3.87)	2.66 (2.23,4.05)	NS	2.12 (1.73,2.60)	1.71 (1.37,2.38)	P=0.018
<i>PVA (mmHg.ml)</i>	15961 (13050,21389)	9657 (6626,14485)	P<0.001	11254 (8818,14518)	5412 (4149,9308)	P<0.001
<i>SW (ml.mmHg)</i>	12804 (9602,15221)	5813 (4520,9861)	P<0.001	8220 (5989,10703)	3537 (2171,6645)	P<0.001
<i>PRSW (mmHg)</i>	100 (87,109)	62 (54,80)	P<0.001	59 (53,68)	34 (27,57)	P<0.001
<i>Zva (mmHg/ml/m²)</i>	3.46 (2.72,4.20)	4.13 (3.39,5.56)	P=0.001	2.74 (2.21,3.20)	3.50 (2.54,4.17)	P=0.038

CARDIAC-CORONARY COUPLING PRE- AND POST-TAVI

Table 7-4: The impact of TAVI (pre- vs post) on full pressure volume loop results during each physiological setting in all paired datasets

	Baseline (n=18)			Hyperaemia (n=17)			Pacing (n=18)		
	<i>Pre-TAVI</i>	<i>Post-TAVI</i>		<i>Pre-TAVI</i>	<i>Post-TAVI</i>		<i>Pre-TAVI</i>	<i>Post-TAVI</i>	
<i>SV (ml)</i>	77 (66,96)	82 (62,92)	NS	84 (65,95)	85 (59,89)	NS	56 (41,68)	48 (34,66)	NS
<i>EDP (mmHg)</i>	17 (12,27)	17 (10,26)	NS	19 (13,26)	18 (8,27)	NS	16 (12,26)	15 (8,20)	NS
<i>ESP (mmHg)</i>	151 (126,172)	110 (104,126)	P<0.001	149 (125,168)	101 (95,121)	P=0.001	130 (106,169)	90 (72,102)	P=0.001
<i>EDV (ml)</i>	135 (104,152)	132 (108,148)	NS	133 (107,159)	126 (101,147)	NS	101 (81,120)	100 (80,111)	NS
<i>ESV (ml)</i>	50 (38,56)	545 (46,58)	P=0.090	49 (40,66)	53 (39,64)	NS	49 (33,64)	49 (43,60)	NS
<i>EF (%)</i>	61 (56,68)	62 (55,66)	NS	60 (53,68)	63 (52,69)	NS	54 (44,65)	52 (40,62)	NS
<i>CO (l/min)</i>	5.4 (4.3,6.5)	6.0 (4.0,7.1)	NS	5.3 (4.3,7.3)	5.5 (3.7,6.8)	NS	6.7 (4.8,8.2)	5.8 (4.1,8.1)	NS
<i>Ea (mmHg/ml)</i>	1.9 (1.6,2.5)	1.5 (1.2,1.8)	P=0.090	1.7 (1.4,2.6)	1.4 (1.1,1.9)	P=0.020	2.4 (1.9,3.0)	2.0 (1.4,2.3)	P=0.030
<i>Ees (mmHg/ml)</i>	3.0 (2.4,3.9)	2.0 (1.7,2.6)	P<0.001	2.7 (2.2,3.6)	2.1 (1.7,2.5)	P=0.001	2.7 (2.2,4.0)	1.7 (1.4,2.4)	P=0.001
<i>VA</i>	0.63 (0.48,0.79)	0.63 (0.51,0.84)	NS	0.66 (0.48,0.90)	0.60 (0.46,0.92)	NS	0.85 (0.55,1.26)	0.94 (0.60,1.5)	NS
<i>SCI (mmHg/ml/s)</i>	10.2 (8.1,14.8)	7.9 (6.1,10.0)	P<0.001	10.5 (7.9,13.2)	7.9 (5.8,9.4)	P<0.001	14.0 (10.5,15.8)	10.7 (8.1,14.2)	P<0.001
<i>Tau (ms)</i>	40 (36,53)	52 (37,423)	P=0.014	41 (37,58)	89 (40,415)	P=0.023	44 (36,69)	68 (41,219)	P=0.060
<i>dP/dt+ (mmHg/s)</i>	1397 (1156,1563)	960 (833,1095)	P<0.001	1430 (1106,1558)	864 (742,1036)	P<0.001	1405 (1078,1781)	1023 (860,270)	P<0.001
<i>dP/dt- (mmHg/s)</i>	-1297 (-1595,-1065)	-834 (-1071,-715)	P<0.001	-1309 (-1577,-999)	-741 (-900,-657)	P<0.001	-1029 (-1424,-750)	-679 (-905,-514)	P=0.001
<i>EDPVR (mmHg/ml)</i>	0.14 (0.10,0.17)	0.13 (0.79,0.20)	NS	0.13 (0.09,0.16)	0.13 (0.07,0.24)	NS	0.17 (0.10,0.28)	0.14 (0.08,0.23)	NS
<i>ESPVR (mmHg/ml)</i>	3.15 (2.37,3.87)	2.12 (1.73,2.60)	P<0.001	2.76 (2.25,3.66)	2.12 (1.69,2.55)	P=0.001	2.66 (2.23,4.05)	1.71 (1.37,2.38)	P<0.001
<i>PVA (mmHg.ml)</i>	15961 (13050,21389)	11254 (8818,14518)	P<0.001	15149 (12954,20714)	9707 (7612,13349)	P<0.001	9657 (6626,14485)	5412 (4149,9308)	P=0.001
<i>SW (ml.mmHg)</i>	12804 (9602,15221)	8220 (5989,10702)	P<0.001	12336 (9356,15868)	7439 (4323,9459)	P<0.001	5813 (4520,9861)	3537 (2171,6645)	P<0.001
<i>PRSW (mmHg)</i>	100 (87,109)	59 (53,68)	P<0.001	90 (81,107)	57 (49,65)	P<0.001	62 (54,80)	34 (27,57)	P<0.001
<i>Zva (mmHg/ml/m²)</i>	3.46 (2.72,4.20)	2.74 (2.21,3.20)	P=0.099	3.12 (2.41,4.30)	2.56 (1.90,3.49)	P=0.031	4.13 (3.39,5.56)	3.50 (2.54,4.17)	P=0.030

7.2.1 Haemodynamic Changes with Intervention

The haemodynamic effects of hyperaemia, pacing and the changes following TAVI are shown in Table 7-2, Table 7-3, Table 7-4 and

Table 7-5. TAVI impacted the relative change in response to physiological settings. From baseline to hyperaemia, there was an increase in ESV ($+8\pm 29\%$) before TAVI rather than a reduction ($-6\pm 9\%$) following intervention ($p=0.036$). There were also differences in EDV ($+1\%$ [$-1,+7$] vs -1% [$-3,+1$], $p=0.011$), dP/dt^+ (-1% [$-4,+1$] vs -4% [$-8,0$], $p=0.035$), dP/dt^- (-2% [$-6,+4$], vs -5% [$-15,-1$], $p=0.040$) and PVA (0% [$-3,+3$], vs -4% [$-10,-2$], $p=0.005$) between these settings.

The relative change between LGAS and HGAS also differed. At baseline following intervention, compared to pre-TAVI, there was a less profound drop in ESP in LGAS patients ($-9\pm 19\%$ vs $-34\pm 11\%$, $p=0.004$) and lesser reduction in both dP/dt^+ ($-19\pm 15\%$ vs $-37\pm 9\%$, $p=0.013$) and dP/dt^- ($-17\pm 19\%$ vs $-39\pm 15\%$, $p=0.015$). PVA also reduced less profoundly in the LGAS group ($-21\pm 18\%$ vs $-39\pm 15\%$, $p=0.037$). Pacing induced minimal change in LGAS patients but a significant drop in ejection fraction in HGAS patients pre-TAVI at 90bpm ($-1\pm 15\%$ vs $-19\pm 12\%$, $p=0.016$) when compared to LGAS patients.

Post-TAVI, hyperaemia also induced a less significant reduction in the relative change in dP/dt^- (-3% [$-11,+1$] vs -10% [$-18,-6$], $p=0.024$), dP/dt^+ ($-2\pm 5\%$ vs $-11\pm 10\%$, $p=0.032$) and SCI (-1% [$-5,+7$] vs -5% [$-11,-3$], $p=0.050$) from baseline in the LGAS patients. There was therefore more ventricular impact with hyperaemia, pacing and aortic valve intervention in patients with HGAS, which raises the suspicion of poor remodelling and compliance in the LGAS patients.

In this study, Tau increased immediately following TAVI, at baseline, hyperaemia and rapid pacing, but there was no difference between LGAS and HGAS cohorts. There was significant correlation between pre-TAVI CFR and resting Tau ($R=-0.525$, $p=0.030$).

PVA fell with rapid pacing pre- and post-TAVI and with hyperaemia post-TAVI. Like-for-like following TAVI, during resting state, hyperaemia and pacing, PVA fell significantly ($p<0.001$). Baseline, hyperaemic and paced PVA was lower in LGAS patients, suggesting reduced oxygen consumption in this cohort.

7.2.2 VA results

I found that pre-TAVI, VA increased during pacing both before ($p=0.003$) and after ($p=0.008$) TAVI (Table 7-3). Post-TAVI, hyperaemia also induced a drop in VA ($p=0.048$) (Table 7-2). Resting VA closely correlated with resting LVEDVi ($R=0.687$, $p=0.002$), LVESVi ($R=0.696$, $p=0.001$), indexed stroke volume by MRI ($R=0.532$, $p=0.023$), cardiac output by MRI ($R=0.558$, $p=0.016$), ejection fraction by MRI ($R=-0.512$, $p=0.030$) and pressure-volume loops ($R=-0.689$, $p=0.002$), peak radial strain ($R=-0.505$, $p=0.039$), SCI ($R=-0.682$, $p=0.002$) and PRSW ($R=-0.520$, $p=0.027$).

LGAS patients had lower VA coupling during pacing at 90bpm (0.65 ± 0.38 vs 1.20 ± 0.44 , $p=0.019$), and a trend towards lower values during hyperaemia (0.57 ± 0.25 vs 0.88 ± 0.42 , $p=0.092$) and pacing at 120bpm (0.74 ± 0.38 vs 1.15 ± 0.44 , $p=0.055$) pre-TAVI (

Table 7-5). There was no difference following intervention. This would suggest that the low flow ventricle is more compliant despite reduced maximum and minimum dP/dt , supported by a trend toward increased E_{es} in LGAS patients during rapid pacing pre-TAVI.

CARDIAC-CORONARY COUPLING PRE- AND POST-TAVI

Table 7-5: Full pressure-volume loop results in LGAS and HGAS cohorts pre-TAVI. Results displayed when P<0.010 for LGAS then HGAS with SD or IQR in brackets. No differences were found post-TAVI between cohorts.

	REST		HYPERAEMIA		RAPID PACING	
<i>HR (bpm)</i>		NS		NS		NS
<i>SV (ml)</i>		NS		NS		NS
<i>Svi (ml/m²)</i>		NS		NS		NS
<i>CO (l/min)</i>		NS		NS		NS
<i>EDP (mmHg)</i>		NS		NS		NS
<i>ESP (mmHg)</i>	127 (115,147)/169 (151,181)	P=0.004	125 (111,157)/163 (150,180)	P=0.021	117±35/150±36	P=0.060
<i>EDV (ml)</i>		NS		NS	90±15/119±28	P=0.015
<i>ESV (ml)</i>		NS	43±15/67±25	P=0.040	37±14/61±17	P=0.003
<i>EF (%)</i>		NS	65±11/55±12	P=0.088	60±13/48±10	P=0.053
<i>Ea (mmHg/ml)</i>		NS		NS		NS
<i>Ees (mmHg/ml)</i>		NS		NS		NS
<i>VA</i>		NS	0.57±0.25/0.88±0.42	P=0.092	0.74±0.38/1.15±0.44	P=0.055
<i>SCI (mmHg/ml/s)</i>		NS		NS		NS
<i>Tau (ms)</i>		NS		NS		NS
<i>dP/dt+ (mmHg/s)</i>	1267 (1047,1408)/1509 (1289,1736)	P=0.031		NS		NS
<i>dP/dt- (mmHg/s)</i>	-1066 (-1494,-974)/-1475 (-1640,-1174)	P=0.050	-1045 (-1462,-938)/-1493 (-1725,-1222)	P=0.074		NS
<i>EDPVR (mmHg/ml)</i>		NS		NS		NS
<i>ESPVR (mmHg/ml)</i>		NS		NS		NS
<i>PVA (mmHg.ml)</i>	13583±2975/20598±7123	P=0.020	13579±2337/21118±7549	P=0.026	7972±2659/13606±5423	P=0.017
<i>SW (ml.mmHg)</i>	10745±2424/15212±4356	P=0.019	10741±1749/15089±4887	P=0.042		NS
<i>PRSW (mmHg)</i>	91±13/ 107±12	P=0.013		NS		NS

7.3 Summary

Gotzmann *et al* recently demonstrated that the left ventricle in LGAS exhibits increased stiffness and reduced contractility when compared to other cohorts of AS²⁷⁶, in addition to impaired vascular function – a pattern similar to that in heart failure with preserved ejection fraction (HFpEF). In this study, there was no significant difference in Ea and Ees between cohorts. In addition, despite reduced maximum and minimum dP/dt, there was lower VA coupling in LGAS patients suggesting more favorable compliance.

The immediate response to TAVI was significant. There was a fall in ESP, Ees, SCI, ESPVR, PVA, maximum and minimum dP/dt, SW, PRSW, and Zva. End systolic pressure was lower in patients with LGAS and LV volumes smaller during hyperaemia and pacing. Reduced baseline dP/dt values in LGAS were combined with lower SW, PRSW and PVA – pointing towards less severe ventricular impact from aortic stenosis, or toward increased stiffness. Disparate features of cardiac efficiency were observed between cohorts which highlights the clinical challenges with this disease entity.

8 SYNTHESIS

8.1 Introduction

“Aortic stenosis is a simple mechanical fault, which, if severe enough, imposes a heavy burden on the left ventricle and sooner or later overcomes it.”

P Wood 1958

Aortic stenosis is a disease of the valve, ventricle and microvasculature. The aim of this descriptive physiological study was to:

- Determine the detailed effects of hyperaemia, rapid pacing, and valve implantation in patients with severe symptomatic aortic stenosis (AS) with preserved left ventricular systolic function.
- Provide insight into the distinct features exhibited by low gradient (LGAS) and high gradient aortic stenosis (HGAS).
- Pair meticulous invasive physiology with that of non-invasive techniques and assess short term remodelling phenomena.

The study included 19 patients, recruited over a 2-year period from the transcatheter aortic valve implantation waiting list, where all patients were deemed to have severe, symptomatic aortic stenosis by the heart team. Very few patients met inclusion and exclusion criteria and many potential LGAS recruits were in atrial fibrillation as is known to be prevalent in this disease entity. Whilst final analysis compared LGAS and HGAS, further subdivision to low-flow or normal-flow cohorts was abandoned due to disparate measurements of stroke volume obtained from echocardiography and MRI, and small recruitment numbers (see Table 3-1).

8.2 Ventricular Disparity between LGAS and HGAS

Patients with HGAS exhibited significantly higher aortic valve calcium scores and NT-proBNP levels fell more significantly in the HGAS group. Subendocardial late gadolinium enhancement was only observed within the LGAS group (despite lower left ventricular

SYNTHESIS

pressures), and mid wall late gadolinium enhancement was only observed within the HGAS group. Interstitial fibrosis was no different between cohorts. These non-invasive findings suggest a different pattern of disease in LGAS – a myopathic disease with a degree of aortic stenosis which allows the cardiac physiology to reach tipping point. This is further supported by a shorter baseline ejection time and lower left ventricular mass, volume and pressure. The LGAS cohort displayed reduced baseline parameters of contractility and lusitropy (maximum and minimum dP/dt , SW, PRSW), and this was combined with lower PVA, which indicates reduced oxygen consumption in this group. Despite no difference in E_a between groups (i.e., afterload), a trend towards lower VA was seen during hyperaemia and rapid pacing in the LGAS group, in line with lower alternative markers of contractility such as dP/dt^+ .

HGAS patients had higher end systolic pressure which reduced to a greater degree following TAVI, and pre-TAVI, rapid pacing induced increasing end systolic volumes and a plunge in the ejection fraction – contrary to that found in the LGAS cohort. Following intervention, PVA (signifying oxygen consumption) reduced more profoundly in the HGAS group, and hyperaemia induced a fall in dP/dt^+ . These findings would suggest more favourable malleability and response to various physiological settings – a divergent effect from the unwavering monotony of the LGAS group where unfavourable remodelling appears to allow minimal impact.

8.3 Coronary Disparity between LGAS and HGAS

The novel invasive coronary findings of this study demonstrate significant differences in the coronary flow between patients with LGAS and HGAS. At baseline, LGAS patients exhibit reduced acceleratory BEW, increased inhibitory FEW and lower microcirculatory-derived coronary flow (are above WI^-). During hyperaemia following TAVI, HGAS exhibited greater FCW, and the change from baseline following TAVI revealed that in LGAS patients the BEW reduced, but increased in HGAS patients. This distinct maladaptive coronary flow in response to vasodilatation is pathological and provides more insight into this challenging clinical and physiological condition.

Coronary and aortic Alx, and reflection coefficient were significantly lower in LGAS at rest and during hyperaemia pre-TAVI, likely to be related to lower left ventricular mass and reduced aortic stiffness. Contrasting trends were observed in tension time index (TTI) and BI following TAVI: an increase in TTI in LGAS signifying increased oxygen demand (decrease in HGAS patients) and decrease in BI in LGAS indicating subendocardial ischaemia (increase in HGAS). Importantly, a relative reduction in diastolic time fraction was seen in the LGAS cohort, in comparison to an increase in the HGAS cohort. Ejection time (although shorter at baseline in LGAS patients) was significantly shortened in the HGAS group but remained static in LGAS patients. It is clear that this study does not support the notion that LGAS is a condition of increased vascular stiffness.

Post-TAVI, the change in perfusion efficiency from baseline to hyperaemia reduced in LGAS but increased in HGAS patients, and during hyperaemia the LGAS group's response to augment accelerating waves was significantly blunted. In addition, post-procedure diastolic hyperaemic microvascular resistance was greater in LGAS patients suggesting underlying endothelial dysfunction, supported by a trend towards reduced baseline myocardial perfusion reserve index in LGAS patients.

8.4 Structural and Functional Effects of TAVI

Following balloon-expandable TAVI prosthesis implantation in this cohort, coronary VTI, APV and perfusion efficiency fell, possibly representing a period of ventricular stunning in the immediate aftermath of rapid pacing for valve deployment. In keeping with this, hyperaemia post-TAVI, in comparison to pre-TAVI, demonstrated significantly reduced backward expansion waves and reduced overall distal-originating waves. There was, however, evidence of improved forward flow with reduced ejection time, and increased diastolic time fraction and Buckberg Index during pacing stress, signifying improved myocardial oxygen supply-demand ratio. There was no immediate change in coronary flow reserve. Coronary augmentation pressure and augmentation index fell following TAVI, presumably related to a reduction in systemic vascular resistance. I also observed

SYNTHESIS

a significant decrease in end systolic pressure, effective arterial elastance (E_a), end systolic elastance (E_{es}), Starling contractile state index (SCI), end systolic pressure volume relationship (ESPVR), pressure volume area (PVA), maximum and minimum dP/dt , stroke work (SW), preload recruitable stroke work (PRSW), and valvulo-arterial impedance (Z_{va}) following TAVI. There is therefore strong evidence of reduction in load-independent indices of ventricular contractility. The effects of hyperaemia on the post-TAVI ventricle were more profound than on the pre-TAVI ventricle: reduced ESP, E_a , VA, PVA, SW, Z_{va} , and maximum and minimum dP/dt . Prior to valve implantation, it is likely that vasodilatory capacity is exhausted and there is therefore a more prominent effect with hyperaemia following TAVI.

Follow up cardiac magnetic resonance imaging demonstrated improved left ventricular ejection fraction and a preferential reduction in LV mass over cavity size, with improved global myocardial perfusion reserve index and global 3-dimensional strain. There was favourable delayed remodelling as assessed non-invasively in comparison to the immediate invasively-assessed parameters.

Limitations

The main limitation of this study was the modest patient numbers. Additional patient recruitment would have increased statistical power and improved characterisation of both disease processes. Whilst all physiological indices were assessed at the end of the study, aside from MRI perfusion assessment, it was not possible to fully blind the results from the researcher. There was also no opportunity to repeat scans or invasive measurements, so we have not assessed the test/retest repeatability and have not re-analysed results to present inter-observer variability based on the raw data. Statistical analysis using repeated T-tests rather than ANOVA where relevant may have increased the risk of inaccurate (falsely positive) results. Up to date echocardiography within 24-hours of the invasive and non-invasive protocols would have allowed full and accurate assessment of the aortic valve gradient. In addition, there are multiple comparisons and since this is an exploratory, hypothesis generating study, there is no Bonferroni correction.

Future Directions

This hypothesis-generating study has provided new insight into the disease processes described. The distorted coronary blood flow in LGAS is corrected by TAVI following which minimal difference is observed between groups. Many of the clinical challenges of paradoxical low gradient aortic stenosis are still prominent even in the detailed physiology described. In LGAS patients, AS is certainly contributory, but it remains unclear why this subset of valvular heart disease pose a higher risk with previously published poor outcomes. Detrimental coronary flow and distinct remodelling is evident from this work.

Physiological assessment in the immediate aftermath of TAVI may represent, at least in part, ventricular stunning due to rapid pacing. Delayed invasive physiological assessment after a period of time to allow cardiac remodelling would be of extreme interest to determine the effects of valve intervention in combination with structural and functional changes observed by cardiac magnetic resonance imaging. In addition, studying the immediate effects between patients treated with balloon-expanding, versus self-expanding TAVI prosthesis may help unravel the immediate deterioration in left ventricular parameters described here. The non-invasive assessment of detailed ventricular lusitropy and compliance would allow a more translational application of this work. Changes in preload and afterload and peripheral vascular studies would also provide additional insight in these cohorts which may exhibit vascular disease contributory to the overall condition.

References

1. Christian HA. Aortic Stenosis with Calcification of the Cusps. Journal of the American Medical Association 1931;97.
2. Schwarz F, Flameng W, Schaper J, et al. Myocardial structure and function in patients with aortic valve disease and their relation to postoperative results. Am J Cardiol 1978;41:661-9.
3. Ross J, Jr., Braunwald E. Aortic stenosis. Circulation 1968;38:61-7.
4. Harvey WL, C. D. Exercitatio anatomica de motu cordis et sanguinis in animalibus / by William Harvey ; with an English translation and annotations by Chauncey D. Leake. The Collegiate Press, Menasha, Wisconsin Thomas C, 1928.
5. Sabiston DC, Jr., Gregg DE. Effect of cardiac contraction on coronary blood flow. Circulation 1957;15:14-20.
6. Ahn JH, Kim SM, Park SJ, et al. Coronary Microvascular Dysfunction as a Mechanism of Angina in Severe AS: Prospective Adenosine-Stress CMR Study. J Am Coll Cardiol 2016;67:1412-22.
7. Lancellotti P, Nchimi A. Coronary microvascular reserve and outcome in aortic stenosis: Pathophysiological significance vs. clinical relevance. Eur Heart J 2017;38:1230-2.
8. Laxson DD, Dai XZ, Homans DC, Bache RJ. Coronary vasodilator reserve in ischemic myocardium of the exercising dog. Circulation 1992;85:313-22.
9. Downey HF, Crystal GJ, Bashour FA. Asynchronous transmural perfusion during coronary reactive hyperaemia. Cardiovasc Res 1983;17:200-6.
10. Goto M, Flynn AE, Doucette JW, et al. Cardiac contraction affects deep myocardial vessels predominantly. Am J Physiol 1991;261:H1417-29.
11. Algranati D, Kassab GS, Lanir Y. Mechanisms of myocardium-coronary vessel interaction. Am J Physiol Heart Circ Physiol 2010;298:H861-73.
12. Westerhof N, Boer C, Lamberts RR, Sipkema P. Cross-talk between cardiac muscle and coronary vasculature. Physiol Rev 2006;86:1263-308.
13. Hess DS, Bache RJ. Transmural distribution of myocardial blood flow during systole in the awake dog. Circ Res 1976;38:5-15.

SYNTHESIS

14. Downey JM, Kirk ES. Inhibition of coronary blood flow by a vascular waterfall mechanism. *Circ Res* 1975;36:753-60.
15. Blumenthal MR, Wang HH, Wang SC. Effect of acute experimental aortic stenosis on coronary circulation. *Circ Res* 1962;11:727-35.
16. Komaru T, Kanatsuka H, Shirato K. Coronary microcirculation. *Pharmacology & Therapeutics* 2000;86:217-61.
17. Heusch G. Alpha-adrenergic coronary vasoconstriction in humans. *J Am Coll Cardiol* 2010;55:1278.
18. Stanojevic D, Gunasekaran P, Tadros P, et al. Intravenous Adenosine Infusion is Safe and Well Tolerated During Coronary Fractional Flow Reserve Assessment in Elderly Patients With Severe Aortic Stenosis. *J Invasive Cardiol* 2016;28:357-61.
19. Lumley M, Williams R, Asrress KN, et al. Coronary Physiology During Exercise and Vasodilation in the Healthy Heart and in Severe Aortic Stenosis. *J Am Coll Cardiol* 2016;68:688-97.
20. Scarsini R, Pesarini G, Zivelonghi C, et al. Coronary physiology in patients with severe aortic stenosis: Comparison between fractional flow reserve and instantaneous wave-free ratio. *Int J Cardiol* 2017;243:40-6.
21. Krams R, Kofflard MJ, Duncker DJ, et al. Decreased coronary flow reserve in hypertrophic cardiomyopathy is related to remodeling of the coronary microcirculation. *Circulation* 1998;97:230-3.
22. Blows LJ, Redwood SR. The pressure wire in practice. *Heart* 2007;93:419-22.
23. Di Gioia G, Pellicano M, Toth GG, et al. Fractional Flow Reserve-Guided Revascularization in Patients With Aortic Stenosis. *Am J Cardiol* 2016;117:1511-5.
24. Ahmad Y, Gotberg M, Cook C, et al. Coronary Hemodynamics in Patients With Severe Aortic Stenosis and Coronary Artery Disease Undergoing Transcatheter Aortic Valve Replacement: Implications for Clinical Indices of Coronary Stenosis Severity. *JACC Cardiovasc Interv* 2018;11:2019-31.
25. Duncker DJ, Bache RJ. Regulation of coronary blood flow during exercise. *Physiol Rev* 2008;88:1009-86.
26. Bell JR, Fox AC. Pathogenesis of subendocardial ischemia. *Am J Med Sci* 1974;268:3-13.

SYNTHESIS

27. Downey JM, Kirk ES. The transmural distribution of coronary blood flow during maximal vasodilation. *Proc Soc Exp Biol Med* 1975;150:189-93.
28. Archie JP. Intramyocardial pressure: Effect of preload on transmural distribution of systolic coronary blood flow. *The American Journal of Cardiology* 1975;35:904-11.
29. Giezeman MJ, VanBavel E, Grimbergen CA, Spaan JA. Compliance of isolated porcine coronary small arteries and coronary pressure-flow relations. *Am J Physiol* 1994;267:H1190-8.
30. Wusten B, Buss DD, Deist H, Schaper W. Dilatory capacity of the coronary circulation and its correlation to the arterial vasculature in the canine left ventricle. *Basic Res Cardiol* 1977;72:636-50.
31. Vermeltfoort IA, Raijmakers PG, Lubberink M, et al. Feasibility of subendocardial and subepicardial myocardial perfusion measurements in healthy normals with (15)O-labeled water and positron emission tomography. *J Nucl Cardiol* 2011;18:650-6.
32. Merkus D, Kajiya F, Vink H, et al. Prolonged diastolic time fraction protects myocardial perfusion when coronary blood flow is reduced. *Circulation* 1999;100:75-81.
33. Davies JE, Whinnett ZI, Francis DP, et al. Evidence of a dominant backward-propagating "suction" wave responsible for diastolic coronary filling in humans, attenuated in left ventricular hypertrophy. *Circulation* 2006;113:1768-78.
34. Davies JE, Sen S, Broyd C, et al. Arterial pulse wave dynamics after percutaneous aortic valve replacement: fall in coronary diastolic suction with increasing heart rate as a basis for angina symptoms in aortic stenosis. *Circulation* 2011;124:1565-72.
35. Rolandi MC, Wiegerinck EM, Casadonte L, et al. Transcatheter Replacement of Stenotic Aortic Valve Normalizes Cardiac-Coronary Interaction by Restoration of Systolic Coronary Flow Dynamics as Assessed by Wave Intensity Analysis. *Circ Cardiovasc Interv* 2016;9:e002356.
36. Raphael CE, Cooper R, Parker KH, et al. Mechanisms of Myocardial Ischemia in Hypertrophic Cardiomyopathy: Insights From Wave Intensity Analysis and Magnetic Resonance. *J Am Coll Cardiol* 2016;68:1651-60.
37. De Silva K, Foster P, Guilcher A, et al. Coronary wave energy: a novel predictor of functional recovery after myocardial infarction. *Circ Cardiovasc Interv* 2013;6:166-75.

SYNTHESIS

38. Claridge S, Chen Z, Jackson T, et al. Effects of Epicardial and Endocardial Cardiac Resynchronization Therapy on Coronary Flow: Insights From Wave Intensity Analysis. *J Am Heart Assoc* 2015;4.
39. Lockie TP, Rolandi MC, Guilcher A, et al. Synergistic adaptations to exercise in the systemic and coronary circulations that underlie the warm-up angina phenomenon. *Circulation* 2012;126:2565-74.
40. Asrress KN, Williams R, Lockie T, et al. Physiology of Angina and Its Alleviation With Nitroglycerin: Insights From Invasive Catheter Laboratory Measurements During Exercise. *Circulation* 2017;136:24-34.
41. Arri S, Williams R, Asrress K, et al. Unravelling the Mechanisms of Mental Stress Induced Myocardial Ischaemia: Novel Insights from Intracoronary Measurements during Cardiac Catherisation. *J Am Coll Cardiol* 2017;69.
42. Williams R, Asrress K, Lumley M, et al. Use of novel intracoronary technology to investigate the effect of cold air inhalation during exercise on coronary microvascular resistance and blood flow in coronary artery disease: a cross-sectional study. *The Lancet* 2016;387.
43. Peeters F, Meex SJR, Dweck MR, et al. Calcific aortic valve stenosis: hard disease in the heart: A biomolecular approach towards diagnosis and treatment. *Eur Heart J* 2018;39:2618-24.
44. Carabello BA. The relationship of left ventricular geometry and hypertrophy to left ventricular function in valvular heart disease. *J Heart Valve Dis* 1995;4 Suppl 2:S132-8; discussion S8-9.
45. Mahmood M, Francis JM, Pal N, et al. Myocardial perfusion and oxygenation are impaired during stress in severe aortic stenosis and correlate with impaired energetics and subclinical left ventricular dysfunction. *J Cardiovasc Magn Reson* 2014;16:29.
46. Rajappan K, Rimoldi OE, Dutka DP, et al. Mechanisms of coronary microcirculatory dysfunction in patients with aortic stenosis and angiographically normal coronary arteries. *Circulation* 2002;105:470-6.
47. Galiuto L, Lotrionte M, Crea F, et al. Impaired coronary and myocardial flow in severe aortic stenosis is associated with increased apoptosis: a transthoracic Doppler and myocardial contrast echocardiography study. *Heart* 2006;92:208-12.

SYNTHESIS

48. Breisch EA, Houser SR, Carey RA, Spann JF, Bove AA. Myocardial blood flow and capillary density in chronic pressure overload of the feline left ventricle. *Cardiovasc Res* 1980;14:469-75.
49. Miyagawa S, Masai T, Fukuda H, et al. Coronary microcirculatory dysfunction in aortic stenosis: myocardial contrast echocardiography study. *Ann Thorac Surg* 2009;87:715-9.
50. Gould KL, Carabello BA. Why angina in aortic stenosis with normal coronary arteriograms? *Circulation* 2003;107:3121-3.
51. Cioffi G, Faggiano P, Vizzardi E, et al. Prognostic effect of inappropriately high left ventricular mass in asymptomatic severe aortic stenosis. *Heart* 2011;97:301-7.
52. Broyd CJ, Davies JE, Escaned JE, Hughes A, Parker K. Wave intensity analysis and its application to the coronary circulation. *Global Cardiology Science and Practice* 2015;2015.
53. Geske JB, Cullen MW, Sorajja P, Ommen SR, Nishimura RA. Assessment of left ventricular outflow gradient: hypertrophic cardiomyopathy versus aortic valvular stenosis. *JACC Cardiovasc Interv* 2012;5:675-81.
54. Banovic MD, Vujisic-Tesic BD, Kujacic VG, et al. Coronary flow reserve in patients with aortic stenosis and nonobstructed coronary arteries. *Acta Cardiol* 2011;66:743-9.
55. Camici PG, Crea F. Coronary microvascular dysfunction. *N Engl J Med* 2007;356:830-40.
56. Kozakova M, Palombo C, Pratali L, Pittella G, Galetta F, L'Abbate A. Mechanisms of coronary flow reserve impairment in human hypertension. An integrated approach by transthoracic and transesophageal echocardiography. *Hypertension* 1997;29:551-9.
57. Beyerbach HP, Lamb HJ, van Der Laarse A, et al. Aortic valve replacement in patients with aortic valve stenosis improves myocardial metabolism and diastolic function. *Radiology* 2001;219:637-43.
58. Kenny A, Wisbey CR, Shapiro LM. Profiles of coronary blood flow velocity in patients with aortic stenosis and the effect of valve replacement: a transthoracic echocardiographic study. *Br Heart J* 1994;71:57-62.

SYNTHESIS

59. Yotti R, Bermejo J, Gutierrez-Ibanez E, et al. Systemic vascular load in calcific degenerative aortic valve stenosis: insight from percutaneous valve replacement. *J Am Coll Cardiol* 2015;65:423-33.
60. Wiegerinck EM, van de Hoef TP, Rolandi MC, et al. Impact of Aortic Valve Stenosis on Coronary Hemodynamics and the Instantaneous Effect of Transcatheter Aortic Valve Implantation. *Circ Cardiovasc Interv* 2015;8:e002443.
61. Garcia D, Camici PG, Durand LG, et al. Impairment of coronary flow reserve in aortic stenosis. *J Appl Physiol* (1985) 2009;106:113-21.
62. Vassalli G, Kaufmann P, Villari B, et al. Reduced epicardial coronary vasodilator capacity in patients with left ventricular hypertrophy. *Circulation* 1995;91:2916-23.
63. Marcus ML, Doty DB, Hiratzka LF, Wright CB, Eastham CL. Decreased coronary reserve: a mechanism for angina pectoris in patients with aortic stenosis and normal coronary arteries. *N Engl J Med* 1982;307:1362-6.
64. Steadman CD, Jerosch-Herold M, Grundy B, et al. Determinants and functional significance of myocardial perfusion reserve in severe aortic stenosis. *JACC Cardiovasc Imaging* 2012;5:182-9.
65. Crea F, Camici PG, Bairey Merz CN. Coronary microvascular dysfunction: an update. *Eur Heart J* 2014;35:1101-11.
66. Dunn RB, Griggs DM, Jr. Ventricular filling pressure as a determinant of coronary blood flow during ischemia. *Am J Physiol* 1983;244:H429-36.
67. Gould KL, Johnson NP. Ischemia in Aortic Stenosis: New Insights and Potential Clinical Relevance. *J Am Coll Cardiol* 2016;68:698-701.
68. Hongo M, Goto T, Watanabe N, et al. Relation of phasic coronary flow velocity profile to clinical and hemodynamic characteristics of patients with aortic valve disease. *Circulation* 1993;88:953-60.
69. Kern MJ. Changing reflections of the coronary microcirculation after percutaneous aortic valve replacement: novel observations with arterial pulsed wave dynamics. *Circulation* 2011;124:1505-7.
70. Ben-Dor I, Malik R, Minha S, et al. Coronary blood flow in patients with severe aortic stenosis before and after transcatheter aortic valve implantation. *Am J Cardiol* 2014;114:1264-8.

SYNTHESIS

71. von Knobelsdorff-Brenkenhoff F, Karunaharamoorthy A, Trauzeddel RF, et al. Evaluation of Aortic Blood Flow and Wall Shear Stress in Aortic Stenosis and Its Association With Left Ventricular Remodeling. *Circ Cardiovasc Imaging* 2016;9:e004038.
72. Fallen EL, Elliott WC, Gorlin R. Mechanisms of angina in aortic stenosis. *Circulation* 1967;36:480-8.
73. Julius BK, Spillmann M, Vassalli G, Villari B, Eberli FR, Hess OM. Angina pectoris in patients with aortic stenosis and normal coronary arteries. Mechanisms and pathophysiological concepts. *Circulation* 1997;95:892-8.
74. Gutierrez-Barrios A, Gamaza-Chulian S, Agarrado-Luna A, et al. Invasive assessment of coronary flow reserve impairment in severe aortic stenosis and echocardiographic correlations. *Int J Cardiol* 2017;236:370-4.
75. Omran H, Fehske W, Rabahieh R, Hagendorff A, Luderitz B. Relation between symptoms and profiles of coronary artery blood flow velocities in patients with aortic valve stenosis: a study using transoesophageal Doppler echocardiography. *Heart* 1996;75:377-83.
76. Hildick-Smith DJR, Shapiro LM. Coronary flow reserve improves after aortic valve replacement for aortic stenosis: an adenosine transthoracic echocardiography study. *Journal of the American College of Cardiology* 2000;36:1889-96.
77. Singh A, Greenwood JP, Berry C, et al. Comparison of exercise testing and CMR measured myocardial perfusion reserve for predicting outcome in asymptomatic aortic stenosis: the PROgnostic Importance of Microvascular Dysfunction in Aortic Stenosis (PRIMID AS) Study. *Eur Heart J* 2017;38:1222-9.
78. Rajappan K, Rimoldi OE, Camici PG, Bellenger NG, Pennell DJ, Sheridan DJ. Functional changes in coronary microcirculation after valve replacement in patients with aortic stenosis. *Circulation* 2003;107:3170-5.
79. Yamanaga K, Tsujita K, Komura N, et al. Physiological basis of discordance between coronary flow velocity reserve and hyperemic microvascular resistance for evaluating coronary microvascular dysfunction in patients without atherosclerotic obstruction. *Int J Cardiol* 2015;201:535-7.
80. Gould KL, Johnson NP. Imaging Coronary Blood Flow in AS: Let the Data Talk, Again. *J Am Coll Cardiol* 2016;67:1423-6.

SYNTHESIS

81. Pibarot P, Dumesnil JG. Paradoxical low-flow, low-gradient aortic stenosis adding new pieces to the puzzle. *J Am Coll Cardiol* 2011;58:413-5.
82. Bhattacharyya S, Mittal T, Abayalingam M, et al. Classification of Aortic Stenosis by Flow and Gradient Patterns Provides Insights into the Pathophysiology of Disease. *Angiology* 2016;67:664-9.
83. Minners J, Allgeier M, Gohlke-Baerwolf C, Kienzle RP, Neumann FJ, Jander N. Inconsistencies of echocardiographic criteria for the grading of aortic valve stenosis. *Eur Heart J* 2008;29:1043-8.
84. Dayan V, Vignolo G, Magne J, Clavel MA, Mohty D, Pibarot P. Outcome and Impact of Aortic Valve Replacement in Patients With Preserved LVEF and Low-Gradient Aortic Stenosis. *J Am Coll Cardiol* 2015;66:2594-603.
85. Rimoldi O, Rosen SD, Camici PG. The blunting of coronary flow reserve in hypertension with left ventricular hypertrophy is transmural and correlates with systolic blood pressure. *J Hypertens* 2014;32:2465-71; discussion 71.
86. Murthy VL, Naya M, Foster CR, et al. Association between coronary vascular dysfunction and cardiac mortality in patients with and without diabetes mellitus. *Circulation* 2012;126:1858-68.
87. Gjesdal O, Bluemke DA, Lima JA. Cardiac remodeling at the population level--risk factors, screening, and outcomes. *Nat Rev Cardiol* 2011;8:673-85.
88. Herrmann S, Stork S, Niemann M, et al. Low-gradient aortic valve stenosis myocardial fibrosis and its influence on function and outcome. *J Am Coll Cardiol* 2011;58:402-12.
89. Hachicha Z, Dumesnil JG, Bogaty P, Pibarot P. Paradoxical low-flow, low-gradient severe aortic stenosis despite preserved ejection fraction is associated with higher afterload and reduced survival. *Circulation* 2007;115:2856-64.
90. Awtry E, Davidoff R. Low-flow/low-gradient aortic stenosis. *Circulation* 2011;124:e739-41.
91. Barasch E, Fan D, Chukwu EO, et al. Severe isolated aortic stenosis with normal left ventricular systolic function and low transvalvular gradients: pathophysiologic and prognostic insights. *J Heart Valve Dis* 2008;17:81-8.

SYNTHESIS

92. Hachicha Z, Dumesnil JG, Pibarot P. Usefulness of the valvuloarterial impedance to predict adverse outcome in asymptomatic aortic stenosis. *J Am Coll Cardiol* 2009;54:1003-11.
93. Pibarot P, Dumesnil JG. Low-flow, low-gradient aortic stenosis with normal and depressed left ventricular ejection fraction. *J Am Coll Cardiol* 2012;60:1845-53.
94. Eleid MF, Sorajja P, Michelena HI, Malouf JF, Scott CG, Pellikka PA. Survival by stroke volume index in patients with low-gradient normal EF severe aortic stenosis. *Heart* 2015;101:23-9.
95. Rusinaru D, Bohbot Y, Ringle A, Marechaux S, Diouf M, Tribouilloy C. Impact of low stroke volume on mortality in patients with severe aortic stenosis and preserved left ventricular ejection fraction. *Eur Heart J* 2018;39:1992-9.
96. Pibarot P. Aortic stenosis: flow matters. *Heart* 2015;101:5-6.
97. Christensen KL, Ivarsen HR, Thuesen L, Kristensen BO, Egeblad H. Aortic valve stenosis: fatal natural history despite normal left ventricular function and low invasive peak-to-peak pressure gradients. *Cardiology* 2004;102:147-51.
98. Clavel MA, Dumesnil JG, Capoulade R, Mathieu P, Senechal M, Pibarot P. Outcome of patients with aortic stenosis, small valve area, and low-flow, low-gradient despite preserved left ventricular ejection fraction. *J Am Coll Cardiol* 2012;60:1259-67.
99. Clavel MA, Fuchs C, Burwash IG, et al. Predictors of outcomes in low-flow, low-gradient aortic stenosis: results of the multicenter TOPAS Study. *Circulation* 2008;118:S234-42.
100. Debry N, Sudre A, Amr G, et al. Transcatheter aortic valve implantation for paradoxical low-flow low-gradient aortic stenosis patients. *Catheter Cardiovasc Interv* 2016;87:797-804.
101. Dumesnil JG, Pibarot P, Carabello B. Paradoxical low flow and/or low gradient severe aortic stenosis despite preserved left ventricular ejection fraction: implications for diagnosis and treatment. *Eur Heart J* 2010;31:281-9.
102. Eleid MF, Sorajja P, Michelena HI, Malouf JF, Scott CG, Pellikka PA. Flow-gradient patterns in severe aortic stenosis with preserved ejection fraction: clinical characteristics and predictors of survival. *Circulation* 2013;128:1781-9.

SYNTHESIS

103. Herrmann HC, Pibarot P, Hueter I, et al. Predictors of mortality and outcomes of therapy in low-flow severe aortic stenosis: a Placement of Aortic Transcatheter Valves (PARTNER) trial analysis. *Circulation* 2013;127:2316-26.
104. Lancellotti P, Magne J, Donal E, et al. Clinical outcome in asymptomatic severe aortic stenosis: insights from the new proposed aortic stenosis grading classification. *J Am Coll Cardiol* 2012;59:235-43.
105. Le Ven F, Freeman M, Webb J, et al. Impact of low flow on the outcome of high-risk patients undergoing transcatheter aortic valve replacement. *J Am Coll Cardiol* 2013;62:782-8.
106. Mehrotra P, Jansen K, Flynn AW, et al. Differential left ventricular remodelling and longitudinal function distinguishes low flow from normal-flow preserved ejection fraction low-gradient severe aortic stenosis. *Eur Heart J* 2013;34:1906-14.
107. Mohty D, Boulogne C, Magne J, et al. Prevalence and long-term outcome of aortic prosthesis-patient mismatch in patients with paradoxical low-flow severe aortic stenosis. *Circulation* 2014;130:S25-31.
108. Mohty D, Magne J, Deltreuil M, et al. Outcome and impact of surgery in paradoxical low-flow, low-gradient severe aortic stenosis and preserved left ventricular ejection fraction: a cardiac catheterization study. *Circulation* 2013;128:S235-42.
109. Pai RG, Varadarajan P, Razzouk A. Survival benefit of aortic valve replacement in patients with severe aortic stenosis with low ejection fraction and low gradient with normal ejection fraction. *Ann Thorac Surg* 2008;86:1781-9.
110. Jander N, Minners J, Holme I, et al. Outcome of patients with low-gradient "severe" aortic stenosis and preserved ejection fraction. *Circulation* 2011;123:887-95.
111. Maes F, Boulif J, Pierard S, et al. Natural history of paradoxical low-gradient severe aortic stenosis. *Circ Cardiovasc Imaging* 2014;7:714-22.
112. Malkin CJ, Long WR, Baxter PD, et al. Impact of left ventricular function and transaortic gradient on outcomes from transcatheter aortic valve implantation: data from the UK TAVI Registry. *EuroIntervention* 2016;11:1161-9.
113. Tribouilloy C, Rusinaru D, Marechaux S, et al. Low-gradient, low-flow severe aortic stenosis with preserved left ventricular ejection fraction: characteristics, outcome, and implications for surgery. *J Am Coll Cardiol* 2015;65:55-66.

SYNTHESIS

114. Elmariah S. Patterns of left ventricular remodeling in aortic stenosis: therapeutic implications. *Curr Treat Options Cardiovasc Med* 2015;17:391.
115. Baumgartner H, Falk V, Bax JJ, et al. 2017 ESC/EACTS Guidelines for the management of valvular heart disease. *Eur Heart J* 2017;38:2739-91.
116. Nishimura RA, Otto CM, Bonow RO, et al. 2017 AHA/ACC Focused Update of the 2014 AHA/ACC Guideline for the Management of Patients With Valvular Heart Disease: A Report of the American College of Cardiology/American Heart Association Task Force on Clinical Practice Guidelines. *J Am Coll Cardiol* 2017;70:252-89.
117. Levy F, Laurent M, Monin JL, et al. Aortic valve replacement for low-flow/low-gradient aortic stenosis operative risk stratification and long-term outcome: a European multicenter study. *J Am Coll Cardiol* 2008;51:1466-72.
118. Spethmann S, Baldenhofer G, Dreger H, et al. Recovery of left ventricular and left atrial mechanics in various entities of aortic stenosis 12 months after TAVI. *Eur Heart J Cardiovasc Imaging* 2014;15:389-98.
119. Schewel J, Schluter M, Schmidt T, Kuck KH, Frerker C, Schewel D. Early haemodynamic changes and long-term outcome of patients with severe low-gradient aortic stenosis after transcatheter aortic valve replacement. *EuroIntervention* 2020;15:1181-9.
120. Chadha G, Bohbot Y, Rusinaru D, Marechaux S, Tribouilloy C. Outcome of Normal-Flow Low-Gradient Severe Aortic Stenosis With Preserved Left Ventricular Ejection Fraction: A Propensity-Matched Study. *J Am Heart Assoc* 2019;8:e012301.
121. Chin CWL, Ding ZP, Lam CSP, Ling LH. Paradoxical Low-Gradient Aortic Stenosis: The HFpEF of Aortic Stenosis. *J Am Coll Cardiol* 2016;67:2447-8.
122. Lorell BH, Carabello BA. Left ventricular hypertrophy: pathogenesis, detection, and prognosis. *Circulation* 2000;102:470-9.
123. Bursac N. Cardiac fibroblasts in pressure overload hypertrophy: the enemy within? *J Clin Invest* 2014;124:2850-3.
124. Biernacka AF, N. G. Aging and Cardiac Fibrosis. *Aging and disease* 2011:158–73.

SYNTHESIS

125. Beach JM, Mihaljevic T, Rajeswaran J, et al. Ventricular hypertrophy and left atrial dilatation persist and are associated with reduced survival after valve replacement for aortic stenosis. *J Thorac Cardiovasc Surg* 2014;147:362-9 e8.
126. Gosse P. Left ventricular hypertrophy as a predictor of cardiovascular risk. *J Hypertens Suppl* 2005;23:S27-33.
127. Shah AS, Chin CW, Vassiliou V, et al. Left ventricular hypertrophy with strain and aortic stenosis. *Circulation* 2014;130:1607-16.
128. Anderson KR, Sutton MG, Lie JT. Histopathological types of cardiac fibrosis in myocardial disease. *J Pathol* 1979;128:79-85.
129. Krayenbuehl HP, Hess OM, Monrad ES, Schneider J, Mall G, Turina M. Left ventricular myocardial structure in aortic valve disease before, intermediate, and late after aortic valve replacement. *Circulation* 1989;79:744-55.
130. Schaper J, Speiser B. The extracellular matrix in the failing human heart. *Basic Res Cardiol* 1992;87 Suppl 1:303-9.
131. Villari B, Campbell SE, Hess OM, et al. Influence of collagen network on left ventricular systolic and diastolic function in aortic valve disease. *J Am Coll Cardiol* 1993;22:1477-84.
132. Azevedo CF, Nigri M, Higuchi ML, et al. Prognostic significance of myocardial fibrosis quantification by histopathology and magnetic resonance imaging in patients with severe aortic valve disease. *J Am Coll Cardiol* 2010;56:278-87.
133. Dweck MR, Joshi S, Murigu T, et al. Midwall fibrosis is an independent predictor of mortality in patients with aortic stenosis. *J Am Coll Cardiol* 2011;58:1271-9.
134. Hess OM, Villari B, Krayenbuehl HP. Diastolic dysfunction in aortic stenosis. *Circulation* 1993;87:IV73-6.
135. Hein S, Arnon E, Kostin S, et al. Progression from compensated hypertrophy to failure in the pressure-overloaded human heart: structural deterioration and compensatory mechanisms. *Circulation* 2003;107:984-91.
136. Chin CW, Messika-Zeitoun D, Shah AS, et al. A clinical risk score of myocardial fibrosis predicts adverse outcomes in aortic stenosis. *Eur Heart J* 2016;37:713-23.

SYNTHESIS

137. Chin CW, Shah AS, McAllister DA, et al. High-sensitivity troponin I concentrations are a marker of an advanced hypertrophic response and adverse outcomes in patients with aortic stenosis. *Eur Heart J* 2014;35:2312-21.
138. Bull SC, Loudon M, Joseph J, et al. 151 Myocardial Perfusion, Strain and Pre-Contrast T1 Values in Moderate Asymptomatic Aortic Stenosis. *Heart* 2013;99:A89.1-A.
139. Debl K, Djavidani B, Buchner S, et al. Delayed hyperenhancement in magnetic resonance imaging of left ventricular hypertrophy caused by aortic stenosis and hypertrophic cardiomyopathy: visualisation of focal fibrosis. *Heart* 2006;92:1447-51.
140. Heymans S, Schroen B, Vermeersch P, et al. Increased cardiac expression of tissue inhibitor of metalloproteinase-1 and tissue inhibitor of metalloproteinase-2 is related to cardiac fibrosis and dysfunction in the chronic pressure-overloaded human heart. *Circulation* 2005;112:1136-44.
141. Rudolph A, Abdel-Aty H, Bohl S, et al. Noninvasive detection of fibrosis applying contrast-enhanced cardiac magnetic resonance in different forms of left ventricular hypertrophy relation to remodeling. *J Am Coll Cardiol* 2009;53:284-91.
142. Weidemann F, Herrmann S, Stork S, et al. Impact of myocardial fibrosis in patients with symptomatic severe aortic stenosis. *Circulation* 2009;120:577-84.
143. Barone-Rochette G, Pierard S, De Meester de Ravenstein C, et al. Prognostic significance of LGE by CMR in aortic stenosis patients undergoing valve replacement. *J Am Coll Cardiol* 2014;64:144-54.
144. Chin CW, Pawade TA, Newby DE, Dweck MR. Risk Stratification in Patients With Aortic Stenosis Using Novel Imaging Approaches. *Circ Cardiovasc Imaging* 2015;8:e003421.
145. Chin CWL, Everett RJ, Kwiecinski J, et al. Myocardial Fibrosis and Cardiac Decompensation in Aortic Stenosis. *JACC Cardiovasc Imaging* 2017;10:1320-33.
146. Holmes AA, Taub CC, Garcia MJ, Shan J, Slovut DP. Paradoxical low-flow aortic stenosis is defined by increased ventricular hydraulic load and reduced longitudinal strain. *J Cardiovasc Med (Hagerstown)* 2017;18:87-95.
147. Lee SP, Kim YJ, Kim JH, et al. Deterioration of myocardial function in paradoxical low-flow severe aortic stenosis: two-dimensional strain analysis. *J Am Soc Echocardiogr* 2011;24:976-83.

SYNTHESIS

148. Sato K, Seo Y, Ishizu T, et al. Prognostic value of global longitudinal strain in paradoxical low-flow, low-gradient severe aortic stenosis with preserved ejection fraction. *Circ J* 2014;78:2750-9.
149. Dumesnil JG, Shoucri RM, Laurenceau JL, Turcot J. A mathematical model of the dynamic geometry of the intact left ventricle and its application to clinical data. *Circulation* 1979;59:1024-34.
150. Henein MY, Gibson DG. Normal long axis function. *Heart* 1999;81:111-3.
151. Lafitte S, Perlant M, Reant P, et al. Impact of impaired myocardial deformations on exercise tolerance and prognosis in patients with asymptomatic aortic stenosis. *Eur J Echocardiogr* 2009;10:414-9.
152. Clavel MA, Pibarot P. Assessment of low-flow, low-gradient aortic stenosis: multimodality imaging is the key to success. *EuroIntervention* 2014;10 Suppl U:U52-60.
153. Kato S, Saito N, Kirigaya H, et al. Impairment of Coronary Flow Reserve Evaluated by Phase Contrast Cine-Magnetic Resonance Imaging in Patients With Heart Failure With Preserved Ejection Fraction. *J Am Heart Assoc* 2016;5.
154. Lee JF, Barrett-O'Keefe Z, Garten RS, et al. Evidence of microvascular dysfunction in heart failure with preserved ejection fraction. *Heart* 2016;102:278-84.
155. Marcus ML, Harrison DG, Chilian WM, et al. Alterations in the coronary circulation in hypertrophied ventricles. *Circulation* 1987;75:119-25.
156. Sucato V, Evola S, Novo G, et al. Angiographic Evaluation of Coronary Microvascular Dysfunction in Patients with Heart Failure and Preserved Ejection Fraction. *Microcirculation* 2015;22:528-33.
157. de Boer RA, Lok DJ, Jaarsma T, et al. Predictive value of plasma galectin-3 levels in heart failure with reduced and preserved ejection fraction. *Ann Med* 2011;43:60-8.
158. de Boer RA, Voors AA, Muntendam P, van Gilst WH, van Veldhuisen DJ. Galectin-3: a novel mediator of heart failure development and progression. *Eur J Heart Fail* 2009;11:811-7.
159. Baldenhofer G, Zhang K, Spethmann S, et al. Galectin-3 predicts short- and long-term outcome in patients undergoing transcatheter aortic valve implantation (TAVI). *Int J Cardiol* 2014;177:912-7.

SYNTHESIS

160. Arangalage D, Nguyen V, Robert T, et al. Determinants and prognostic value of Galectin-3 in patients with aortic valve stenosis. *Heart* 2016;102:862-8.
161. Chin C. Paradoxical low-flow low-gradient aortic stenosis: advanced severe disease, a new entity or a progression of disease? *Heart* 2015;101:1079.
162. Dahl JS, Eleid MF, Pislaru SV, Scott CG, Connolly HM, Pellikka PA. Development of paradoxical low-flow, low-gradient severe aortic stenosis. *Heart* 2015;101:1015-23.
163. Herrmann S, Fries B, Liu D, et al. Differences in natural history of low- and high-gradient aortic stenosis from nonsevere to severe stage of the disease. *J Am Soc Echocardiogr* 2015;28:1270-82 e4.
164. Pislaru SV, Pellikka PA. The spectrum of low-output low-gradient aortic stenosis with normal ejection fraction. *Heart* 2016;102:665-71.
165. Fearon WF, Nishi T, De Bruyne B, et al. Clinical Outcomes and Cost-Effectiveness of Fractional Flow Reserve-Guided Percutaneous Coronary Intervention in Patients With Stable Coronary Artery Disease: Three-Year Follow-Up of the FAME 2 Trial (Fractional Flow Reserve Versus Angiography for Multivessel Evaluation). *Circulation* 2018;137:480-7.
166. Xaplanteris P, Fournier S, Pijls NHJ, et al. Five-Year Outcomes with PCI Guided by Fractional Flow Reserve. *N Engl J Med* 2018;379:250-9.
167. Kikoine J, Lebon M, Gouffran G, Millischer D, Cattan S, Nallet O. [Measurement of fractional flow reserve in patients with severe aortic stenosis: A valid test?]. *Ann Cardiol Angeiol (Paris)* 2016;65:366-9.
168. Danson E, Hansen P, Sen S, Davies J, Meredith I, Bhindi R. Assessment, treatment, and prognostic implications of CAD in patients undergoing TAVI. *Nat Rev Cardiol* 2016;13:276-85.
169. Pesarini G, Scarsini R, Zivelonghi C, et al. Functional Assessment of Coronary Artery Disease in Patients Undergoing Transcatheter Aortic Valve Implantation: Influence of Pressure Overload on the Evaluation of Lesions Severity. *Circ Cardiovasc Interv* 2016;9.
170. Lester SJ, Heilbron B, Gin K, Dodek A, Jue J. The natural history and rate of progression of aortic stenosis. *Chest* 1998;113:1109-14.

SYNTHESIS

171. Nemes A, Balazs E, Csanady M, Forster T. Long-term prognostic role of coronary flow velocity reserve in patients with aortic valve stenosis - insights from the SZEGED Study. *Clin Physiol Funct Imaging* 2009;29:447-52.
172. Vesey AT, Esson G, Chin C, Dweck M, Newby D. Detection of Cardiac Fibrosis and Cell Death in Patients with Aortic Stenosis. *Journal of the American College of Cardiology* 2015;65.
173. Chin CW, Djohan AH, Lang CC. The role of cardiac biochemical markers in aortic stenosis. *Biomarkers* 2016;21:316-27.
174. Anand A, Chin C, Shah ASV, et al. Cardiac myosin-binding protein C is a novel marker of myocardial injury and fibrosis in aortic stenosis. *Heart* 2018;104:1101-8.
175. Banovic M, Vujisic-Tesic B, Bojic S, et al. Diagnostic value of NT-proBNP in identifying impaired coronary flow reserve in asymptomatic moderate or severe aortic stenosis. *Biomark Med* 2013;7:221-7.
176. Mosteller RD. Simplified calculation of body-surface area. *N Engl J Med* 1987;317:1098.
177. Plein S, Schwitter J, Suerder D, Greenwood JP, Boesiger P, Kozerke S. k-Space and time sensitivity encoding-accelerated myocardial perfusion MR imaging at 3.0 T: comparison with 1.5 T. *Radiology* 2008;249:493-500.
178. Cerqueira MD, Weissman NJ, Dilsizian V, et al. Standardized myocardial segmentation and nomenclature for tomographic imaging of the heart. A statement for healthcare professionals from the Cardiac Imaging Committee of the Council on Clinical Cardiology of the American Heart Association. *Int J Cardiovasc Imaging* 2002;18:539-42.
179. Kremers FP, Hofman MB, Groothuis JG, et al. Improved correction of spatial inhomogeneities of surface coils in quantitative analysis of first-pass myocardial perfusion imaging. *J Magn Reson Imaging* 2010;31:227-33.
180. Kramer CM, Barkhausen J, Bucciarelli-Ducci C, Flamm SD, Kim RJ, Nagel E. Standardized cardiovascular magnetic resonance imaging (CMR) protocols: 2020 update. *J Cardiovasc Magn Reson* 2020;22:17.
181. Ishida M, Schuster A, Morton G, et al. Development of a universal dual-bolus injection scheme for the quantitative assessment of myocardial perfusion cardiovascular magnetic resonance. *J Cardiovasc Magn Reson* 2011;13:28.

SYNTHESIS

182. Moon JC, Messroghli DR, Kellman P, et al. Myocardial T1 mapping and extracellular volume quantification: a Society for Cardiovascular Magnetic Resonance (SCMR) and CMR Working Group of the European Society of Cardiology consensus statement. *J Cardiovasc Magn Reson* 2013;15:92.
183. Baan J, van der Velde ET, de Bruin HG, et al. Continuous measurement of left ventricular volume in animals and humans by conductance catheter. *Circulation* 1984;70:812-23.
184. Burkhoff D, van der Velde E, Kass D, Baan J, Maughan WL, Sagawa K. Accuracy of volume measurement by conductance catheter in isolated, ejecting canine hearts. *Circulation* 1985;72:440-7.
185. van der Velde ET, van Dijk AD, Steendijk P, et al. Left ventricular segmental volume by conductance catheter and Cine-CT. *Eur Heart J* 1992;13 Suppl E:15-21.
186. Bastos MB, Burkhoff D, Maly J, et al. Invasive left ventricle pressure-volume analysis: overview and practical clinical implications. *Eur Heart J* 2020;41:1286-97.
187. Siebes M, Verhoeff BJ, Meuwissen M, de Winter RJ, Spaan JA, Piek JJ. Single-wire pressure and flow velocity measurement to quantify coronary stenosis hemodynamics and effects of percutaneous interventions. *Circulation* 2004;109:756-62.
188. Jenni R, Buchi M, Zweifel HJ, Ritter M. Impact of Doppler guidewire size and flow rates on intravascular velocity profiles. *Cathet Cardiovasc Diagn* 1998;45:96-100.
189. Kaufmann PA, Jenni R. Coronary flow reserve assessment from average peak velocity profiles alone must be judged with caution. *Journal of the American College of Cardiology* 2000;35:1363-4.
190. Ofili EO, Kern MJ, Labovitz AJ, et al. Analysis of coronary blood flow velocity dynamics in angiographically normal and stenosed arteries before and after endolumen enlargement by angioplasty. *J Am Coll Cardiol* 1993;21:308-16.
191. Davies JE, Whinnett ZI, Francis DP, et al. Use of simultaneous pressure and velocity measurements to estimate arterial wave speed at a single site in humans. *Am J Physiol Heart Circ Physiol* 2006;290:H878-85.
192. De Bruyne B, Pijls NH, Barbato E, et al. Intracoronary and intravenous adenosine 5'-triphosphate, adenosine, papaverine, and contrast medium to assess fractional flow reserve in humans. *Circulation* 2003;107:1877-83.

SYNTHESIS

193. Buckberg G, Eber L, Herman M, Gorlin R. Ischemia in aortic stenosis: hemodynamic prediction. *Am J Cardiol* 1975;35:778-84.
194. Thormann J, Schlepper M. Comparison of myocardial flow, hemodynamic changes, and lactate metabolism during isoproterenol stress in patients with coronary heart disease and severe aortic stenosis. *Clin Cardiol* 1979;2:437-45.
195. Klotz S, Hay I, Dickstein ML, et al. Single-beat estimation of end-diastolic pressure-volume relationship: a novel method with potential for noninvasive application. *Am J Physiol Heart Circ Physiol* 2006;291:H403-12.
196. Salton CJ, Chuang ML, O'Donnell CJ, et al. Gender differences and normal left ventricular anatomy in an adult population free of hypertension. A cardiovascular magnetic resonance study of the Framingham Heart Study Offspring cohort. *J Am Coll Cardiol* 2002;39:1055-60.
197. To AC, Flamm SD, Marwick TH, Klein AL. Clinical utility of multimodality LA imaging: assessment of size, function, and structure. *JACC Cardiovasc Imaging* 2011;4:788-98.
198. Hor KN, Gottliebson WM, Carson C, et al. Comparison of magnetic resonance feature tracking for strain calculation with harmonic phase imaging analysis. *JACC Cardiovasc Imaging* 2010;3:144-51.
199. Sammut E, Zarinabad N, Wesolowski R, et al. Feasibility of high-resolution quantitative perfusion analysis in patients with heart failure. *J Cardiovasc Magn Reson* 2015;17:13.
200. Schuster A, Sinclair M, Zarinabad N, et al. A quantitative high resolution voxel-wise assessment of myocardial blood flow from contrast-enhanced first-pass magnetic resonance perfusion imaging: microsphere validation in a magnetic resonance compatible free beating explanted pig heart model. *Eur Heart J Cardiovasc Imaging* 2015;16:1082-92.
201. Scannell CM, Villa ADM, Lee J, Breeuwer M, Chiribiri A. Robust Non-Rigid Motion Compensation of Free-Breathing Myocardial Perfusion MRI Data. *IEEE Trans Med Imaging* 2019;38:1812-20.

SYNTHESIS

202. Flett AS, Hayward MP, Ashworth MT, et al. Equilibrium contrast cardiovascular magnetic resonance for the measurement of diffuse myocardial fibrosis: preliminary validation in humans. *Circulation* 2010;122:138-44.
203. Cowell SJ, Newby DE, Burton J, et al. Aortic valve calcification on computed tomography predicts the severity of aortic stenosis. *Clin Radiol* 2003;58:712-6.
204. Baumgartner H, Hung J, Bermejo J, et al. Recommendations on the Echocardiographic Assessment of Aortic Valve Stenosis: A Focused Update from the European Association of Cardiovascular Imaging and the American Society of Echocardiography. *J Am Soc Echocardiogr* 2017;30:372-92.
205. Devereux RB, Alonso DR, Lutas EM, et al. Echocardiographic assessment of left ventricular hypertrophy: comparison to necropsy findings. *Am J Cardiol* 1986;57:450-8.
206. Zoghbi WA, Farmer KL, Soto JG, Nelson JG, Quinones MA. Accurate noninvasive quantification of stenotic aortic valve area by Doppler echocardiography. *Circulation* 1986;73:452-9.
207. Esper SA, Pinsky MR. Arterial waveform analysis. *Best Pract Res Clin Anaesthesiol* 2014;28:363-80.
208. Arani DT, Carleton RA. Assessment of aortic valvular stenosis from the aortic pressure pulse. *Circulation* 1967;36:30-5.
209. Kotval PS. Doppler waveform parvus and tardus. A sign of proximal flow obstruction. *J Ultrasound Med* 1989;8:435-40.
210. O'Rourke MF, Staessen JA, Vlachopoulos C, Duprez D, Plante GE. Clinical applications of arterial stiffness; definitions and reference values. *Am J Hypertens* 2002;15:426-44.
211. Sarnoff SJ, Braunwald E, Welch GH, Jr., Case RB, Stainsby WN, Macruz R. Hemodynamic determinants of oxygen consumption of the heart with special reference to the tension-time index. *Am J Physiol* 1958;192:148-56.
212. Buckberg GD, Fixler DE, Archie JP, Hoffman JI. Experimental subendocardial ischemia in dogs with normal coronary arteries. *Circ Res* 1972;30:67-81.
213. Buckberg GD, Towers B, Paglia DE, Mulder DG, Maloney JV. Subendocardial ischemia after cardiopulmonary bypass. *J Thorac Cardiovasc Surg* 1972;64:669-84.

SYNTHESIS

214. Smucker ML, Tedesco CL, Manning SB, Owen RM, Feldman MD. Demonstration of an imbalance between coronary perfusion and excessive load as a mechanism of ischemia during stress in patients with aortic stenosis. *Circulation* 1988;78:573-82.
215. Ladwiniec A, White PA, Nijjer SS, et al. Diastolic Backward-Travelling Decompression (Suction) Wave Correlates With Simultaneously Acquired Indices of Diastolic Function and Is Reduced in Left Ventricular Stunning. *Circ Cardiovasc Interv* 2016;9.
216. Westerhof N, Segers P, Westerhof BE. Wave Separation, Wave Intensity, the Reservoir-Wave Concept, and the Instantaneous Wave-Free Ratio: Presumptions and Principles. *Hypertension* 2015;66:93-8.
217. De Silva K, Lumley M, Kailey B, et al. Coronary and microvascular physiology during intra-aortic balloon counterpulsation. *JACC Cardiovasc Interv* 2014;7:631-40.
218. Williams RP, Asrress KN, Lumley M, et al. Deleterious Effects of Cold Air Inhalation on Coronary Physiological Indices in Patients With Obstructive Coronary Artery Disease. *J Am Heart Assoc* 2018;7:e008837.
219. Sen S, Escaned J, Malik IS, et al. Development and validation of a new adenosine-independent index of stenosis severity from coronary wave-intensity analysis: results of the ADVISE (ADenosine Vasodilator Independent Stenosis Evaluation) study. *J Am Coll Cardiol* 2012;59:1392-402.
220. Meuwissen M, Chamuleau SA, Siebes M, et al. Role of variability in microvascular resistance on fractional flow reserve and coronary blood flow velocity reserve in intermediate coronary lesions. *Circulation* 2001;103:184-7.
221. Williams RP, de Waard GA, De Silva K, et al. Doppler Versus Thermodilution-Derived Coronary Microvascular Resistance to Predict Coronary Microvascular Dysfunction in Patients With Acute Myocardial Infarction or Stable Angina Pectoris. *Am J Cardiol* 2018;121:1-8.
222. Neill WA, Fluri-Lundeen JH. Myocardial oxygen supply in left ventricular hypertrophy and coronary heart disease. *Am J Cardiol* 1979;44:746-53.
223. Muller C, Golasch G, Schachinger S, et al. Transcatheter aortic valve replacement (TAVR) leads to an increase in the subendocardial viability ratio assessed by pulse wave analysis. *PLoS One* 2018;13:e0207537.

SYNTHESIS

224. Broyd CJ, Rigo F, Nijjer S, et al. Regression of left ventricular hypertrophy provides an additive physiological benefit following treatment of aortic stenosis: Insights from serial coronary wave intensity analysis. *Acta Physiol (Oxf)* 2018;224:e13109.
225. Ganau A, Devereux RB, Roman MJ, et al. Patterns of left ventricular hypertrophy and geometric remodeling in essential hypertension. *Journal of the American College of Cardiology* 1992;19:1550-8.
226. Dweck MR, Joshi S, Murigu T, et al. Left ventricular remodeling and hypertrophy in patients with aortic stenosis: insights from cardiovascular magnetic resonance. *J Cardiovasc Magn Reson* 2012;14:50.
227. Levine HJ. Compliance of the left ventricle. *Circulation* 1972;46:423-6.
228. Moore GW, Hutchins GM, Bulkley BH, Tseng JS, Ki PF. Constituents of the human ventricular myocardium: connective tissue hyperplasia accompanying muscular hypertrophy. *Am Heart J* 1980;100:610-6.
229. Yamamoto K, Masuyama T, Sakata Y, et al. Roles of renin-angiotensin and endothelin systems in development of diastolic heart failure in hypertensive hearts. *Cardiovasc Res* 2000;47:274-83.
230. Chahal NS, Lim TK, Jain P, Chambers JC, Kooner JS, Senior R. New insights into the relationship of left ventricular geometry and left ventricular mass with cardiac function: A population study of hypertensive subjects. *Eur Heart J* 2010;31:588-94.
231. Sorop O, Heinonen I, van Kranenburg M, et al. Multiple common comorbidities produce left ventricular diastolic dysfunction associated with coronary microvascular dysfunction, oxidative stress, and myocardial stiffening. *Cardiovasc Res* 2018;114:954-64.
232. Westerhof N, Bosman F, De Vries CJ, Noordergraaf A. Analog studies of the human systemic arterial tree. *J Biomech* 1969;2:121-43.
233. van den Bos GC, Westerhof N, Randall OS. Pulse wave reflection: can it explain the differences between systemic and pulmonary pressure and flow waves? A study in dogs. *Circ Res* 1982;51:479-85.
234. Westerhof N, Sipkema P, van den Bos GC, Elzinga G. Forward and backward waves in the arterial system. *Cardiovasc Res* 1972;6:648-56.

SYNTHESIS

235. Hashimoto J, Imai Y, O'Rourke MF. Indices of pulse wave analysis are better predictors of left ventricular mass reduction than cuff pressure. *Am J Hypertens* 2007;20:378-84.
236. Sharman JE, Davies JE, Jenkins C, Marwick TH. Augmentation index, left ventricular contractility, and wave reflection. *Hypertension* 2009;54:1099-105.
237. Sera F, Russo C, Iwata S, et al. Arterial wave reflection and aortic valve calcification in an elderly community-based cohort. *J Am Soc Echocardiogr* 2015;28:430-6.
238. Ng ACT, Prihadi EA, Antoni ML, et al. Left ventricular global longitudinal strain is predictive of all-cause mortality independent of aortic stenosis severity and ejection fraction. *Eur Heart J Cardiovasc Imaging* 2018;19:859-67.
239. Galat A, Guellich A, Bodez D, et al. Aortic stenosis and transthyretin cardiac amyloidosis: the chicken or the egg? *Eur Heart J* 2016;37:3525-31.
240. Haloui F, Salaun E, Maysou L, Dehaene A, Habib G. Cardiac amyloidosis: an unusual cause of low flow-low gradient aortic stenosis with preserved ejection fraction. *Eur Heart J Cardiovasc Imaging* 2016;17:383.
241. Longhi S, Lorenzini M, Gagliardi C, et al. Coexistence of Degenerative Aortic Stenosis and Wild-Type Transthyretin-Related Cardiac Amyloidosis. *JACC Cardiovasc Imaging* 2016;9:325-7.
242. Zhao L, Tian Z, Fang Q. Diagnostic accuracy of cardiovascular magnetic resonance for patients with suspected cardiac amyloidosis: a systematic review and meta-analysis. *BMC Cardiovasc Disord* 2016;16:129.
243. Briand M, Dumesnil JG, Kadem L, et al. Reduced systemic arterial compliance impacts significantly on left ventricular afterload and function in aortic stenosis: implications for diagnosis and treatment. *J Am Coll Cardiol* 2005;46:291-8.
244. Gegenava T, Vollema EM, Abou R, et al. Prognostic Value of Thoracic Aorta Calcification Burden in Patients Treated With TAVR. *JACC Cardiovasc Imaging* 2019;12:216-7.
245. Cramariuc D, Cioffi G, Rieck AE, et al. Low-flow aortic stenosis in asymptomatic patients: valvular-arterial impedance and systolic function from the SEAS Substudy. *JACC Cardiovasc Imaging* 2009;2:390-9.

SYNTHESIS

246. Chin CW, Khaw HJ, Luo E, et al. Echocardiography underestimates stroke volume and aortic valve area: implications for patients with small-area low-gradient aortic stenosis. *Can J Cardiol* 2014;30:1064-72.
247. Fabiani I, Pugliese NR, Calogero E, et al. MicroRNAs distribution in different phenotypes of Aortic Stenosis. *Sci Rep* 2018;8:9953.
248. Olah A, Nemeth BT, Matyas C, et al. Physiological and pathological left ventricular hypertrophy of comparable degree is associated with characteristic differences of in vivo hemodynamics. *Am J Physiol Heart Circ Physiol* 2016;310:H587-97.
249. Jugdutt BI. Ventricular remodeling after infarction and the extracellular collagen matrix: when is enough enough? *Circulation* 2003;108:1395-403.
250. Swynghedauw B. Molecular mechanisms of myocardial remodeling. *Physiol Rev* 1999;79:215-62.
251. Cohn JN, Ferrari R, Sharpe N. Cardiac remodeling—concepts and clinical implications: a consensus paper from an international forum on cardiac remodeling. *Journal of the American College of Cardiology* 2000;35:569-82.
252. Liu T, Song D, Dong J, et al. Current Understanding of the Pathophysiology of Myocardial Fibrosis and Its Quantitative Assessment in Heart Failure. *Front Physiol* 2017;8:238.
253. Eghbali M, Blumenfeld OO, Seifter S, et al. Localization of types I, III and IV collagen mRNAs in rat heart cells by in situ hybridization. *J Mol Cell Cardiol* 1989;21:103-13.
254. Porter KE, Turner NA. Cardiac fibroblasts: at the heart of myocardial remodeling. *Pharmacol Ther* 2009;123:255-78.
255. Serini G, Gabbiana G. Modulation of alpha-smooth muscle actin expression in fibroblasts by transforming growth factor-beta isoforms: an in vivo and in vitro study. *Wound Repair Regen* 1996;4:278-87.
256. Hansson GK, Hellstrand M, Rymo L, Rubbia L, Gabbiani G. Interferon gamma inhibits both proliferation and expression of differentiation-specific alpha-smooth muscle actin in arterial smooth muscle cells. *J Exp Med* 1989;170:1595-608.
257. Chen MM, Lam A, Abraham JA, Schreiner GF, Joly AH. CTGF expression is induced by TGF- beta in cardiac fibroblasts and cardiac myocytes: a potential role in heart fibrosis. *J Mol Cell Cardiol* 2000;32:1805-19.

SYNTHESIS

258. Lipson KE, Wong C, Teng Y, Spong S. CTGF is a central mediator of tissue remodeling and fibrosis and its inhibition can reverse the process of fibrosis. *Fibrogenesis Tissue Repair* 2012;5:S24.
259. Kuwahara F, Kai H, Tokuda K, et al. Transforming growth factor-beta function blocking prevents myocardial fibrosis and diastolic dysfunction in pressure-overloaded rats. *Circulation* 2002;106:130-5.
260. Yamamoto K, Masuyama T, Sakata Y, et al. Myocardial stiffness is determined by ventricular fibrosis, but not by compensatory or excessive hypertrophy in hypertensive heart. *Cardiovasc Res* 2002;55:76-82.
261. Hulsmans M, Sam F, Nahrendorf M. Monocyte and macrophage contributions to cardiac remodeling. *J Mol Cell Cardiol* 2016;93:149-55.
262. Zak R. Development and proliferative capacity of cardiac muscle cells. *Circ Res* 1974;35:suppl II:17-26.
263. Vliegen HW, van der Laarse A, Cornelisse CJ, Eulderink F. Myocardial changes in pressure overload-induced left ventricular hypertrophy. A study on tissue composition, polyploidization and multinucleation. *Eur Heart J* 1991;12:488-94.
264. Fielitz J, Leuschner M, Zurbrugg HR, et al. Regulation of matrix metalloproteinases and their inhibitors in the left ventricular myocardium of patients with aortic stenosis. *J Mol Med (Berl)* 2004;82:809-20.
265. Shahi CN, Ghaisas NK, Goggins M, et al. Elevated levels of circulating soluble adhesion molecules in patients with nonrheumatic aortic stenosis. *Am J Cardiol* 1997;79:980-2.
266. Lee SP, Kim HK, Kim YJ, Oh S, Sohn DW. Association of myocardial angiogenesis with structural and functional ventricular remodeling in aortic stenosis patients with normal ejection fraction. *J Cardiovasc Ultrasound* 2014;22:72-9.
267. Runge VM, Clanton JA, Herzer WA, et al. Intravascular contrast agents suitable for magnetic resonance imaging. *Radiology* 1984;153:171-6.
268. Bing R, Cavalcante JL, Everett RJ, Clavel MA, Newby DE, Dweck MR. Imaging and Impact of Myocardial Fibrosis in Aortic Stenosis. *JACC Cardiovasc Imaging* 2019;12:283-96.

SYNTHESIS

269. Treibel TA, Kozor R, Schofield R, et al. Reverse Myocardial Remodeling Following Valve Replacement in Patients With Aortic Stenosis. *J Am Coll Cardiol* 2018;71:860-71.
270. Treibel TA, Fridman Y, Bering P, et al. Extracellular Volume Associates With Outcomes More Strongly Than Native or Post-Contrast Myocardial T1. *JACC Cardiovasc Imaging* 2020;13:44-54.
271. Sarnoff SJ, Berglund E. Ventricular function. I. Starling's law of the heart studied by means of simultaneous right and left ventricular function curves in the dog. *Circulation* 1954;9:706-18.
272. Morita S. Is there a crystal ball for predicting the outcome of cardiomyopathy surgery? Preload recruitable stroke work, may be a possible candidate. *J Cardiol* 2018;71:325-6.
273. Khalafbeigui F, Suga H, Sagawa K. Left ventricular systolic pressure-volume area correlates with oxygen consumption. *Am J Physiol* 1979;237:H566-9.
274. Vanoverschelde JL, Essamri B, Michel X, et al. Hemodynamic and volume correlates of left ventricular diastolic relaxation and filling in patients with aortic stenosis. *J Am Coll Cardiol* 1992;20:813-21.
275. Di Bello V, Giannini C, De Carlo M, et al. Acute improvement in arterial-ventricular coupling after transcatheter aortic valve implantation (CoreValve) in patients with symptomatic aortic stenosis. *Int J Cardiovasc Imaging* 2012;28:79-87.
276. Gotzmann M, Hauptmann S, Hogeweg M, et al. Hemodynamics of paradoxical severe aortic stenosis: insight from a pressure-volume loop analysis. *Clin Res Cardiol* 2019;108:931-9.